INVESTIGATION OF EFFECTS OF BIRD STRIKE ON WING LEADING EDGE
BY USING EXPLICIT FINITE ELEMENT METHOD

A THESIS SUBMITTED TO
THE GRADUATE SCHOOL OF NATURAL AND APPLIED SCIENCES
OF
MIDDLE EAST TECHNICAL UNIVERSITY

BY
OĞUZHAN DEDE

IN PARTIAL FULFILLMENT OF THE REQUIREMENTS
FOR
THE DEGREE OF MASTER OF SCIENCE
IN
AEROSPACE ENGINEERING

FEBRUARY 2015

Approval of the thesis:

INVESTIGATION OF EFFECTS OF BIRD STRIKE PROBLEM ON WING LEADING EDGE BY USING EXPLICIT FINITE ELEMENT METHOD

submitted by **OĞUZHAN DEDE** in partial fulfillment of the requirements for the degree of **Master of Science in Aerospace Engineering Department, Middle East Technical University** by,

Prof. Dr. Gülbin Dural Ünver   _____
Dean, Graduate School of **Natural and Applied Sciences**

Prof. Dr. Ozan Tekinalp   _____
Head of Department, **Aerospace Engineering**

Prof. Dr. Altan Kayran   _____
Supervisor, **Aerospace Engineering Dept., METU**

Examining Committee Members:

Assoc. Prof. Dr. Demirkan Çöker   _____
Aerospace Engineering Dept., METU

Prof. Dr. Altan Kayran   _____
Aerospace Engineering Dept., METU

Asst. Prof. Dr. Ercan Gürses   _____
Aerospace Engineering Dept., METU

Prof. Dr. Orhan Yıldırım   _____
Mechanical Engineering Dept., METU

Oğuzhan Ayısıt, M.Sc.   _____
Chief Research Engineer, TÜBİTAK SAGE

Date: 02/02/2015

I hereby declare that all information in this document has been obtained and presented in accordance with academic rules and ethical conduct. I also declare that, as required by these rules and conduct, I have fully cited and referenced all material and results that are not original to this work.

Name, Last Name   : Oğuzhan DEDE

Signature   :

ABSTRACT

INVESTIGATION OF EFFECTS OF BIRD STRIKE PROBLEM ON WING LEADING EDGE BY USING EXPLICIT FINITE ELEMENT METHOD

Dede, Oğuzhan

M.S., Department of Aerospace Engineering

Supervisor   : Prof. Dr. Altan Kayran

February 2015, 98 pages

In aviation industry, bird strike problem causes structural damage and threats to flight safety. Nowadays, designed and produced aircraft have to satisfy "safe flight and landing" requirements. The behavior of the aircraft components during bird strike have be to investigated by numerical methods or experiments. Results obtained from numerical analysis and /or experiments have to be carefully studied to optimize the aircraft structures. However, experiments of bird strike are very costly and require qualified test infrastructures. Also, trial and error method is used in test procedures and it leads to consumption of time and money for aircraft producers. Use of finite element method is continuously increasing to analyze bird strike problems to reduce time and money requirement to validate aircraft structures.

The main aim of this thesis is to apply the explicit finite element analysis procedure for the analysis of bird strike problem on the leading edge of the wing. In addition, another aim of this thesis is to show capabilities and effectiveness of honeycomb material against bird strike when used in the leading edge. For this purpose, LSTC Ls-Dyna is chosen as the explicit finite element solver for the bird strike analysis. To model the soft body impactor (bird), a small benchmark study is performed among different solution formulations such as Eulerian, ALE (Arbitrary Lagrangian Eulerian) and SPH (Smoothed Particle Hydrodynamics). As results of the benchmark study, SPH is chosen as the suitable formulation to model the bird by comparing the

deformation and impact force results. Similarly, suitable material model is selected to model the metallic aircraft structure by conducting a benchmark study between elasto-plastic and elasto-viscoplastic material models. Johnson Cook material model is decided to be used for modeling of metallic aircraft structures. Additionally, laminated composite fabric material model which is available in Ls-Dyna material model library is used for modeling the composite wing leading edge. Material characterization test results are used to determine material parameters and coupon simulations are performed to validate material model of the composite fabric material.

After the selection of suitable solution formulation for soft body impactor and material models for metallic and composite aircraft structure, bird strike analyses on the wing leading edge are performed for both metallic and composite case studies. Effect of bird strike is investigated for metallic and composite leading edges and it is clearly seen that bird strike problem may lead to catastrophic failure during flight if proper design measures are not taken.

Finally, reinforcement study of the wing leading edge is done by using the honeycomb material. Honeycomb material is added to metallic and composite wing leading edge and bird strike analyses repeated to investigate the effect of honeycomb on the bird strike problem. It is seen that honeycomb exhibits excellent stiffness against soft body impact. It is concluded that honeycomb materials are very effective materials for bird strike problem with low ratio of weight / impact stiffness.

Keywords: Explicit finite element, bird strike, wing, leading edge, Eulerian, ALE, SPH, Honeycomb

ÖZ

KANAT HÜCUM KENARI KUŞ ÇARPMASI PROBLEMİNİN AÇIK SONLU ELEMAN METODU İLE İNCELENEMESİ

Dede, Oğuzhan

Yüksek Lisans, Havacılık ve Uzay Mühendisliği Bölümü

Tez Yöneticisi   : Prof. Dr. Altan Kayran

Şubat 2015, 98 sayfa

Havacılık sektöründe, kuş çarpması maddi zararlara yol açan ve uçuş güvenliğini tehdit eden önemli bir sorun olarak kabul edilmektedir. Günümüzde tasarlanan ve üretilen havacılık yapılarının güvenli uçuş ve iniş gereksinimlerine uyum sağlamaları zorunludur. Bu gereksinimleri sağlayabilmek için, sonlu elemanlar yöntemi ve/veya testler ile yapısal parçaların, kuş çarpmasına karşı davranışları incelenmektedir. Elde edilen sonuçlar ile tasarım sürecinde iyileştirme çalışmaları yapılıp, daha dayanıklı ve güvenli araçların üretilmesi hedeflenmektedir. Fakat test maliyetlerinin yüksek olması ve "deneme-yanılma yönteminin" test sayısını arttırması, üreticileri hem zaman hem de maddi olarak zorlamaktadır.

Bu tezin amacı, kanat hücum kenarı kuş çarpması problem için tavsiye niteliğinde analiz yöntemi oluşturmaktır. Ayrıca, bal peteği yapısının kuş çarpması problemlerine karşı etkili bir güçlendirme yöntemi olduğunu göstermek, bu tezin bir diğer amacıdır. Çözücü olarak, Ls-Dyna çözücüsü kullanılmıştır. Basit bir model üzerinde, çözücüde bulunan farklı çözüm yöntemleri; SPH (Smoothed Particle Hyrodynamics), Eulerian, ALE (Arbitrary Lagrangian Eulerian) kıyaslanmıştır. Deformasyon ve çarpma kuvveti sonuçları kıyaslanarak, SPH yönteminin kuş modellemede en iyi sonucu verdiği görülmüştür. Metalik yapıları modellemek için malzeme modeli seçimi yapılmıştır. Elastik-plastik ve elastik-viskoplastik malzeme modelleri kıyaslanarak en uygun malzeme modeli seçilmiştir. Johnson Cook

malzeme modelinin metalik yapıları modellemede uygun bir model olduğu anlaşılmıştır. Bunlara ek olarak, kompozit malzeme modellemek için Ls-Dyna malzeme modeli kütüphanesinde bulunan laminated composite fabric kullanılmıştır. Malzeme karakterizasyonu için yapılan kupon testleriyle, kupon analizleri kıyaslanarak malzeme modeli doğrulanmıştır.

Uygun çözüm yöntemi ve malzeme modellerinin seçilmesinin ardından metalik ve kompozit kanat hücum kenarları için kuş çarpması analizleri yapılmış ve sonuçlar incelenmiştir. Elde edilen sonuçlara göre, uçuş sırasında olabilecek kuş çarpması problemleri uçuş güvenliğini tehdit edebilmektedir.

Son olarak, kuş çarpması problemine önlem olarak güçlendirme çalışmaları yapılmıştır. Bu kapsamda, bal peteği malzemesi kullanılmıştır. Metalik ve kompozit hücum kenarlarına bal peteği eklenmiş ve analizler tekrarlanmıştır. Analiz sonuçları incelendiğinde, bal peteği yapısının, kuş çarpması problemlerine karşı etkili bir güçlendirme yöntemi olduğu belirlenmiştir.

Anahtar Kelimeler: Sonlu Eleman Metodu, Kuş Çarpma, Kanat, Hücum Kenarı, Eulerian, ALE, SPH, Bal Peteği

To My Lovely Wife

ACKNOWLEDGEMENTS

I would like to express my endless thanks to Prof. Dr. Altan Kayran for his effort to this thesis. Without his supervision and constant helps, this thesis would not have been possible.

I would like to thank Bias Engineering and Ender Koç for providing required software and their technical support.

I would also like to thank Suphi Yılmaz, Cem Cenç, Mert Atasoy and Okan Çınar from Aselsan Inc. for consent to include copyrighted pictures and test data as a part of my dissertation.

Finally, I would like to express my deepest appreciation to my family for their understanding and their support.

TABLE OF CONTENTS

LIST OF FIGURES

FIGURES

LIST OF TABLES

TABLES

LIST OF SYMBOLS

FEM	Finite Element Method
ALE	Arbitrary Lagrangian Eulerian
SPH	Smoothed Particle Hydrodynamics
CFL	Courant-Friedrichs-Lewy condition
EOS	Equation of State
m	Mass
d	Displacement
v	Velocity
a	Acceleration
J	Impulse
σ	Stress
ε^p	Plastic Strain
ε^f	Failure Strain
ϕ	Yield Surface
σ_y	Yield Stress
w_{ij}	Damage Parameters
ro	Density
E	Young's Modulus
E_a	Elastic Modulus at Longitudinal Direction
E_b	Elastic Modulus at Transverse Direction
pr	Poisson's Ratio
G	Shear Modulus
G_{ab}	Shear Modulus in ab plane
G_{bc}	Shear Modulus in bc plane
G_{ac}	Shear Modulus in ac plane
V_C	Cruise Speed
V_H	Hover Speed
c	Speed of Sound

Δt_{crit}	Critical Time Step
W	Kernel Function
P	Pressure
T	Temperature
e	Internal Energy
v	Specific Volume
ρ	Density
P_N	Normalized Pressure
P_S	Stagnation Pressure
A	Initial Yield Stress
B	Hardening Modulus
C	Strain Rate
ϕ	Yield Function

CHAPTER 1

INTRODUCTION

Foreign object damage is a very important problem for aircraft structures. Although aircraft structures are faced with various threats of foreign object damage like tire rubber or runway debris, bird strike problem causes about 90% of all incidences [1]. Especially in civil aviation, bird strike causes a significant financial problem and threats to the flight safety. According to the Federal Aviation Administration's (FAA) National Wildlife Strike Database, threats to aviation safety due to wildlife impacts upon civil and military aircraft have killed more than 200 people and destroyed 186 aircraft since 1988, globally [1].

Wings, nose/radome, windshield, engines and fuselages were reported as most common aircraft components struck by birds. Figure 1-1 shows an illustration of aircraft components which have a risk in terms of bird strike.
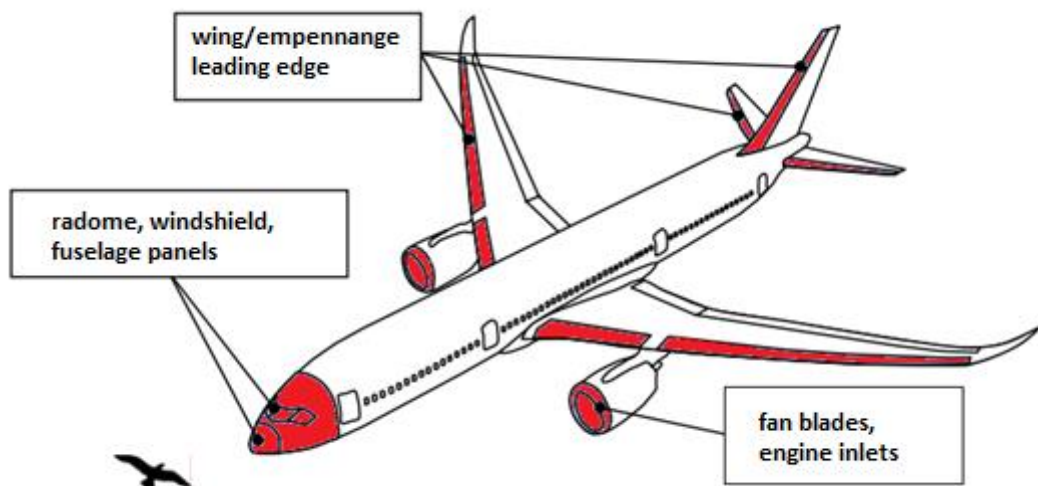
Figure 1-1 Aircraft Components Exposed to the Risk of Bird Strike

An aircraft must satisfy "continued safe flight and landing" requirements. To satisfy these requirements, prior to the final certification test, validation studies are usually

performed during the design process. These studies are mainly based on the bird strike tests. However, performing bird strike tests requires well qualified test infrastructure and needs huge amount of time and money. After the initial design, manufacturer has to produce prototypes and prepares the test system. This leads to complicated designs for "bird-strike proof" aircraft. Nowadays, complicated and highly nonlinear problems can be modeled together with improved computer and software technologies. Design methodology slightly changes with increasing usage of finite element software packages. Firstly, bird strike proof designs are validated by using computer simulations and the final design is tested. This brings some advantages such as reduced design time, lower testing budget and safer designs.

1.1   Literature Review

Empirical formulas are traditionally used for analyzing bird strike problems to determine the required thickness of structural components to able to resist bird impacts. However, the airworthiness requirements are slightly changed and empirical formulas cannot handle today's optimized complex aircraft structures adequately. In the last few decades, many researchers focused their bird strike research by using computers and the related software.

McCallum and Constantinou from BAE systems studied on the effect of bird shape during bird strike. They used explicit finite element solver (LSTC Ls-Dyna). They firstly analyzed traditional bird shape impacting on the square flat panel by using ALE and SPH techniques. After the selection of suitable solution techniques, they modeled detailed bird model. Finally, they concluded that modeling of detailed bird model may have an important consequence for damage initiation and failure of the target [2]. The difference in pressure results were provided in this study. More realistic representation of the bird shape influenced the stagnation pressure and it is given in Figure 1-2 [2].

2
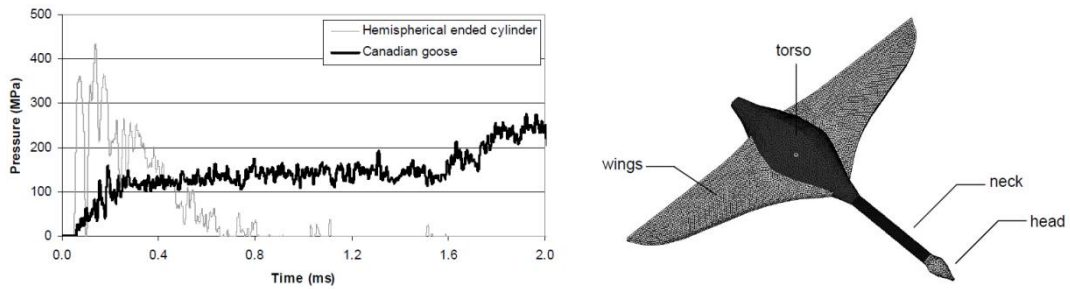
Figure 1-2 Stagnation Pressure (left) and Bird Shape (right) [2]

In Guida's study [3], main aim was to design with the help of finite element analysis and the experimental tests, an aircraft wing leading edge structure with innovative materials that satisfies the optimization of requirements such as weight and performance. Material characterization was the first step of this study. Selections of suitable material model were selected. Bird strike on aircraft empennage was performed by using SPH solution technique. [3].

Bird strike analysis and comparison with real test were conducted by Guida M., et al. [4] In this study, a numerical investigation of the capability of a fiber metal sandwich wing leading edge construction subject to bird strike was done by using finite element method coupled to smooth particle hydrodynamic method. Excellent qualitative correlations with the experimental data were achieved [4]. Comparison of the test and simulation is given in Figure 1-3 [4].
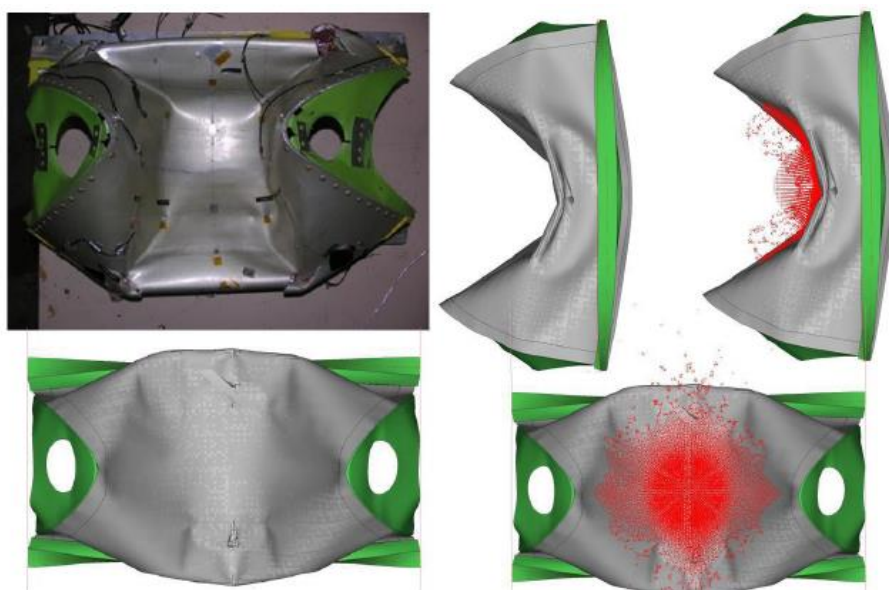
Figure 1-3 Numerical and Experimental Shape after the Impact [4]

3

Lavoie et al. used SPH method to analyze bird strike on rigid target and compared analysis results with test results. The paper is demonstration of accuracy of SPH method for the bird impact. After validation of the SPH method, bird impact on wing leading edge analysis was given in this paper [5]. Bird strike analysis results are given in Figure 1-4 [5]. It can be concluded that "SPH method can be used to obtain accurate results for bird impact simulations and it is suitable for complex problems that cannot be successfully solved using other numerical methods"
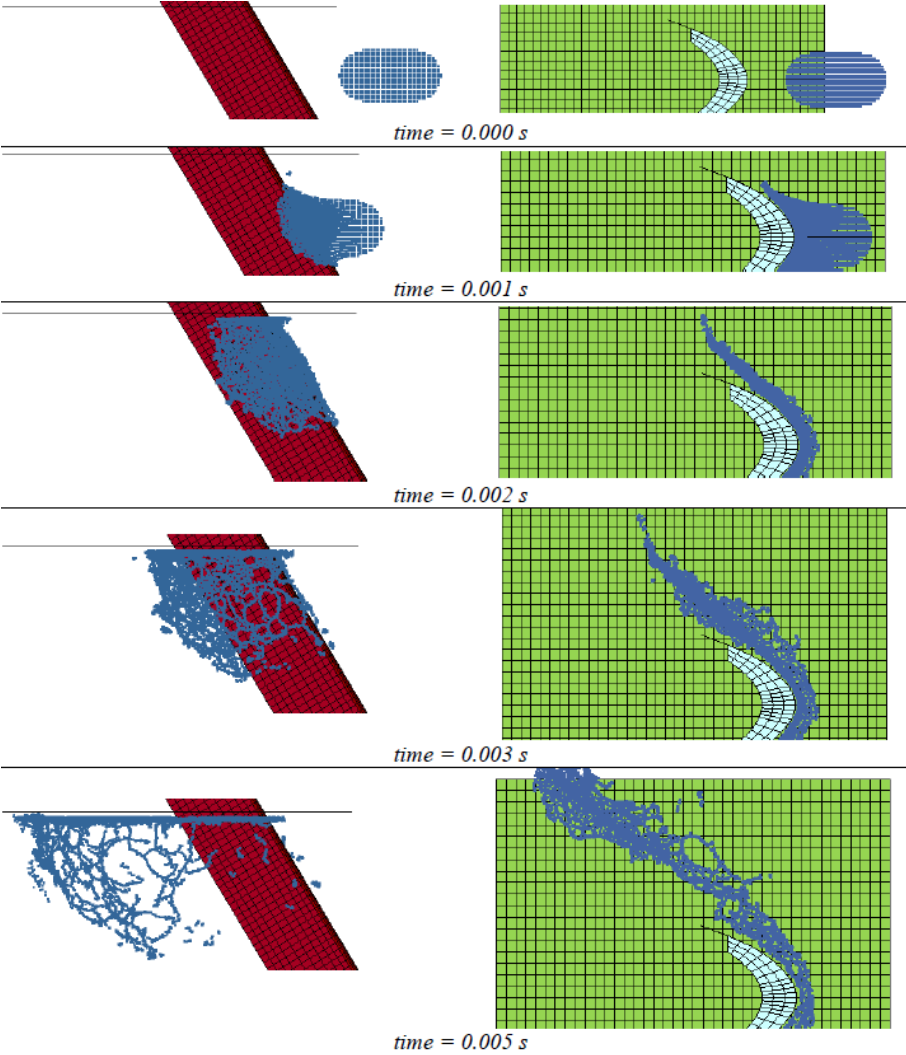
Figure 1-4 Bird Impact Analysis Results [5]

Another bird impact related study was presented by Shmotin Y., N., et al. at the 7th European Ls-Dyna Conference. This study was mainly focused on the bird impact on jet engine fan. Large dynamic deformation of the blades is caused by high speed impact of bird onto rotating fan blades. Comparison of experimental data and Ls-Dyna analysis results was performed. The paper indicated that the numerical

simulations were very important for development of engine fan design and construction [6].

Sebastian Heimbs from EADS worked on bird strike simulations on composite aircraft structures. Firstly, bird strikes on rigid plate analyses were performed to validate modeling methods. Stacked shell models, cohesive elements, preloading and soft body impactor modeling were presented in this paper. The study showed that final simulation results correlate well with the experimental test data [7].

Rotor Spinner bird strike analyses was performed by Tho, C., and Smith, M., R., from Bell Helicopter Textron Inc. Bird strike phenomenon was briefly explained and some explanatory information on the modeling approach was given in the paper. Rotor spinner bird strike analyses and experimental tests were done and comparison results were also given in this paper [8]. Moreover, bird strike simulation was done for BA609 empennage structure. Bird was modeled by using SPH solution technique. Simulation results were compared with test results and it is clearly seen that SPH formulation provided acceptable results. Comparison of the test and simulation is given in Figure 1-5 [8].
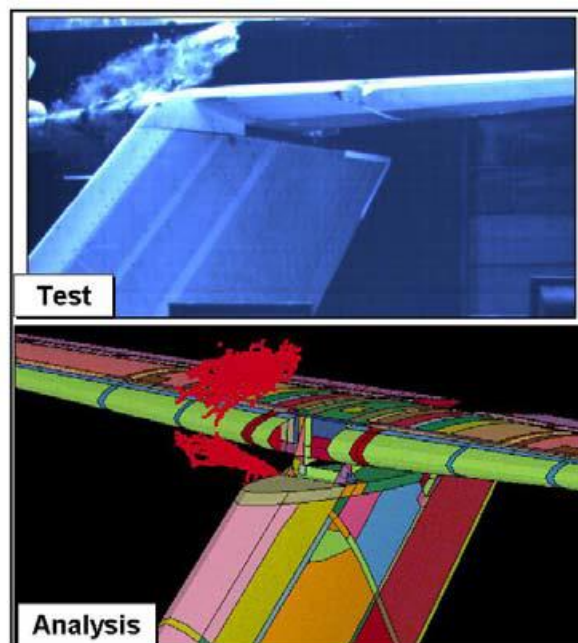
Figure 1-5 BA609 Horizontal Stabilizer Bird Strike Correlation [8]

SPH method was used to model bird strike analysis by Goyal, V., K., et al. This paper mainly focused on the SPH solution methodology to model bird strike problem. One dimensional beam centered impact problem was modeled and compared with the analytical and the numerical approach. After the validation process, bird strike problem on tapered plate was performed. They concluded that SPH approach is suitable for bird-strike events within 10% error. [9]

Soft impact damage on composite fan stage assemblies was investigated by Kim, M., et al. In their study, impact on static single blade and rotating fan assembly were simulated. ALE and SPH techniques were used to model soft impact damage. They concluded that "bird impact composite damage modeling approach developed is a critical step towards the development of an extensive methodology for evaluating the crashworthiness of future propulsion systems subject to soft impact damage." [10]

A study about bird strike simulations was conducted by Sebastian Heimbs from European Aeronautic Defense and Space [11]. This paper provides a review about applications of different soft body impactor modeling methods. Advantages and disadvantages of various solution techniques were summarized. A benchmark study was performed for each solution techniques such as Lagrangian, Eulerian, ALE and SPH. According to comparison study, Lagrangian method provided reliable results until large distortion occurred during analysis. ALE technique needed high computational time compared to SPH and questionable results due to severe deformation of the moving mesh. In Eulerian case, the numerical-experimental correlation was not satisfying, which was expressed with the highest relative error in terms of impact force. Analysis result of SPH is given in Figure 1-6. The SPH method is the recommended approach in this study, due to high stability, low cost and good correlation with experimental observations in terms of scattering particles.
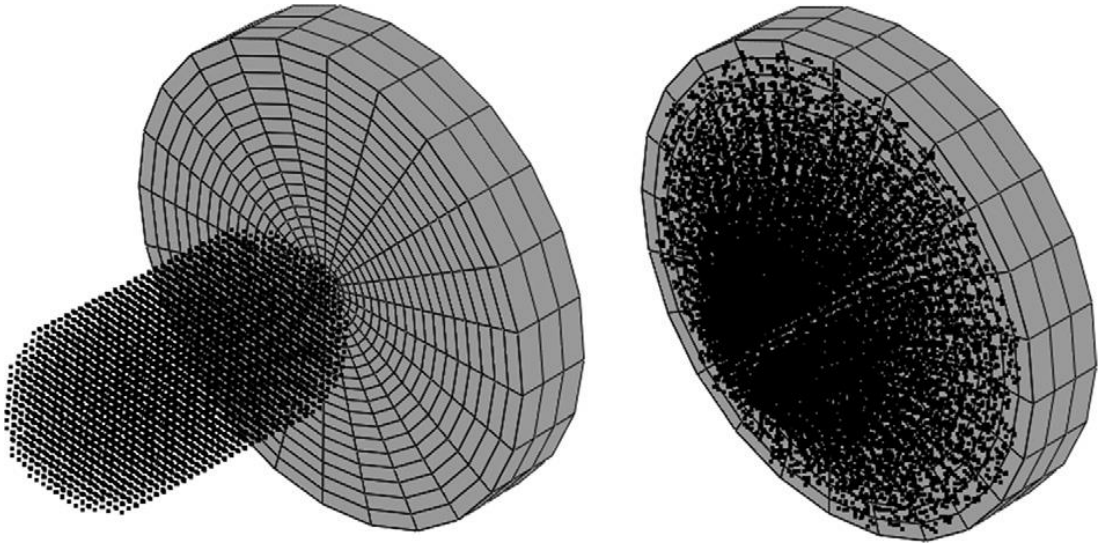
Figure 1-6 Deformation History of SPH Method [11]

Another bird strike related study was conducted by Liu., J. et al [12]. Experiments and simulations were conducted for bird impact with a flat plate at different velocities. Elastic-plastic material with a defined failure limit was offered at low impact speeds. The isotropic elastic – plastic hydrodynamic solid model was best suited for the bird strike simulation at intermediate impact velocities. Finally, the SPH method with Gruneisen EOS definition for solid element provided for the bird strike simulation at high impact speed.

Bird strike on a flat plate simulations were conducted in Hyperworks Technology Conference by Salem S. C. et al [13]. This paper discussed different solution techniques for bird modeling, Lagrangian, ALE and SPH. Based on this study, the SPH model was chosen for the prediction of bird impact effect on a typical aircraft wing leading edge. The deformation characteristic of leading edge matched with experiments. Deformation profile of test and simulation is given in Figure 1-7.
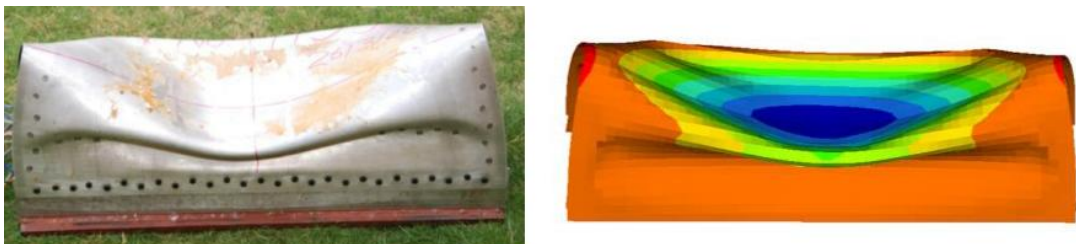
Figure 1-7 Deformation of Leading Edge for Test and Simulation [13]

Finally, experimental and simulation bird strike results for aluminum foam based sandwich panels was carried out by Hanssen A. G. et all at International Journal of Impact Engineering [14]. The bird was modeled by using ALE solution technique whereas sandwich panel was described by Lagrangian method. According to this study, the model was able to represent failure of both the aluminum cover plates as well as the aluminum foam core. Deformation results of impact simulation for aluminum foam based sandwich panel are given in Figure 1-8.
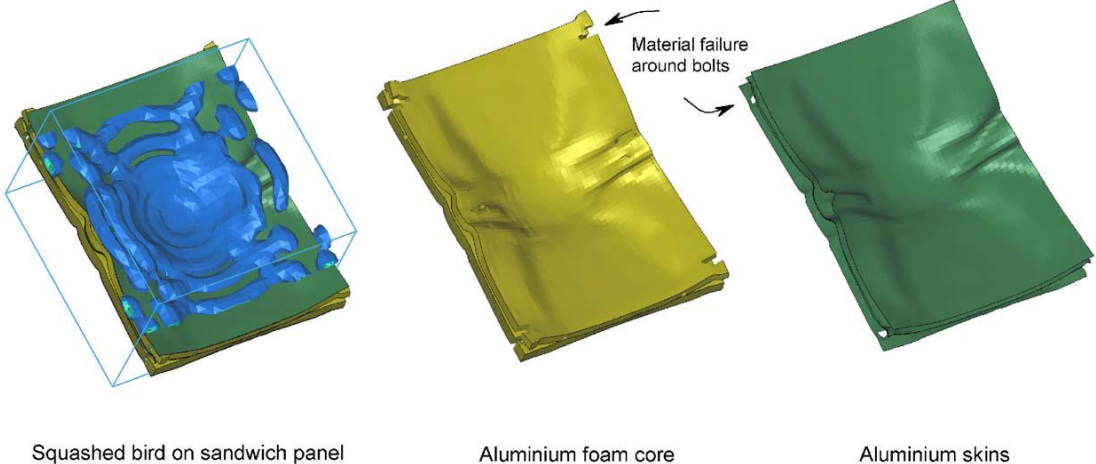
Figure 1-8 Deformation Result of Aluminum Foam Based Sandwich Panel [14]

1.2 Objective and Scope of the Thesis

The main aim of this thesis is to determine an analysis procedure for bird strike problem on wing leading edge. Explicit finite element method is used to analyze this type of short duration highly nonlinear impact problem. Firstly, bird strike analyses methodology is given in Chapter 2. The methodology simply contains problem description and standard research, determination of bird impactor modeling technique, selection of suitable material models for metallic and composite aircraft structures and finally performing bird strike analyses.

In chapter 3, technical details of explicit finite element method basically introduced. Available solution techniques such as Lagrangian, ALE (Arbitrary Lagrangian Eulerian), Eulerian and SPH (Smoothed Particle Hydrodynamics) are described briefly. Also, the theory of equation of state (EOS) is explained.

In chapter 4, benchmark study among solution techniques to select suitable bird impactor method. Cylindrical with hemi-spherical ends bird geometry is modeled by using Eulerian, ALE and SPH solution method. Bird models are impacted with 100 m/s initial velocity to rigid square plate. According to deformation history, reaction force and literature review, suitable modeling technique of soft body impactor (bird) is selected.

In chapter 5, suitable material model for metallic aircraft structure is determined by performing benchmark study. Deformation behavior, internal/external energy history results are compared to determine effectiveness of elasto-plastic and elasto-viscoplastic material models in bird impact problem. Similarly, material model for composite aircraft structure is introduced. Material parameters are explained and illustrated physical meaning of these parameters in graphically. Coupon tests are performed for plain woven carbon fiber fabric material and the test results are validated with coupon simulations.

In chapter 6, after determining suitable solution formulation for bird modeling and selection of material models, analyses of bird strike problem on wing leading edge are performed. Impact behavior of metallic and composite leading edge is investigated. Aerodynamic profile of metallic leading edge is highly distorted during impact while catastrophic failure does not happen because of ductile mechanical property of aluminum. On the other hand, catastrophic failure occurs during impact in composite leading edge case because of brittle behavior of composite material.

In Chapter 7, reinforcement study is performed against bird strike problem. One of the suitable solutions is to use honeycomb materials in impact region. Bird strike analyses are repeated for honeycomb reinforced metallic and composite leading edges to investigate effectiveness of honeycomb material in impact problem. Excellent impact resistant behavior is provided by honeycomb material. Aerodynamic profile of both metallic and composite leading edge is not distorted too much and catastrophic failure does not happen in composite leading edge. This study shows that honeycomb material can be freely used for this type of impact problem.

Finally, in chapter 8, bird impact problem solution methodology is summarized and future studies are indicated.

CHAPTER 2

BIRD STRIKE PROBLEM ANALYSIS METHODOLOGY

2.1   Simulation Steps

Analysis of the bird strike problem can be divided into four main parts. Firstly, the problem has to be described and related aviation standards have to be determined. In this content, impact location, bird shape and weight, impact speed has to be clearly assessed. Secondly, suitable solution method has to be chosen. Also, required material model for the soft impactor should be selected. Thirdly, material models have to be determined according to metallic and nonmetallic aircraft structures. Finally, the bird strike simulation is performed. In Figure 2-1, flowchart for the suggested procedure of bird strike analysis on aircraft structures is given.
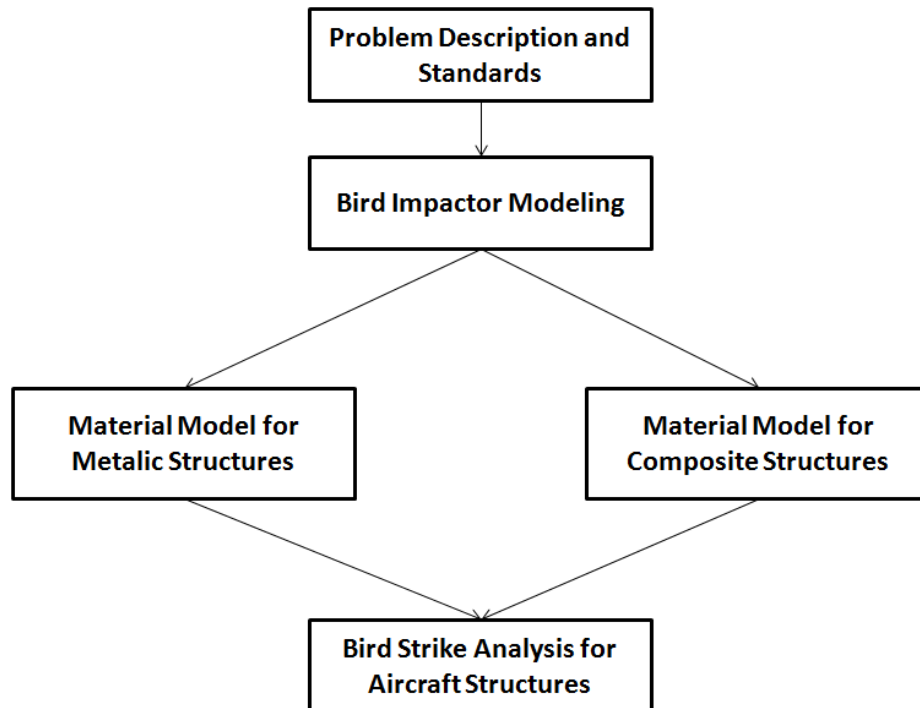
Figure 2-1 Flowchart for Suggested Procedure of Bird Strike Analysis

2.2 Problem Description and Standards

In this thesis, bird strike on wing leading edge is investigated for a general aviation aircraft. Bird impactor dimension are given in Figure 2-2 [15]. The geometry is simply described as cylinder with hemi-spherical ends.
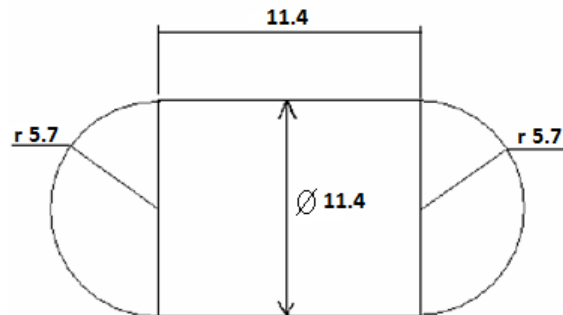
Figure 2-2 Bird Impactor Dimensions (all dimension is given by cm) [15]

Federal Aviation Administration (FAA) also states the bird strike test condition. According to FAA's Issue Paper G-1, bird strike test condition is given by the parameters in Table 2-1[16].

Table 2-1 FAA Bird Strike Test Condition [16]

Test Condition	Bird Weight	Impact Speed	14 CFR
Airplane	4.0 lb (1.8 kg)	V_C at sea level	§ 25.631
VTOL/conversion	2.2 lb (1.0 kg)	V_H at 8000 ft	§ 29.631

The bird strike he requirement is specified in § 25.631 [16] as

(a) *The aircraft must be capable of continued safe flight and landing during which likely structural damage or system failure occurs as a result of –*
   (1) *In airplane mode, impact with a 4-pound bird when the velocity of the aircraft relative to the bird along the aircraft's flight path is equal to Vc at sea level or 0.85Vc at 8,000 ft, whichever is more critical;*
   (2) *In VTOL/conversion mode, impact with a 2.2 pound bird at V_{con} or V_H (whichever is less) at altitude up to 8,000ft.*
(b) *Compliance must be shown by tests or by analysis based on tests carried out on sufficiently representative structures of similar design.*

where, V_C is cruise speed and V_H indicates the hover speed.

In this thesis, the following procedure implemented for the analysis of the bird strike problem:

I. Explicit finite element methodology is defined and solution techniques in Ls-Dyna are introduced.

II. Bird strike on a rigid plate study is performed by using different bird modeling technique to determine the suitable/accurate solution technique among ALE, Eulerian and SPH solution techniques.

III. Material model for metallic aircraft structures is determined among elasto-plastic, elasto-viscoplastic material models available in Ls-Dyna material model library. Similarly, material model in Ls-Dyna for composite aircraft structures is introduced and material parameters are determined utilizing experimental test data.

IV. Leading edge bird strike analyses are performed for both metallic and composite material aircraft structure.

V. Finally, leading edge reinforcement is used to show the effect reinforcement on the structural integrity of the leading edge of the wing

CHAPTER 3

EXPLICIT FINITE ELEMENT METHOD

In this chapter, basic theory of explicit finite element method is described. Also, available solution formulation in explicit finite element theory such as Lagrangian, Eulerian, ALE and SPH are introduced. Finally, equation of state definition which is required during bird strike modeling is briefly explained.

3.1   Explicit Finite Element Method Time Integration Theory

In the Explicit time integration method, internal and external forces are summed at each node point, and nodal acceleration is computed by dividing the force into the nodal mass. The solution is advanced by integrating this acceleration in time. The maximum time step is limited by Courant condition, producing an algorithm which typically requires many relatively inexpensive time steps.

The time integration is expressed as the integration of the equations of motion [17]:

$$ma^n + cv^n + f_{int}^n = f_{ext}^n \tag{3.1}$$

where

m	: Mass matrix
a	: Nodal Acceleration vector
c	: Damping matrix
v	: Velocity vector
F^{ext}	: Nodal external Forces
F^{int}	: Nodal internal Forces
n	: Indicates time step n

The fundamental problem is to calculate the displacement, d^{n+1}, at time t^{n+1}. The conceptual form of explicit time integration can be written as [17]:

$$d^{n+1} = f(d^n, v^n, a^n, d^{n-1}, \dots) \tag{3.2}$$

The equation shows that the solution depends on nodal displacements, velocities and accelerations at state n, quantities which are known. Therefore, the equation can be solved directly.

For the velocity calculation, central difference method can be used [17]:

$$v^{n+1/2} = \frac{d^{n+1} - d^n}{\Delta t^{n+1/2}} \tag{3.3}$$

$$d^{n+1} = v^{n+1/2} \Delta t^{n+1/2} + d^n \tag{3.4}$$

Using $\Delta t^{n+1/2} = t^{n+1} - t^n$ one gets:

$$d^{n+1} = v^{n+1/2}(t^{n+1} - t^n) + d^n \tag{3.5}$$

The velocity can be also expressed using the acceleration:

$$a^n = \frac{v^{n+1/2} - v^{n-1/2}}{t^{n+1/2} - t^{n-1/2}} \tag{3.6}$$

With $\Delta t^n = t^{n+1/2} - t^{n-1/2}$ the velocity is given by:

$$v^{n+1/2} = v^{n-1/2} + \Delta t^n a^n \tag{3.7}$$

As previously shown, the equation of motion is in the form:

$$ma^n = f_{ext}^n - f_{int}^n - cv^n \tag{3.8}$$

Therefore, the acceleration at a^{n+1} can be calculated as:

$$a^{n+1} = m^{-1}(f_{ext}^{n+1} - f_{int}^{n+1} - cv^{n+1/2}) \tag{3.9}$$

Note that the damping force is expressed at $v^{n+1/2}$.

The new velocity is found based on the old velocity and acceleration. From that, displacement can be updated. Finally with the new internal and external forces, one can calculate the new acceleration.

First, all variables initialized at t = 0. Then, velocity and displacements are updated. Computation of internal and external forces is performed. Finally, acceleration values for each nodal point are calculated.

To summarize the explicit time integration, flowchart for explicit time integration is given in Figure 3-1.
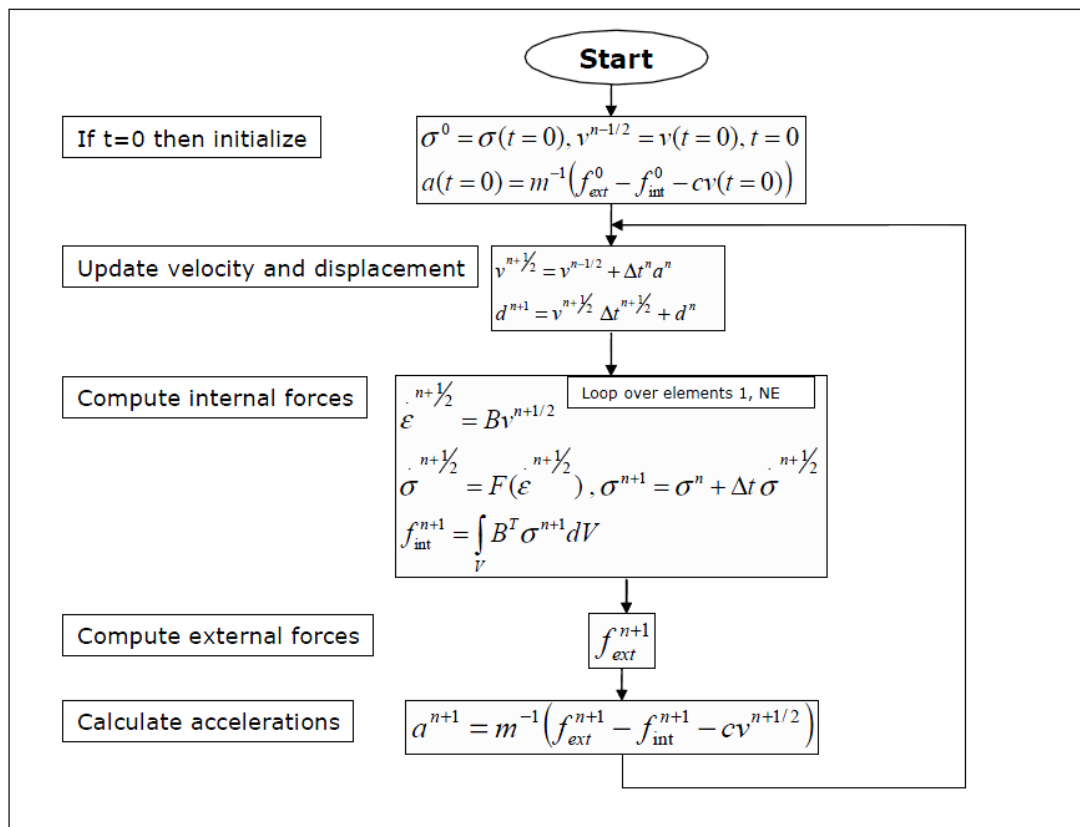
Figure 3-1 Flowchart for Ls-Dyna Explicit

To provide stability in explicit finite element method, CFL (Courant-Friedrichs-Lewy) law has to be applied. Courant-Friedrichs-Lewy law states that

$$c \leq \Delta x / \Delta t \text{ for stability} \tag{3.10}$$

Therefore, the critical time step in explicit finite element method is given by

$$\Delta t_{crit} \leq \frac{l_{min}}{c} \qquad (3.11)$$

where

l_{min} is the smallest element length

c is the speed of sound in the material
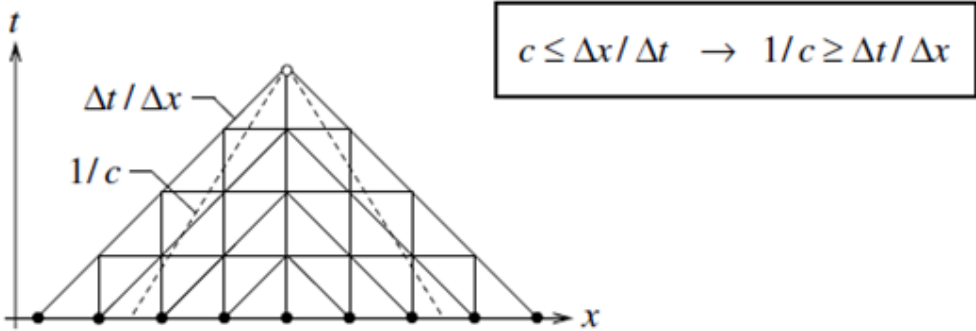
Figure 3-2 CFL Law for Stability in Explicit Finite Element Method

According to Figure 3-2, information velocity in the algorithm has to be larger than physical stress wave velocity. In other words, stress wave in the material propagates with speed of sound in the physical material while stress wave propagates with calculated critical time step in the algorithm.

3.2 Lagrange Solution Technique

In the Lagrangian solution technique, the nodes of the mesh are attached to the imaginary material "points". These nodes move and deform with the material. The Lagrange elements contain the same material throughout the calculation. In other words, mesh deforms with the material. This is shown in Figure 3-3. Generally, Lagrange solution method is not suitable for the case of extreme mesh distortion problem because of some instability problems [17].
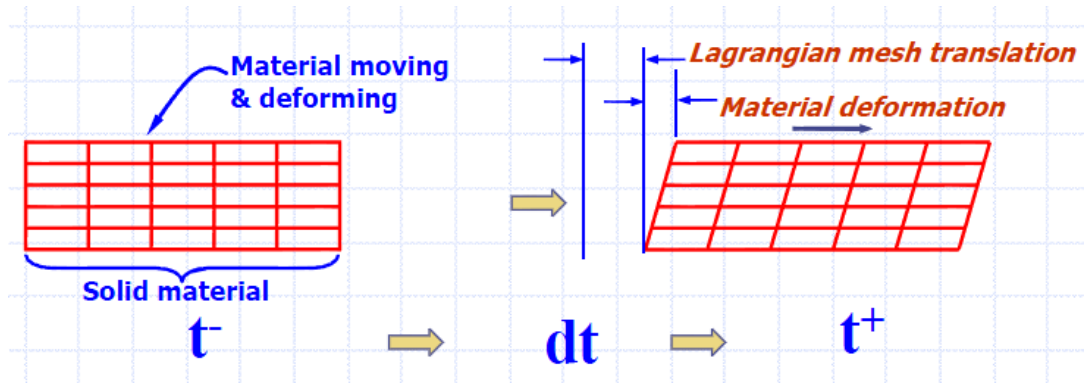
Figure 3-3 Lagrange Solution Technique

3.3 Eulerian Solution Technique

Hypothetically considering of two overlapping meshes, one is a background reference mesh which is fixed in space and the other is a virtual mesh attached to the material which "flows" through the reference mesh. This is visualized in Figure 3-4 [17].
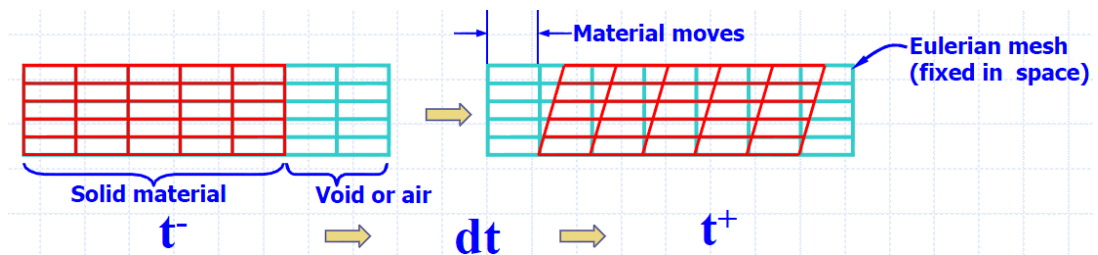
Figure 3-4 Eulerian Solution Technique

In the Eulerian solution technique, first, the material is deformed in a Lagrangian step just like the Lagrangian formulation. Then, the element state variables in the virtual "Lagrangian elements" are remapped or transported back into the fixed reference Eulerian mesh.

3.4   ALE (Arbitrary Lagrangian Eulerian) Solution Technique

Consider two overlapping meshes, one is a background mesh which can move arbitrarily in space, and the other is a virtual mesh attached to the material which "flows" through the former moving mesh. This may be visualized in two steps. First, the material is deformed in a Lagrangian step just like the Lagrangian formulation. Then, the element state variables in the virtual "Lagrange elements" are remapped or transported back into the moving (background) reference ALE mesh [17]. Illustrative description of ALE method is given in Figure 3-5.
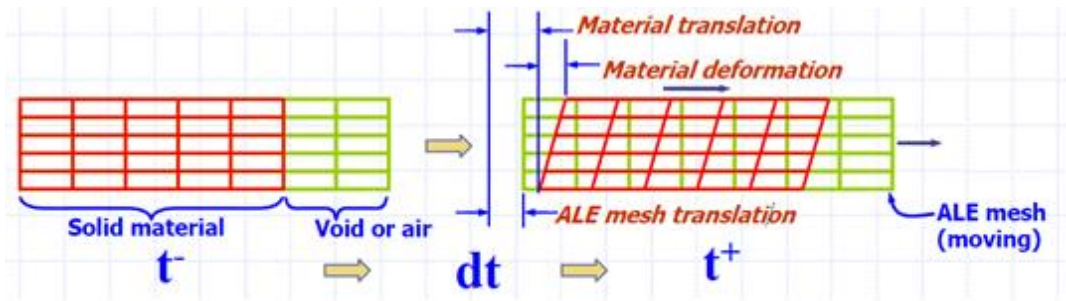
Figure 3-5 ALE Solution Technique

3.5   SPH (Smoothed Particle Hydrodynamics) Solution Technique

Smoothed Particle Hydrodynamics (SPH) is an N-body integration formulation developed by Lucy 1977 [18]. The method was developed to avoid the limitations of mesh distortion which is faced with in extreme deformation problems that one faces with in the finite element solution. Absence of grid is the main difference between the classical method and the SPH. Therefore, the particles are the computational framework on which the governing equations are resolved. The new model requires a new calculation method, which is briefly explained in the following [18]

The particle approximation of a function is:

$$\Pi^h f(x) = \int f(y) W(x - y, h) dy \qquad (3.12)$$

where W is the kernel function.

The Kernel function W is defined using the function θ by the relation:

$$W(x, h) = \frac{1}{h(x)^d} \theta(x) \tag{3.13}$$

where d is the number of space dimensions and h is the so-called smoothing length which varies in time and in space.

W(x,h) should be a centrally peaked function. The most common smoothing kernel used by the SPH community is the cubic B-spline which is defined by choosing θ as:

$$\theta(u) = C x \begin{cases} 1 - \dfrac{3}{2}u^2 + \dfrac{3}{4}u^3 & for\ |u| \leq 1 \\ \dfrac{1}{4}(2 - u)^3 & for\ 1 \leq |u| \leq 2 \\ 0 & for\ 2 < |u| \end{cases} \tag{3.14}$$

where C is a constant of normalization that depends on the number of space dimensions. SPH particle visualization and the Kernel function is given in Figure 3-6 .
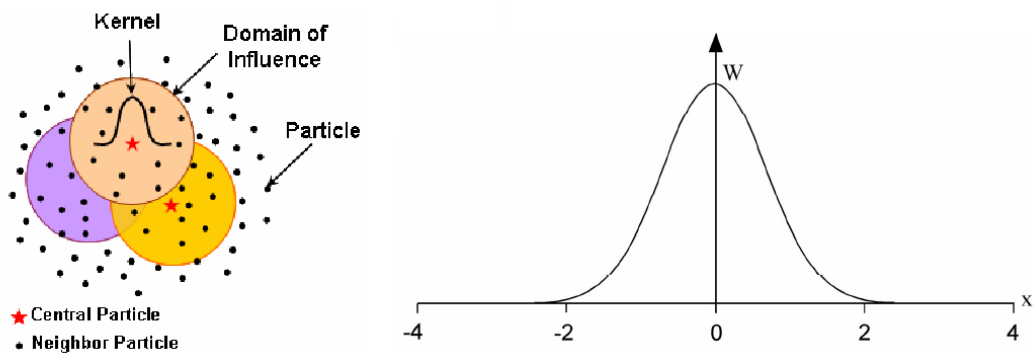
Figure 3-6 SPH Particles and the Kernel Function [8]

3.6   Definition of EOS (Equation of State)

A thermodynamic state of a homogenous material, not undergoing any chemical reaction or phase change, may be defined by two state variables. This relation is generally called an equation of state. For example, a few possible forms relating pressure to two other state variables are given in Eqn. (3.15) [17].

$$P = P(\rho, T) = P(v, e) = P(v_r, e_V) = P(\mu, e_{V0}) \tag{3.15}$$

where,

P is pressure, ρ is density, T is temperature, v is the current specific volume (per mass), e is internal energy per unit mass (also called specific internal energy), v_r is the <u>current</u> relative volume, e_V is internal energy per unit current volume, μ is volumetric parameter and finally e_{V0} is the internal energy per unit <u>reference</u> volume.

This equation form is frequently used to compute pressure. The EOS for solid phase materials is sometimes partitioned into two terms, a cold pressure and a thermal pressure [17].

$$P = P_c(\mu) + P_T(\mu, e_{V0}) \tag{3.16}$$

$P_c(\mu)$is the cold pressure hypothetically evaluated along a 0-degree-Kelvin isotherm. This is sometimes called a 0-K pressure-volume relation or cold compression curve. $P_T(\mu, e_{V0})$ is the thermal pressure component that depends on both volumetric compression and thermal state of the material.

Different forms of the EOS describe different types of material and how their volumetric compression (or expansion) behaves. The coefficients for each EOS model come from data-fitting, phenomenological descriptions, or derivations based on classical thermodynamics, etc.

Gruneisen EOS [19]:

The propagation velocity of a shock front depends on the particle velocity. This effect is taken into account by Gruneisen EOS. The Gruneisen equation of state with cubic shock velocity-particle velocity defines pressure as:

$$P = P_c(\mu) + P_T(\mu, e_{v0}) = A(\mu) + B(\mu)E \qquad (3.17)$$

Cold part is described as elastic interaction between atoms at $0°$ K isotherm

Thermal part is described as kinetic contribution due to molecular motion.

For compression ($\mu > 0$)

$$A(\mu) = \frac{\rho_0 C^2 \mu \left[1 + \left(1 - \frac{\gamma_0}{2}\right)\mu - \frac{a}{2}\mu^2\right]}{\left[1 - (S_1 - 1)\mu - S_2 \frac{\mu^2}{\mu+1} - S_3 \frac{\mu^3}{(\mu+1)^2}\right]^2} \rightarrow \text{cold part}$$

$$B(\mu) = (\gamma_0 + a\mu) \rightarrow \text{thermal part}$$

$$(3.18)$$

For tension ($\mu < 0$)

$$A(\mu) = \rho_0 C^2 \mu \rightarrow cold\ part$$
$$B(\mu) = (\gamma_0 + a\mu) \rightarrow thermal\ part$$
$$(3.19)$$

where, C is the intercept of the u_s-u_p curve; S_1, S_2 and S_3 are the unitless coefficients of the slope of the u_s-u_p curve; γ_0 is the unitless Grunisen coefficient; a is the unitless first order volume correction to γ_0 and finally $\mu = \frac{\rho}{\rho_0} - 1$

where, ρ is current density and ρ_0 is reference density

Finally, u_s-u_p curve definition is given as

$$u_s = C_0 + S_1 u_p + S_2 \left(\frac{u_p}{u_s}\right) u_p + S_3 \left(\frac{u_p}{u_s}\right)^2 u_p \qquad (3.20)$$

CHAPTER 4

BIRD IMPACTOR MODELING AND SELECTION OF THE SOLUTION TECHNIQUE

4.1   Problem Description

In Chapter 3 available solution techniques in Ls-Dyna are explained. It is known that bird (soft body impactor) behaves fluid-like manner during impact, therefore Lagrangian solution technique is not suitable to model bird impactor because heavily distorted elements during soft body impact when the Lagrangian formulation is used. This leads to instability/divergence issues in the explicit finite element solution. To model soft body impactor, Ls-Dyna provides three alternative formulations such as Eulerian, ALE and SPH. A benchmark study is performed to select the suitable/accurate formulation for modeling soft body impactor. The items listed below are followed in the benchmark study:

  I.   Bird dimension is referenced by Federal Aviation Administration (FAA) standards.

  II.   Three different models are prepared and the explicit finite element solution is performed using the Eulerian, ALE and the SPH technique.

 III.   Impact speed is taken as 100 m/s.

 IV.   Bird strikes to a square plate which is totally rigid and there is no deformation on the plate during impact.

Problem definition is schematically shown in Figure 4-1.
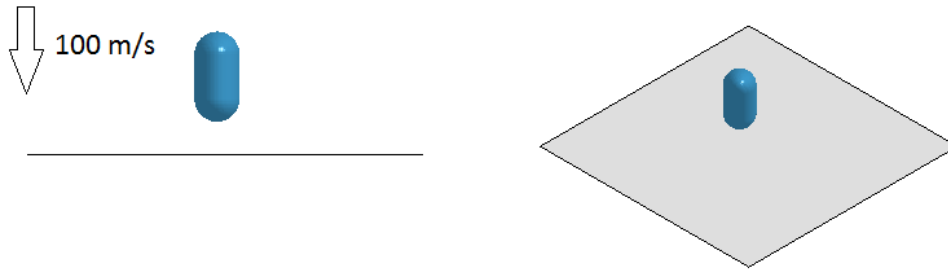
Figure 4-1 Bird Impact Benchmark Study Description

MAT_NULL is selected in Ls-Dyna material model library to model the soft body impactor which behaves fluid like manner during impact.

Material Model NULL [19]:

This material model is used for fluids such as air, water, etc. Equation of state is considered without computing deviatoric stresses. Optionally, a viscosity can be defined. Null material behaves like fluid like and has no yield strength and no shear strength. Material parameter for modeling the bird is given Table 4-1. In Ls-Dyna, this material model is referenced as MAT_009_NULL.

Table 4-1 Material Parameter for Soft Body Impactor

	ro [kg/m^3]	pc [Pa]	mu [Pa*s]
MAT_NULL	950	-1.00E-06	1.00E-03

where, ro is mass density, pc is pressure cut-off and mu is dynamic viscosity.

Gruneisen Equation of State

Bird behaves in a fluid-like manner during impact and its density is very close to the density of water. Therefore, Gruneisen equation of state parameter of water is used for the bird material. The parameters are given in Table 4-2.

Table 4-2 EOS Gruneisen Parameters for the Soft Body Impactor

EOS	C [m/s]	S1	S2	S3	GAMA0	a
GRUNEISEN	1490	1.79	0	0	1.65	0

where C is the intercept of the v_s-v_p curve; S_1, S_2 and S_3 are the unitless coefficients of the slope of the v_s-v_p curve; γ_0 is the unitless Grunisen coefficient; a is the unitless first order volume correction to γ_0 and finally $\mu = \rho/\rho_0 - 1$

Material Model VACUUM [19]:

This material model is used to model the air domain in Eulerian and ALE models. Density is the only parameter which is defined. Typically, density value is chosen close to zero. This material model is indicated as MAT_140_VACUMM in Ls-Dyna.

Illustrative picture of Eulerian, ALE and SPH formulation is given Figure 4-2. Eulerian and ALE methods require a domain which is for moving of the bird material freely without distorting the finite element mesh. This leads to a cubic domain which has bird and air material.
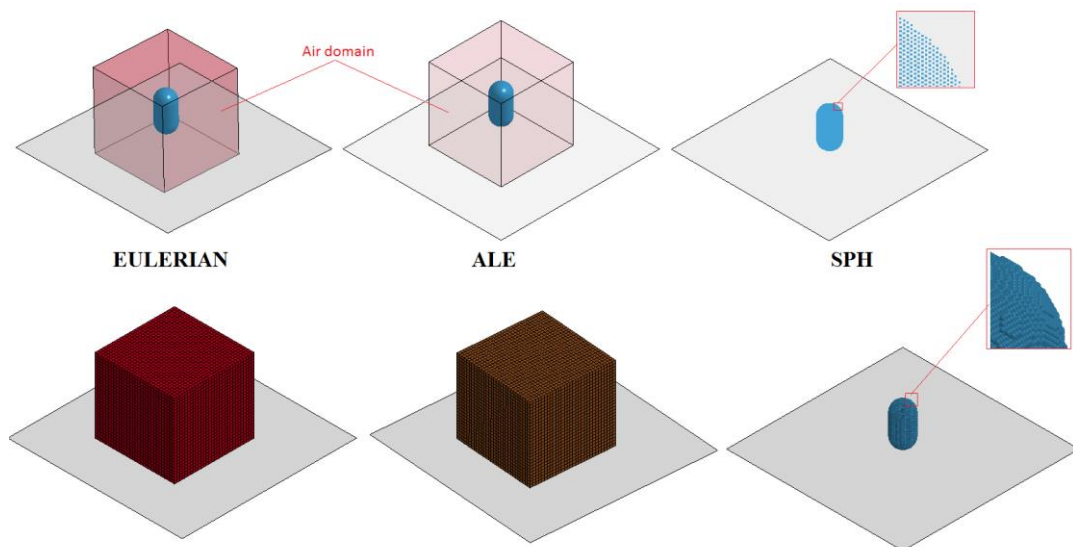
Figure 4-2 Eulerian, ALE and SPH models

Different mesh /particle density cases are modeled to investigate characteristic behavior of solution methods. Summary about the models is provided in Table 4-3.

Table 4-3 Summary of Eulerian, ALE and SPH models

Solution Method	Mesh Density	Number of Element	Element Size
EULERIAN	coarse	30423	15 mm
EULERIAN	fine	219423	7.5 mm
ALE	coarse	30423	15 mm
ALE	fine	219423	7.5 mm
Solution Method	Particle Density	Number of Particles	Particle Distance
SPH	coarse	3789	10 mm
SPH	medium	30309	5 mm
SPH	fine	209076	2 mm

Finite element model of Eulerian and ALE is given in Figure 4-3. Coarse mesh case is given in the left and fine mesh case is provided in right.
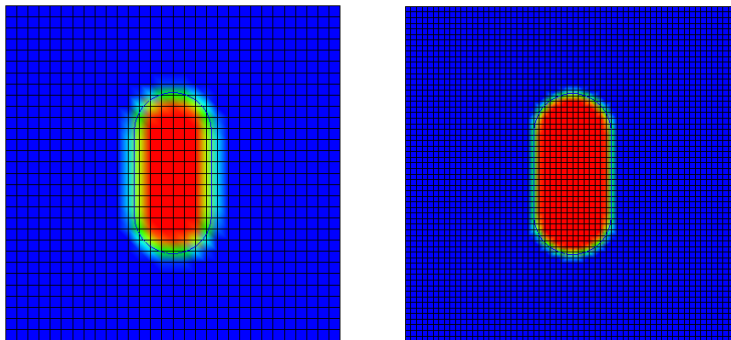
Figure 4-3 Finite Element Model of Eulerian and ALE cases (coarse mesh is left, fine mesh is right)

Illustrative picture about SPH models is given in Figure 4-4. Coarse case is given in left, medium case is in middle and fine case is given in right.
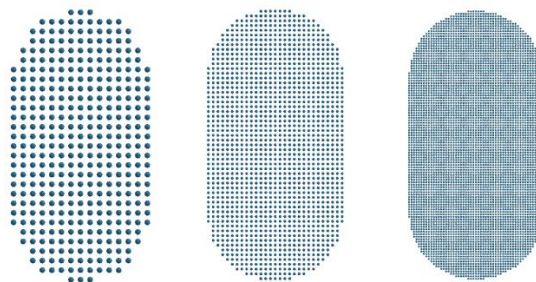
Figure 4-4 Finite Element Model of SPH cases (coarse is left, medium is middle, fine is right)

4.2 Comparison of Eulerian, ALE and SPH Solution Techniques Analysis Results

After analyzing Eulerian, ALE and SPH models, deformation results are given in Figure 4-5. It should be noted that blue region in Eulerian and ALE results represents air domain in Figure 4-5.
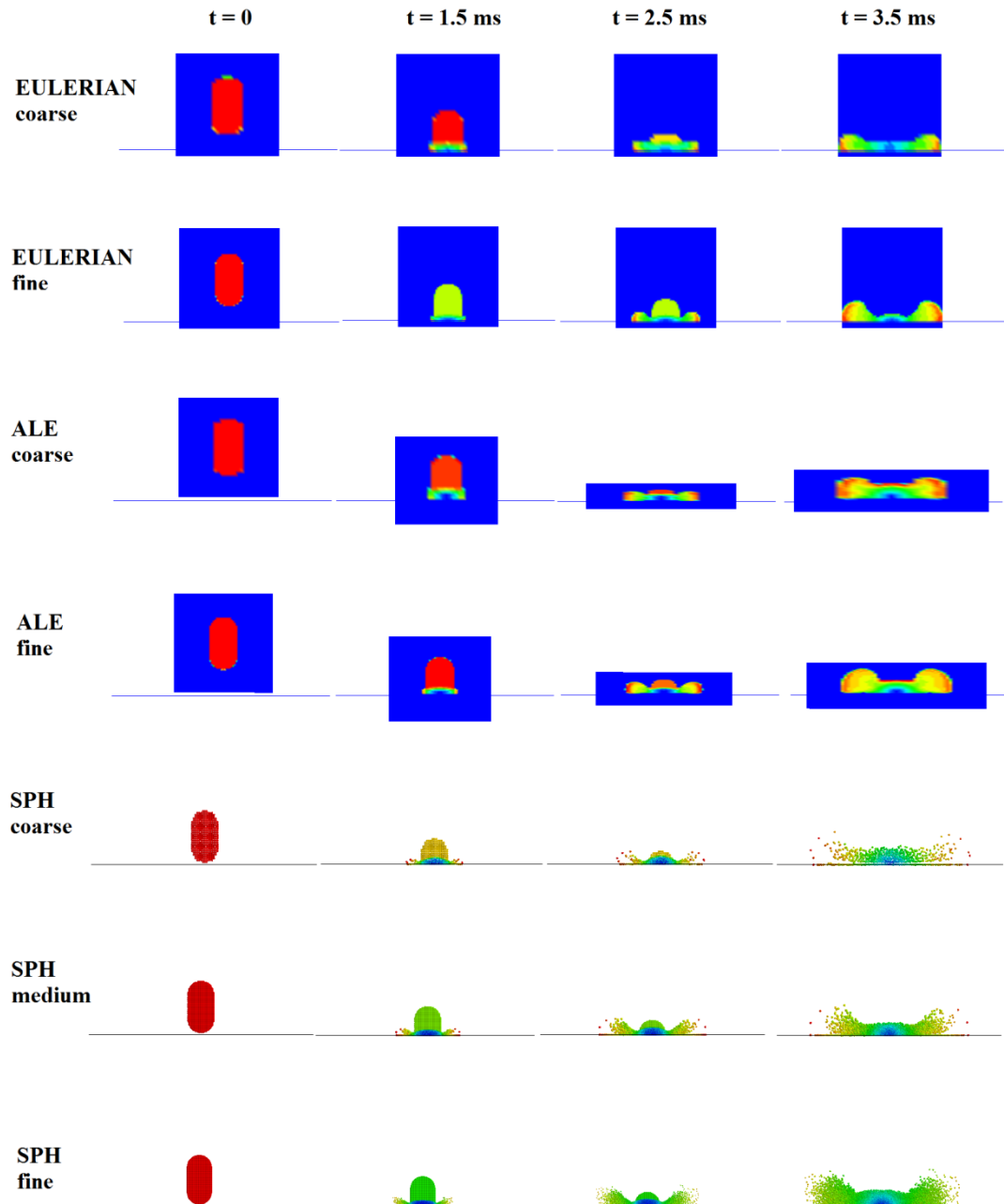
Figure 4-5 Deformation Results of Eulerian, ALE and SPH formulations (side view)

In Figure 4-5, deformation histories are given for the soft body impact to the rigid plate for the Eulerian, ALE and SPH solution techniques. In the Eulerian case, reference elements are fixed in space and bird material moves upon these elements. Similarly, in the ALE case, bird material and finite element model both move. In the SPH case, meshless SPH particles move freely during impact. From Figure 4-5, it is clear that deformation of soft body impactor is influenced from the coarse finite element domain in the Eulerian and the ALE solution techniques. It is also noted that Eulerian and ALE formulations provide closer deformation history when fine element size is used. However, deformation history of the Eulerian and ALE solution is still influenced from the finite element domain. Figure 4-6 shows the top view of the deformation results obtained by the Eulerian, ALE and SPH solution techniques.

TOP VIEW

| EULERIAN coarse | ALE coarse | SPH coarse |

| EULERIAN fine | ALE fine | SPH fine |
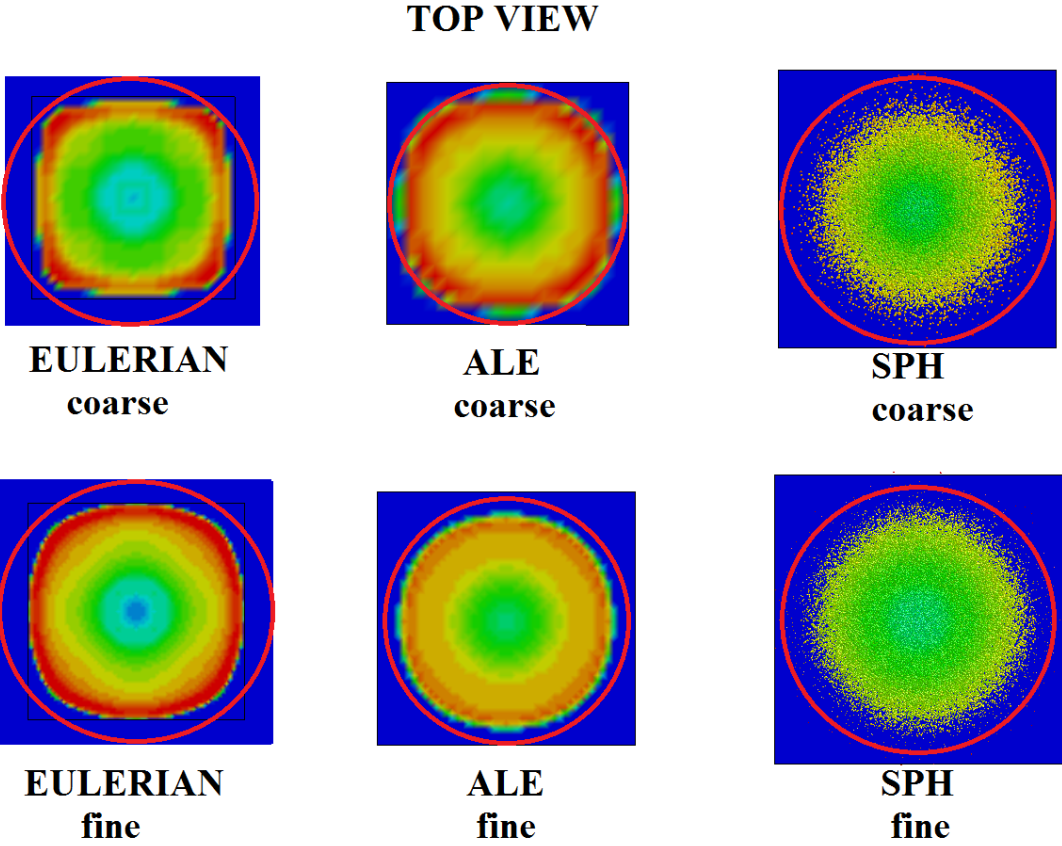
Figure 4-6 Deformation Results of Eulerian, ALE and SPH formulations (top view)

In Figure 4-5 and Figure 4-6, by just comparing the deformation histories, it is seen that SPH method gives more accurate results than the Eulerian and the ALE formulation Eulerian and ALE models behave in a mesh dependent manner. Eulerian

and ALE models provide closer deformation history when finer element size is used. On the other hand, finer mesh size in Eulerian and ALE models yields much higher computational time than SPH models. Solution time summary is provided in Table 4-4 (for Intel® Core™ i7-3630QM 2.40 GHz CPU)

Table 4-4 Summary of Solution Time

Solution Method	Mesh Density	CPU	Solution Time (sec)
EULERIAN	coarse	4	50
EULERIAN	fine	4	497
ALE	coarse	4	51
ALE	fine	4	658
SPH	coarse	4	3
SPH	medium	4	7
SPH	fine	4	113

In Table 4-4, it is clearly seen that Eulerian and ALE models need higher computational time than SPH models.

SPH solution behaves almost in a mesh independent manner. Also, computational time is much lower than Eulerian and ALE models. It is emphasized that mesh independency and low computational time are very useful properties to analyze the bird impact problem.

In the literature, similar soft body impact analyses and tests are performed by Lavoie et al. [5]. In Figure 4-7, test and SPH analysis results obtained by Lavoie et al. are compared with each other. From Figure 4-7, it is seen that SPH solution of the bird impact gives very close deformation histories as the test.
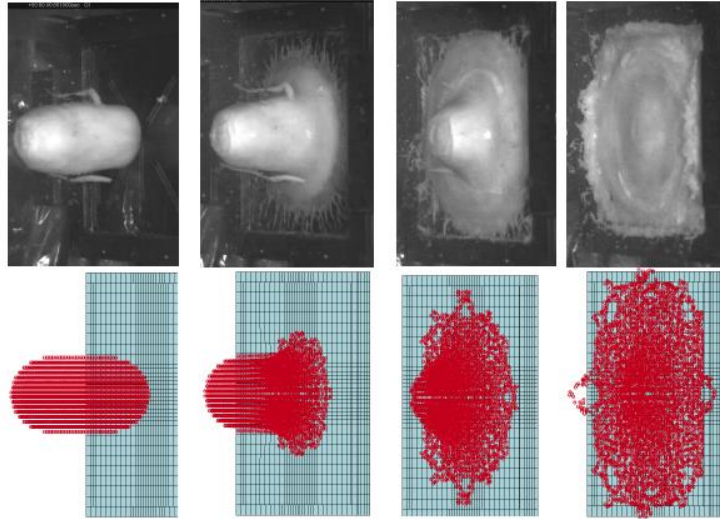
Figure 4-7 Bird Strike Test (top pictures) and Analysis (bottom pictures) Results [5]

Secondly, another study about SPH method was conducted by Goyal, V., K., et al [9]. This paper mainly focused on the SPH solution methodology to model bird strike problem. They concluded that SPH approach is suitable for bird-strike events [9].

In addition to comparing the deformation profiles of Eulerian, ALE and SPH solution of the bird impact problem, investigation of normalized pressure is also helpful in selecting the suitable solution formulation for modeling of the soft body impactor. To calculate normalized pressure, the following relation is used. The main aim of using of normalized pressure is to obtain comparable results from analyses.

$$P_N = \frac{F/A}{P_S} \tag{4.1}$$

$$P_S = \frac{1}{2}\rho v_0^2 \tag{4.2}$$

where,

P_N : Normalized Pressure

F : Impact force (N)

A : Area of the impact region (m^2)

P_S : Stagnation pressure (N/m^2)

ρ : Density (kg/m^3)

v_0 : Impact velocity (m/s^2)

In Figure 4-8, normalized pressure history is given for Eulerian coarse and fine cases. Deformation history is also provided for coarse and fine mesh cases. It is clear that Eulerian solution method is influenced by mesh density. Effect of mesh density is also seen in normalized pressure results. Fine mesh density yields higher normalized pressure in Eulerian models.
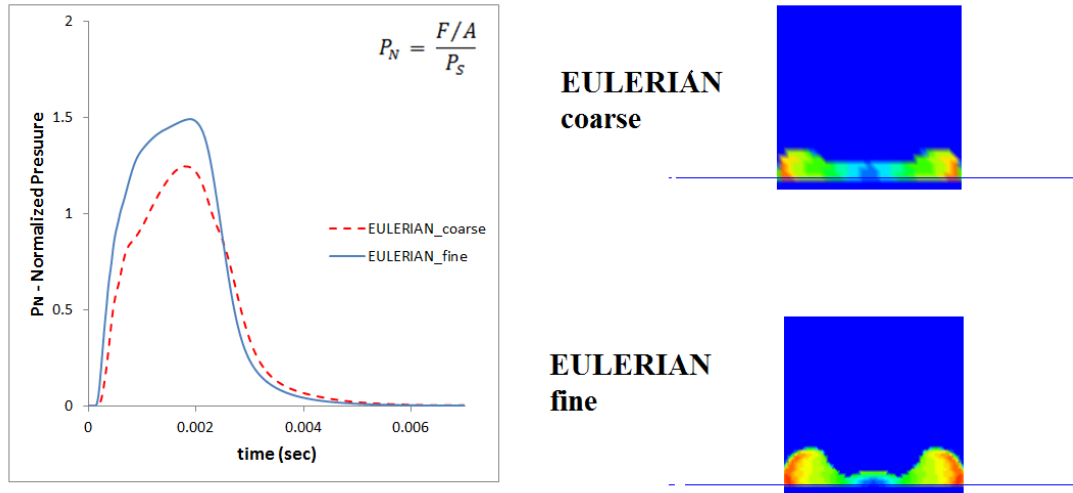
Figure 4-8 Comparison of Normalized Pressure for Eulerian Coarse and Fine Mesh Size

In Figure 4-9, normalized pressure history is provided with deformation plots. Similar to Eulerian case, mesh dependent manner is seen in deformation plots. Peak value of normalized pressure is almost same for both coarse and fine mesh cases although deformation history is influenced from mesh density.
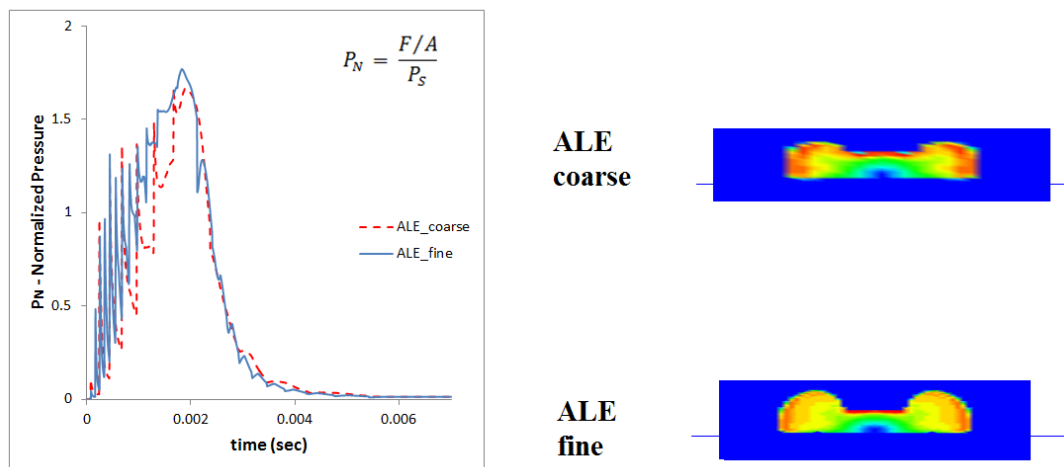
Figure 4-9 Comparison of Normalized Pressure for ALE Coarse and Fine Mesh Size

In Figure 4-10, normalized pressure history is given. Also, deformation plots of SPH models are provided. Normalized pressure distributions are quite similar for coarse, medium and fine particle cases. In addition, deformation profile almost behaves mesh independent manner.
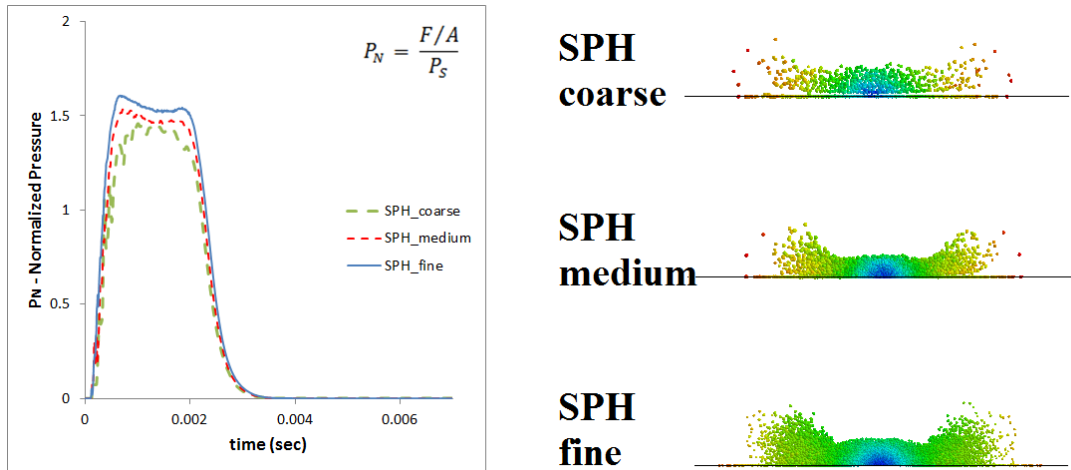
Figure 4-10 Comparion of Normalized Pressure for SPH Coarse, Medium and Fine Particle Distance

In summary:

- Deformation profile of SPH method is closer to the experimental findings in the literature. In addition SPH behaves in a mesh independent manner.
- Experimental test data from study of Lavoie et. al. [5] shows that deformation profile obtained by the SPH method is very close to test data.
- Eulerian and ALE models need higher computational time than SPH models.
- Normalized pressure results of SPH models are very close to each other.

Therefore, SPH method can be used to model soft body impactor in bird strike analyses according to mesh independency, low computational time requirement and literature review.

CHAPTER 5

MATERIAL MODELS FOR THE WING LEADING EDGE

5.1 Material Model for the Metallic Wing Leading Edge

Aluminum alloys are often used in the wing leading edge. Empirical and semi empirical advanced material models can be used to model metallic materials in impact analyses. In Ls-Dyna, there are some advanced material models which are;

> - Steinberg   : Elasto-viscoplastic material model
> - Johnson Cook   : Elasto-viscoplastic material model
> - MTS   : Elasto-viscoplastic material model
> - Piecewise Linear Plasticity   : Elasto-plastic material model

In this chapter, to select suitable material models, a benchmark study is performed. In this respect, Johnson Cook (denoted as JC) and Piecewise Linear Plasticity (denoted as PLP) material models are compared. Main reason of the comparison is to investigate the behavior of elasto-viscoplastic and elasto-plastic constitutive models in the bird strike analysis.

The benchmark study is defined as:

- Bird dimension and impact velocity is taken from FAA standards. Soft body impact is provided on 0.5m x 0.5m flexible square plate which is given in Figure 5-1
- Plate thickness is 1.2 mm
- Plate is fixed at four free edges.
- Plate material is AL 2024 T3 aluminum alloy.
- Soft body impactor (bird) is modeled by using SPH formulation.

Figure 5-1 shows the finite element model prepared in Ls-Dyna.
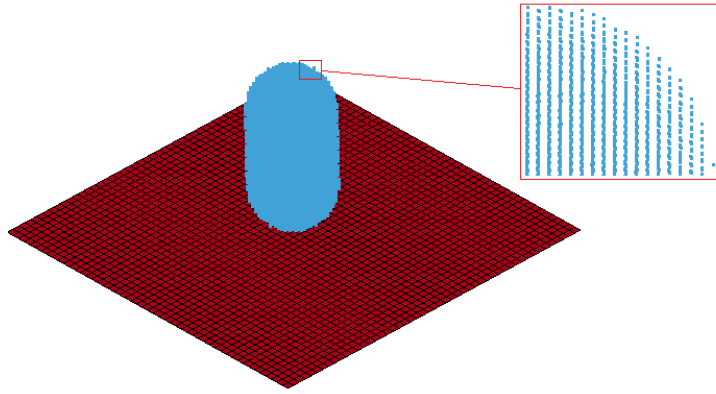
Figure 5-1 0.5m x 0.5 m Plate and Bird Model

Johnson Cook Material Model [19]:

Johson Cook material model can be used to model the high rate deformation of many materials including metals. Metal forming, ballistic penetration of metallic materials and impact problems may be defined as main applications area of the JC material model. This material model is referenced as MAT_015_Johnson_Cook in Ls-Dyna.

In JC material model flow stress expressed as:

$$\sigma_y = \left(A + B\bar{\varepsilon}^{p^n} \right)(1 + C \ln\dot{\varepsilon}^*)(1 - T^{*m}) \tag{5.1}$$

where

  σ : Equivalent stress

  A : Initial yield stress

  B : Hardening modulus

  n : Work hardening exponent

  C : Strain rate dependency

  m : Thermal softening coefficient

  ε : Equivalent strain

  $\dot{\varepsilon}$: Plastic strain rate

  $\dot{\varepsilon}_0$: Reference strain rate

$$\bar{\varepsilon}^p = \text{effective plastic strain} \tag{5.2}$$

$$\dot{\varepsilon}^* = \frac{\dot{\bar{\varepsilon}}^p}{\dot{\varepsilon}_0} \text{ effective plastic strain rate for } \dot{\varepsilon}_0 = 1 \ s^{-1}$$

$$T^* = \frac{T - T_{room}}{T_{melt} - T_{room}}$$

where,

T : Temperature

T_{room} : Room temperature

T_{melt} : Melting temperature

Failure strain is given by:

$$\varepsilon^f = [D_1 + D_2 exp D_3 \sigma^*][1 + D_4 ln\varepsilon^*][1 + D_5 T^*] \qquad (5.3)$$

where D_i ,i=1,..,5 are input constants and σ^* is the ratio of pressure divided by effective stress defined as: $\sigma^* = \frac{P}{\sigma_{eff}}$

Parameters of JC material model and EOS Gruneisen are given for AL 2024 T3 in Table 5-1.

Table 5-1 Parameters of JC Material Model and EOS Gruneisen for AL 2024 T3 [20]

	Material Model	density (kg/m3)	Specific heat (J/kg K)	Melting temp. (K)	A	B	n	C	m
AL 2024T3	Johnson Cook	2770	875	775	265	426	0.34	0.015	1
					D1	D2	D3	D4	D5
					0.13	0.13	-1.5	0.011	0
	EOS	C [m/s]	S1	S2	S3	γ0	a		
	Gruneisen	4551	1.338	0	0	2	0.48		

Piecewise Linear Plasticity Material Model [19] :

Radial return plasticity is main method for the plasticity treatment in this model. Deviatoric stresses are calculated that satisfy the yield function. In Ls-Dyna, this material model is referenced as MAT_024_Piecewise_Linear_Plasticity.

Yield function is defined as:

$$\phi = \frac{1}{2} S_{ij} S_{ij} - \frac{\sigma_y^2}{3} \leq 0 \qquad (5.4)$$

where

$$\sigma_y = \beta \left[\sigma_0 + f_h \left(\varepsilon_{eff}^p \right) \right] \qquad (5.5)$$

where $f_h \left(\varepsilon_{eff}^p \right)$ is defined as hardening function which can be specified in tabular form. Otherwise, linear hardening is given as

$$f_h \left(\varepsilon_{eff}^p \right) = E_p \left(\varepsilon_{eff}^p \right) \qquad (5.6)$$

E_p is defined as plastic hardening modulus.

$$E_p = \frac{E_t \, E}{E - E_t} \qquad (5.7)$$

where E_t is tangent modulus and E is elastic modulus.

Cowper-Symond strain rate model is included to the model to provide strain rate effect which is defined as [19]:

$$\beta = 1 + \left(\frac{\dot{\varepsilon}}{C} \right)^{1/p} \qquad (5.8)$$

Parameters for PLP material model for AL 2024 T3 are given in Table 5-2.

Table 5-2 Parameters of PLP Material model for AL 2024 T3 [4]

	ro [kg/m3]	E [Pa]	pr	sigy [Pa]	etan [Pa]	fail	C	p
piecewise linear plasticity	2770	7.30E+10	0.33	2.80E+08	2.09E+09	0.11	6500	5

where, ro is density, E is elastic moduli, pr is poisson's ratio, sigy is yield stress, etan is tangent moduli, fail is failure strain and finally C and p is Cowper-Symond strain rate parameters.

After performing impact analysis by the two different material models, deformation histories given in Figure 5.2 are obtained.
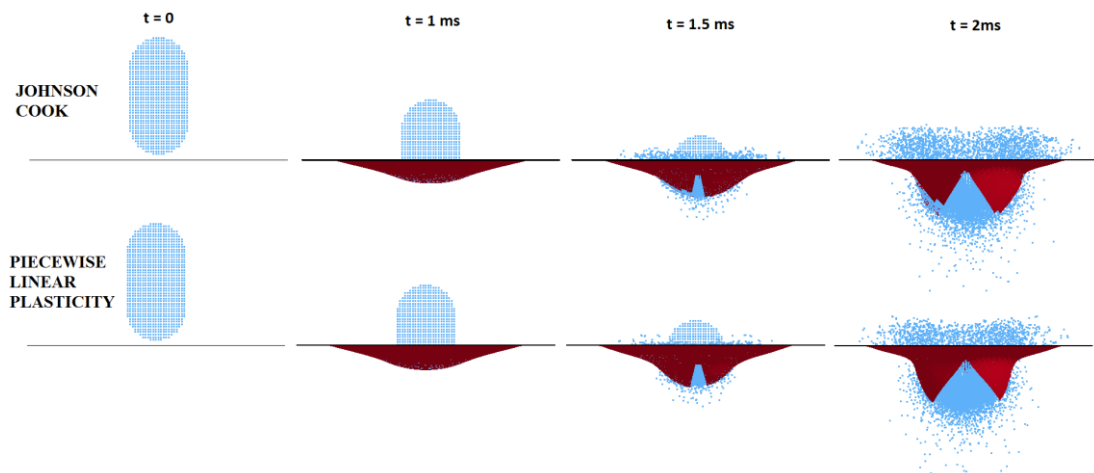
Figure 5-2 Bird Strike Deformation Histories

In Figure 5-2, it is clear that both material models show similar failure behavior for metallic material for this type of problem. At 1 ms, flexible metallic plates deforms similarly for the JC and the PLP material models. At 1.5 ms, failure occurs in the flexible metallic plate. Finally, at 2.5 ms, flexible plates are totally tear out and both material models exhibit almost same behavior during the tear out process. Deformation values of metallic plates are given in Figure 5-3.
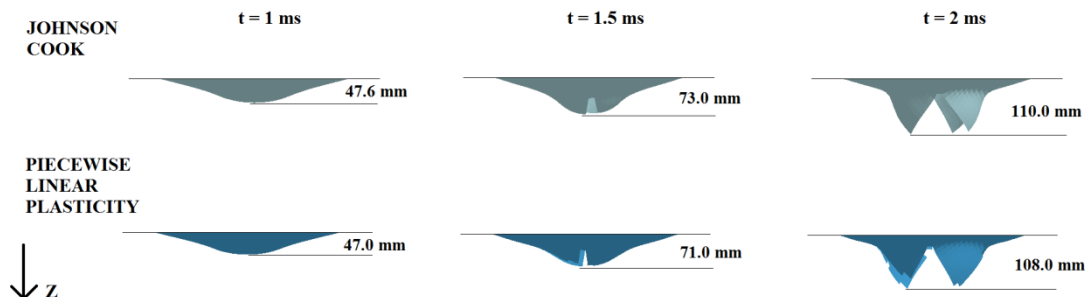
Figure 5-3 Deformation Results of JC and PLP models

Deformation values are tabulated in Table 5-3. It is clear that deformation values are quite similar for JC and PLP material models.

Table 5-3 Summary of Deformation Values

		1 ms	1.5 ms	2 ms
Johnson Cook	deformation [mm]	47.6	73.0	110.0
Piecewise Linear Plasticity		47.0	71.0	108.0

Kinetic and internal energy results of both models are compared in Figure 5-4. PLP denotes piecewise linear plasticity material model and JC denotes Johnson Cook material model.
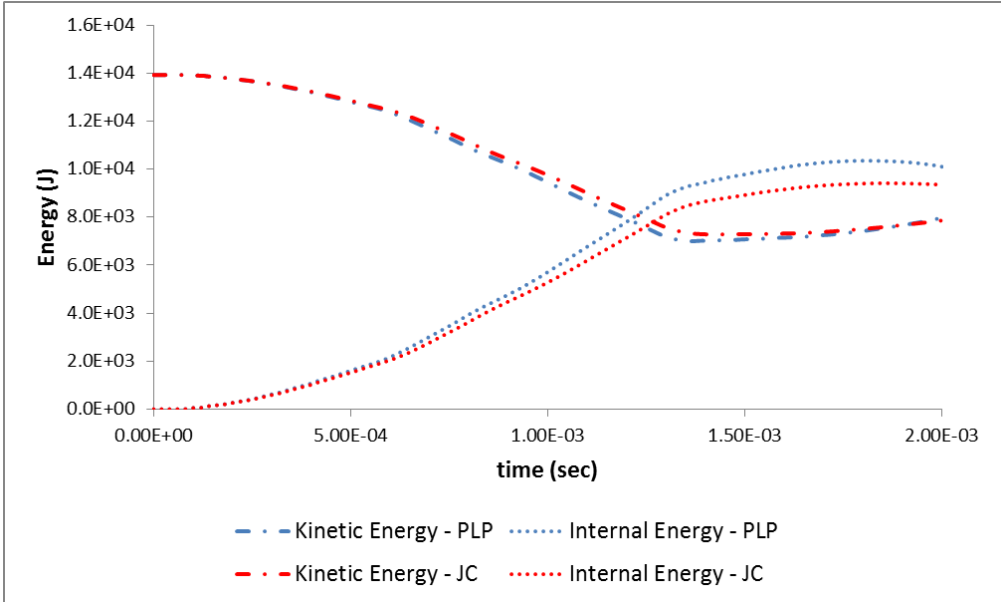
Figure 5-4 Energy vs. Time Graph for the JC and the PLP Models

In Figure 5-4, internal and kinetic energy results for JC and PLP material models also show similar behavior. This means that the flexible metallic plate absorbs almost the same amount of energy during the impact.

Impact force results of both models are also compared in Figure 5-5.
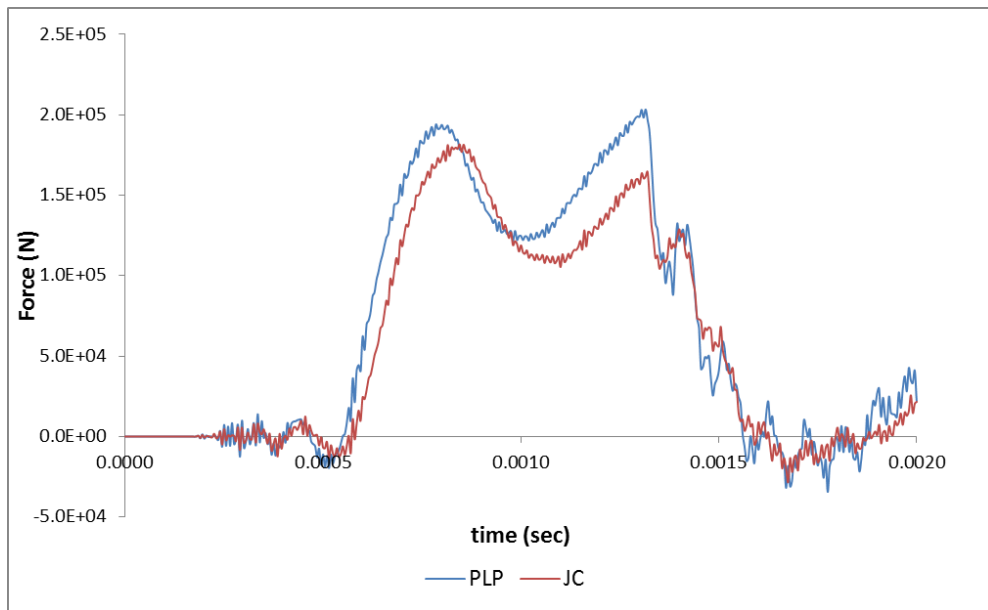
Figure 5-5 Impact Force vs. Time Graph for the JC and the PLP Models

In Figure 5-5, impact force results seem very similar although PLP model behaves more oscillatory than the JC model.

In summary:

- Failure profile of the metallic plate is very similar for both JC and PLP material models.
- Internal and kinetic energy results are calculated to be very close for both JC and PLP models.
- Finally, force history during impact is also very close for both material models.

Therefore, it can be said that JC and PLP material models can be used in this type of problems. In the literature, there are studies in which metallic structures are modeled with the Johnson Cook material model in the bird strike problem [2]. Also, Rueda, et al. from EADS [21] also used Johnson Cook material model for modeling of metallic parts in the bird strike analysis. In the light of comparison study of the JC and PLP material models and the available information in the literature, Johnson Cook material model is selected to model the metallic aircraft structure for the bird strike analysis.

5.2 Material Model for Composite Structures

In aerospace industry, usage of composite materials is continuously increasing due to lightweight requirements. A lot of research is being focused on modeling of composite materials. Ls-Dyna has a few composite material models which are listed below.

- ➢ Orthotropic Elastic
- ➢ Composite Damage
- ➢ Laminated Composite Fabric
- ➢ Shell Composite Failure Shell Model
- ➢ Rate Sensitive Composite Fabric
- ➢ Composite MSC

…

In this thesis, woven fabric composite material is modeled because there are available static and dynamic coupon test results for a specific woven fabric. For woven fabric materials, Ls-Dyna material model library provides suitable material model which is Laminated Composite Fabric. Therefore, to model woven fabric material, Laminated Composite Fabric material model is used.

Laminated Composite Fabric Material Model [19]:

Depending on the type of failure surface, this model can be used to model composite materials with unidirectional layers, complete laminates and woven fabrics. In this model, Continuum Damage Mechanics is used for the failure. This material model is referenced as MAT_058_Laminated_Composite_Fabric in Ls-Dyna. The stress limits are factors used to limit the stress in the softening part to a given value:

$$\sigma_{min} = SLIMxx \, . \, strength \tag{5.7}$$

where, SLIMxx is stress reduction factor after threshold stress exceeded and strength is defined as tension/compression/shear strength values.

Thus, damage value is slightly modified such that elastoplastic like behavior is achieved with the threshold stress. For failure surface type FS=-1, it is assumed that the damage evolution is independent of any of the other stresses. Coupling can be present only via the elastic material parameters.

Required parameters for the Laminated Composite Fabric are given in Table 5-4 [19].

Table 5-4 Parameter Definition of the Laminated Composite Fabric Material Model

Parameter	Description
RO	Density
EA	Ea young's modulus-longitudinal direction
EB	Eb young's modulus-tranverse direction
PRBA	Poisson's ratio
TAU1	Stress and strain limits of the first slightly nonlinear part of the shear stress vs. strain curve
GAMMA1	
GAB	Shear modulus AB
GBC	Shear modulus BC
GCA	Shear modulus CA
SLIMT1	
SLIMC1	Reduction factor in warp and weft direction stress values after threshold stress exceed.
SLIMT2	
SLIMC2	
SLIMS	
AOPT	Material axes option
TSIZE	Time step for automatic element deletion
ERODS	Maximum effective strain for element layer failure
FS	Failure surface type
E11C	Strain in longitudinal compressive strength, a-axis
E22C	Strain in transverse compressive strength, b-axis.
GMS	Engineering shear strain at the shear strength, ab plane.
LCXC	Load curve ID defining longitudinal compressive strength XC vs. strain rate
LCXT	Load curve ID defining longitudinal tensile strength XC vs. strain rate
LCYC	Load curve ID defining tranverse compressive strength XC vs. strain rate
LCYT	Load curve ID defining tranverse tensile strength XC vs. strain rate
LCSC	Load curve ID defining shear strength XC vs. strain rate

To understand the physical meanings of these material parameters, generic stress-strain curves have to be investigated. Firstly, proper coupons have to be prepared to obtain longitudinal and transverse mechanical properties of the composite material. Schematic view of test coupons is given in Figure 5-6.
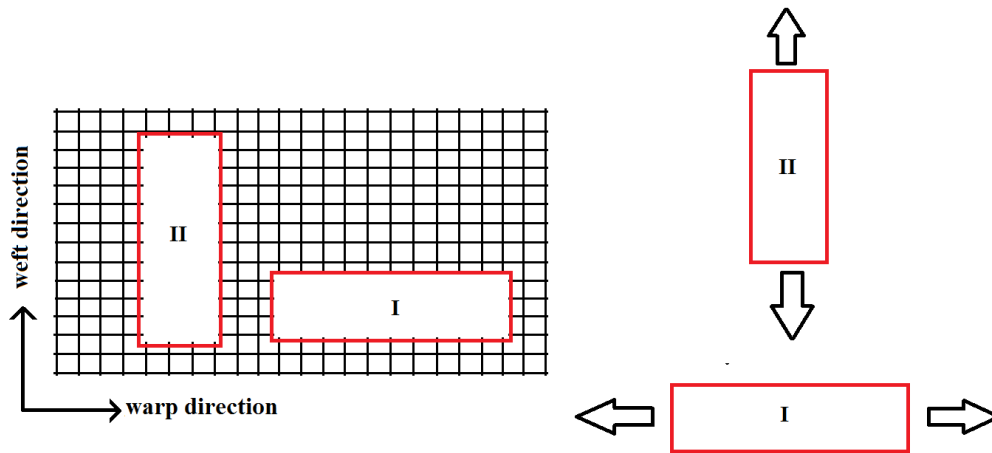
Figure 5-6 Schematic View of Test Coupons

In Figure 5-6, coupon directions are given for longitudinal and transverse cases. Tension/compression coupon tests of case (I) simply gives elastic moduli, failure stress and failure strain in the longitudinal direction. Similarly, tension/compression coupon tests of case (II) gives elastic moduli, failure stress and failure strains in the transverse direction.

Stress strain curves for tension and compression test are given Figure 5-7. Composites are quite brittle materials and that causes almost linear behavior in the longitudinal and in the transverse direction. Because, carbon fibers are dominant in the longitudinal and in the transverse directions for woven fabrics and nonlinear behavior of the resin cannot be measured in fiber directions. After performing coupon tests, elastic moduli values EA and EB are obtained. Also, failure strains, E11C, E11T, E22C and E22T, are measured. Failure stresses such as XC, XT, YC and YT are also obtained from the tests. Finally, strain rate dependent strength graphs such as LCXC, LCXT, LCYC, LCYT and LCS can be obtained by performing coupon tests at different strain rates. For each strain rate value, strength values are measured and they can then be tabulated as an input to the material model.
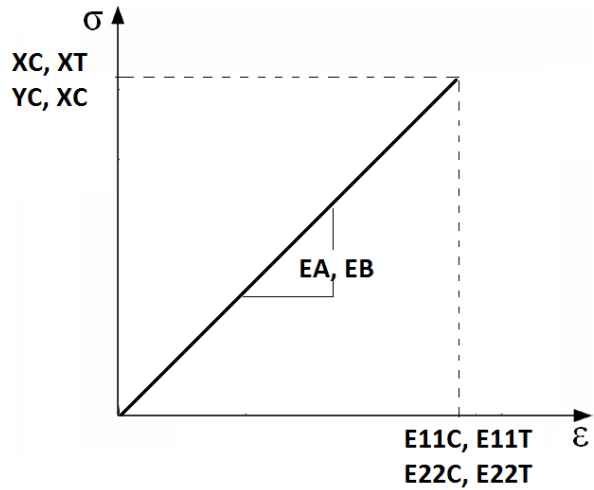
Figure 5-7 Generic Stress-Strain Curves for Tension and Compression Tests

In the longitudinal and in the transverse directions, a linear behavior is observed for a typical woven fabric composite material due to dominant mechanical properties of fibers. However, in shear tests, not only fibers but also the resin material affects the behavior of woven fabrics. Non-linear property of the resin material can be clearly seen in shear tests. Shear modulus; GA, failure strain; GMS and failure stress; SC can be measured from shear tests. Also, nonlinear material parameters TAU1 and GAMMA1 are also obtained from shear tests. Generic stress strain curve for shear tests is given in Figure 5-8. In other words, TAU1 and GAMMA1 parameters are directly obtained from V-notch shear tests while these parameters affect nonlinear behavior of the fabric in shear and off-axis tests. Nonlinearity of off-axis tests are also related to TAU1 and GAMMA1 parameters.
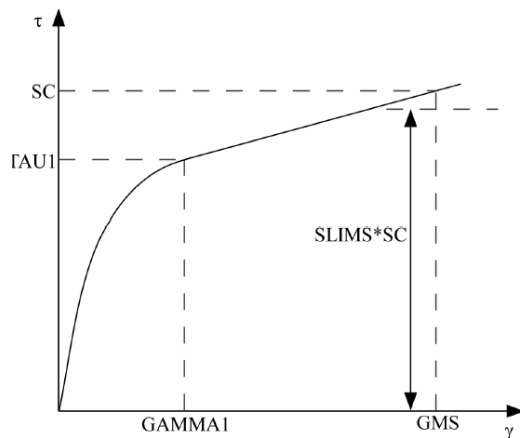
Figure 5-8 Generic Stress-Strain Curves for Shear Tests

There are 3 types of failure surfaces to model composite materials for the laminated composite fabric material model. These failure surfaces are defined in Figure 5-9. In the current study, "Faceted Failure Surface (FS = -1)" option is used for modeling the failure behavior. This option is selected because it includes shear failure control. However, this option provides uncoupled failure behavior.

	unidirectional layers FS=0.0	complete laminates and woven fabrics FS=1.0	FS=-1.0	
tensile fibre mode	$\left(\dfrac{\sigma_{11}}{X_T}\right)^2 = 1$	$\left(\dfrac{\sigma_{11}}{X_T}\right)^2 + \left(\dfrac{\sigma_{12}}{S_C}\right)^2 = 1$	$\left(\dfrac{\sigma_{11}}{X_T}\right)^2 = 1$	$(\sigma_{11} > 0)$
compressive fibre mode	$\left(\dfrac{\sigma_{11}}{X_C}\right)^2 = 1$	$\left(\dfrac{\sigma_{11}}{X_C}\right)^2 + \left(\dfrac{\sigma_{12}}{S_C}\right)^2 = 1$	$\left(\dfrac{\sigma_{11}}{X_C}\right)^2 = 1$	$(\sigma_{11} < 0)$
tensile matrix mode	$\left(\dfrac{\sigma_{22}}{Y_T}\right)^2 + \left(\dfrac{\sigma_{12}}{S_C}\right)^2 = 1$	$\left(\dfrac{\sigma_{22}}{Y_T}\right)^2 + \left(\dfrac{\sigma_{12}}{S_C}\right)^2 = 1$	$\left(\dfrac{\sigma_{22}}{Y_T}\right)^2 = 1$	$(\sigma_{22} > 0)$
compressive matrix mode	$\left(\dfrac{\sigma_{22}}{Y_C}\right)^2 + \left(\dfrac{\sigma_{12}}{S_C}\right)^2 = 1$	$\left(\dfrac{\sigma_{22}}{Y_C}\right)^2 + \left(\dfrac{\sigma_{12}}{S_C}\right)^2 = 1$	$\left(\dfrac{\sigma_{22}}{Y_C}\right)^2 = 1$	$(\sigma_{22} < 0)$
		shear:	$\left(\dfrac{\sigma_{12}}{S_C}\right)^2 = 1$	

Figure 5-9 Types of Failure Surface for the Material Model

Schematic view of these failure surfaces are given in Figure 5-10. "Faceted failure surface" option behaves less conservative than multisurface failure (FS = 0) and smooth failure (FS = 1) cases due to uncoupled manner of faceted failure. However, shear criterion is available in faceted surface case and this is the reason of selecting of faceted failure option.
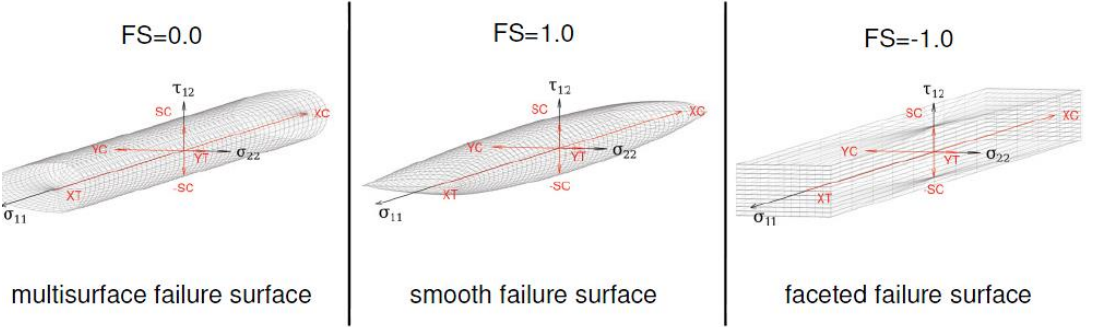
Figure 5-10 Schematic View of Failure Surfaces in the Material Model

Continuum Damage Mechanics theory of laminated composite fabric material model is described in the following.

Effective stresses are given by:

$$\begin{bmatrix} \widehat{\sigma_{11}} \\ \widehat{\sigma_{22}} \\ \widehat{\sigma_{12}} \end{bmatrix} = \begin{bmatrix} 1/(1-w_{11}) & 0 & 0 \\ 0 & 1/(1-w_{22}) & 0 \\ 0 & 0 & 1/(1-w_{12}) \end{bmatrix} \tag{5.8}$$

where w_{ij} : Damage Parameter

Constitutive relation is defined by:

$$\hat{\sigma} = C(w_{ij})\varepsilon$$

$$C(w_{ij}) = \begin{bmatrix} (1-w_{11})E_{11} & (1-w_{11})(1-w_{22})v_{21}E_{22} & 0 \\ (1-w_{11})(1-w_{22})v_{12}E_{11} & (1-w_{22})E_{22} & 0 \\ 0 & 0 & D(1-w_{12})G_{12} \end{bmatrix} \tag{5.9}$$

$$\text{with} : D = 1 - (1-w_{11})(1-w_{22})v_{12}v_{21} > 0$$

Exponential evolution of damage parameters is described by:

$$w_{11} = \begin{cases} w_{11C} \ if \ \sigma_{11} < 0 \\ w_{11T} \ if \sigma_{11} > 0 \end{cases} ; \quad w_{22} = \begin{cases} w_{22C} \ if \ \sigma_{22} < 0 \\ w_{22T} \ if \sigma_{22} > 0 \end{cases}$$

$$w_{11C,T} = 1 - exp\left[-\frac{1}{m_{11C,T}e}\left(\frac{E_{11}\varepsilon_{11}}{X_{C,T}}\right)^{m_{11C,T}}\right]$$

$$w_{22C,T} = 1 - exp\left[-\frac{1}{m_{22C,T}e}\left(\frac{E_{22}\varepsilon_{22}}{Y_{C,T}}\right)^{m_{22C,T}}\right] \tag{5.10}$$

$$w_{12} = 1 - exp\left[-\frac{1}{m_{12S}e}\left(\frac{E_{12}\varepsilon_{12}}{S_C}\right)^{m_{12S}}\right]$$

where;

$$m_{11C,T} = \frac{1}{\ln(\varepsilon_{11C,T}\frac{E_{11}}{X_{C,T}})} ; m_{22C,T} = \frac{1}{\ln(\varepsilon_{22C,T}\frac{E_{22}}{Y_{C,T}})} ; m_{12S} = \frac{1}{\ln(\varepsilon_{12S}\frac{G_{12}}{S_C})} \tag{5.11}$$

$\varepsilon_{11C,T}$: comp./ten. Long. Strain at max strength

$\varepsilon_{22C,T}$: comp./ten. Transv. Strain at max strength

ε_{12S} : Shear strain at max. strength

Range of damage parameters:

$w_{ij} \in [0,1]$ with

$$\begin{cases} w_{ij} = 0 \text{ elastic} \\ w_{ij} = 1 \text{ fully damage} \end{cases}$$

5.2.1 Carbon Prepreg Material Characterization

To create a material model which is prepared according to laminated composite fabric material parameter, coupon tension/compression/shear tests have to be done. In this content, material characterization tests are performed for Hexcel Carbon Prepreg composite material. In the current study, experimental test data are provided by Aselsan Inc.

In total, 96 quasi-static and dynamic coupon tests are done and all data is conducted by Aselsan Inc. The summary of these tests is given in Table 5-5. Dimension and stacking sequence of coupons are given in Appendix A. In addition, instructive information about universal testing machine used in the test is given in Appendix B.

Table 5-5 Carbon Prepreg Material Characterization Tests Summary

Test Type	Standard	Instrument	Replicate	Test Direction	Strain rate (1/s)
Tension	ASTM D3039	*	7	warp	0.003
Tension	ASTM D3039	**	7	warp	5
Tension	ASTM D3039	**	7	warp	50
Tension	ASTM D3039	*	7	weft	0.003
Tension	ASTM D3039	**	7	weft	5
Tension	ASTM D3039	**	7	weft	50
Tension	ASTM D3039	*	7	45^0	0.003
Tension	ASTM D3039	**	7	45^0	5
Tension	ASTM D3039	**	7	45^0	50
Compression	ASTM D6484	*	3	warp	0.003
Compression	ASTM D695	*	7	warp	0.003
Compression	ASTM D6484	*	3	weft	0.003
Compression	ASTM D695	*	7	weft	0.003
Compression	ASTM D6484	*	3	45^0	0.003
Compression	ASTM D695	*	7	45^0	0.003
Shear	ASTM D5379	**	3	-	-

  * Instron 5582 eletromechanical UTM ** Instron 8872 Servohydrolic UTM

where:

ASTM D3039: Standard test method for determining of tensile properties of Polymer matrix composite materials.

ASTM 6484: Standard test method for open-hole compressive strength of polymer matrix composite laminates.

ASTM D 695: Standard test method for compressive properties of rigid plastics.

ASTM D5379: Standard test method for determining of shear properties of composite materials by V-notched beam method.

Pictures of the tension/compression/shear test coupons are given in Figure 5-11 and Figure 5-12.
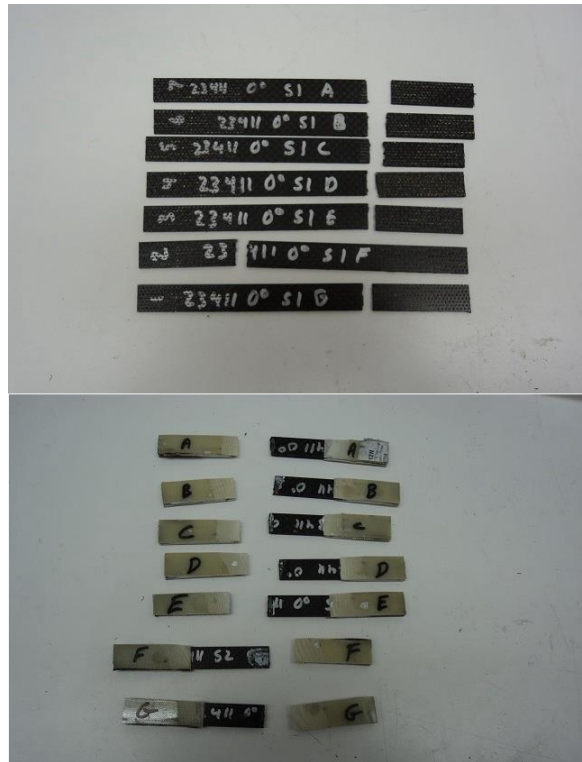

Figure 5-11 Pictures of tension/compression test coupon (courtesy of Aselsan Inc.)
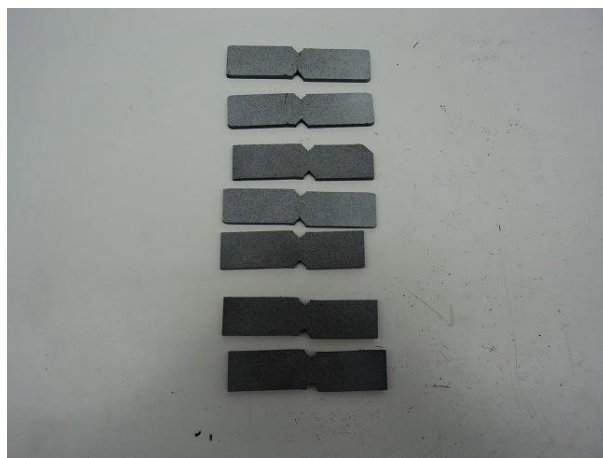
Figure 5-12 Picture of shear test coupon (courtesy of Aselsan Inc.)

After performing tension/compression/shear coupon tests, the following observations are made:

- Differences between moduli and strengths are less than 5 % for warp and weft orientations. This is typical characteristic of woven fabric material. The test results seem correct for warp and weft directions.
- Failure mode of the coupon is almost straight in the warp and weft tension tests and failure occurred near the grips of the test machine.
- In shear tests, the strain is measured using Digital Image Correlation (DIC) system to obtain accurate data. The failure on the shear specimens does not happen brutally and disrupt the specimen completely.

Some of best representative tests results are selected among the 96 tension/compression/shear tests are given in Figure 5-13 - Figure 5-15.
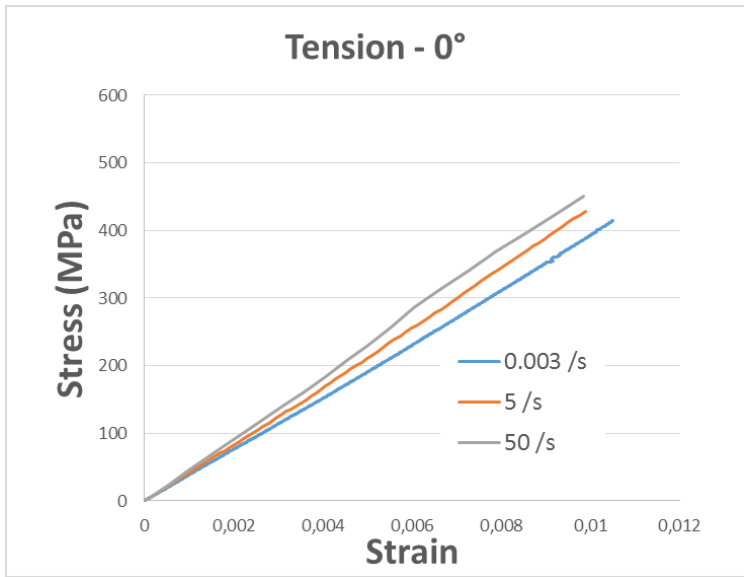
Figure 5-13 Best Representative Tension Test Results in the warp direction

In Figure 5-13, tension tests results at warp direction are given for different strain rates 0.003 /s, 5/s and 50/s. Change in elastic moduli is negligible while strength values are seen to increase with increasing strain rate. From Figure 5-13, it is clear that almost linear behavior is obtained in tension tests because carbon fibers are aligned at warp direction and this leads to almost linear behavior. In other words,

nonlinear behavior which is dominated by the resin material could not be seen in tension/compression tests at warp and weft direction.

Resin material plays an important role for viscoelastic behavior at high strain rates. Strength and elastic moduli values of resin material are rate sensitive because of viscoelastic behavior of the resin material.

Tension tests for warp and weft directions do not provide any information about nonlinear property of composite material due to dominant behavior of fibers in these directions. Therefore, off-axis tests have to be performed to see the nonlinearity in the material response. The results of off-axis tests do not give a direct parameter for laminated composite fabric material model. On the other hand, results of off-axis test are related to the nonlinear material parameters; TAU1 and GAMMA1 which are obtained from shear test results. Off-axis tension test results are given in Figure 5-14.
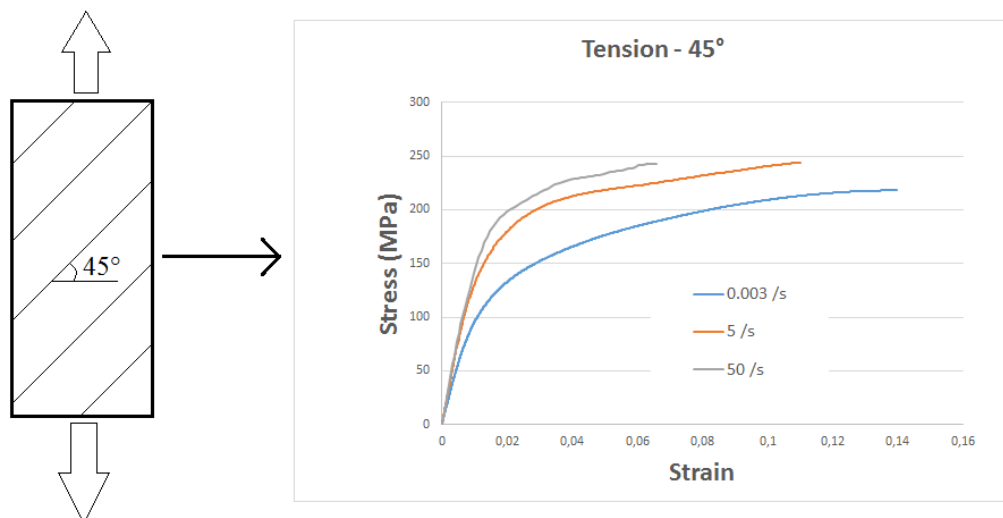
Figure 5-14 Best Representative Tension Test Results at 45° direction

In Figure 5-14, rate sensitive property of composite material is clearly seen. Elastic moduli values slightly increase with increasing strain rate values. Also, strength and failure strain values are influenced with the strain rates. The nonlinear property which is strain rate sensitive can be obtained by performing this type of off -axis tests.

Finally, in-plane shear test result (with V-notch specimen) is provided in Figure 5-15. Similarly, effect of nonlinear, rate sensitive resin property is investigated in shear test. Also, digital image correlation system is used to measure accurate strain values from shear tests. Usage of the digital image correlation system in shear test is illustrated in Figure 5-16
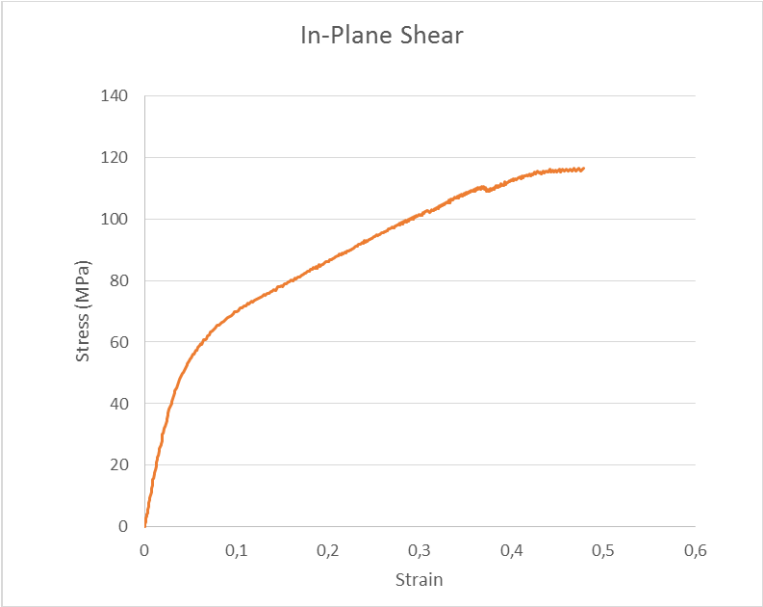
Figure 5-15 Best Representative V-Notch Shear Tests
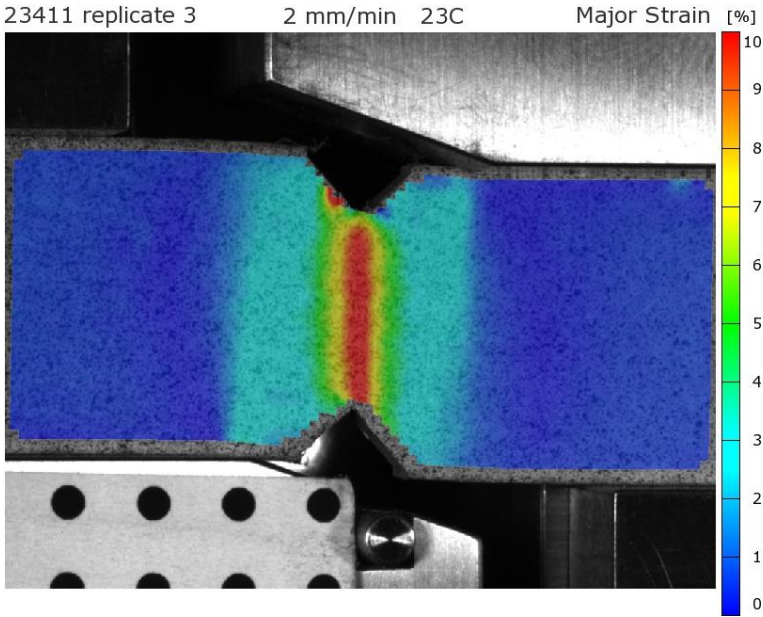
Figure 5-16 Usage of DIC for in-plane Shear Test (courtesy of Aselsan Inc.)

5.2.2 Preparation and Validation of the Material Model

After performing material characterization tests, material parameters are obtained from test data for the laminated composite fabric material model and given in Table 5-6. Some of these parameters do not depend on coupon test results. For example, failure surface selection is completely dependent on the user and in this study faceted failure surface is selected because shear failure criteria is available in faceted failure surface option. Similarly, SLIMxx parameters are often taken as 7.5% which is suggested in the Ls-Dyna theory manual.

Table 5-6 Material Parameters for theMaterial Model

Parameter	Unit	Value	Obtained From
ro	ton/mm3	1.40E-09	--
EA	MPa	37800	Tension test
EB	MPa	39600	Tension test
prba	unitless	0.05	Tension test
tau1	MPa	110	Shear test
gamma1	mm/mm	0.35	Shear test
gab	MPa		Shear test
gbc	MPa	3280	Shear test
gca	MPa		Shear test
slimt1	%		--
slimc1	%		--
slimt2	%	7.50E-02	--
slimc2	%		--
slims	%		--
aopt	unitless	-1	--
tsize	second	2.50E-08	--
erods	mm/mm	0.4	--
fs	unitless	-1	--
e11c	MPa	8.94E-03	Compression test
e22c	MPa	1.03E-02	Compression test
gms	MPa	0.48	Shear test
lcxc	curve ID	201	Compression test
lcxt	curve ID	202	Tension test
lcyc	curve ID	203	Compression test
lcyt	curve ID	204	Tension test
lcsc	curve ID	205	Shear test

Laminated Composite fabric material model also allows strain rate dependent strength values as input. This is very effective to include strain rate effect on the strength values of composite material for the impact problem. In Table 5-7, strain rate vs. strength graphs are given. It should be noted that dynamic coupon tests are performed for only tension with strain rate up to 50 /s. This is the limitation of dynamic test machine. However, during soft body impact analysis, strain rate may be above 50/s. To overcome this issue, available strength values are scaled and predict strength values at higher strain rates.

Table 5-7 Strain Rate vs. Strength Tables for Material Model

LCXC (Curve ID = 201)		LCXT (Curve ID = 202)	
Strain Rate (1/s)	Strength (MPa)	Strain Rate (1/s)	Strength (MPa)
3.00E-03	320	3.00E-03	390
5	335	5	410
50	360	50	425
500	380	500	435

LCYC (Curve ID = 203)		LCYT (Curve ID = 204)	
Strain Rate (1/s)	Strength (MPa)	Strain Rate (1/s)	Strength (MPa)
3.00E-03	360	3.00E-03	395
5	385	5	420
50	410	50	435
500	430	500	450

LCSC (Curve ID = 205)	
Strain Rate (1/s)	Strength (MPa)
3.00E-03	120
5	135
50	150
500	165

Coupon Simulation in Ls-Dyna:

To validate the material model, dynamic coupon tests are simulated in Ls-Dyna. Validation process covers comparison of the failure region and force-deflection curve. Finite element model of the test coupon is given in Figure 5-17. Comparison study is performed for dynamic coupon tension tests such at 5 s^{-1} (75 mm/s → crosshead speed) and at 50s^{-1} (750 mm/s → crosshead speed). Because, simulating the quasi-static coupon tests is very inefficient and impractical by using explicit

finite element method. Explicit finite element method solvers are commonly used for instant, highly nonlinear problems. Dimension and stacking sequence of the coupon are taken same as the real test coupons which are given in Appendix A.
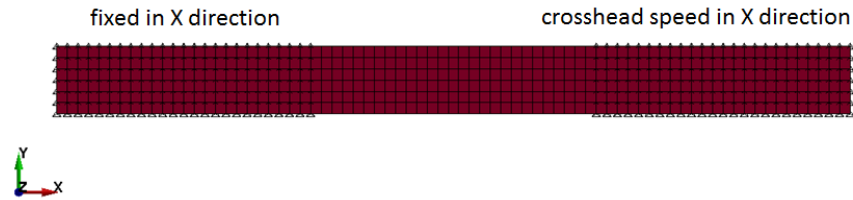

Figure 5-17 Finite Element Model of the Test Coupon

5.2.2.1 Comparison of Coupon Tests and Simulation (Warp Direction Tension)

For the strain rate of 5 s^{-1}, warp direction tension test and simulation results are given in Figure 5-18.

Figure 5-18 Force-Deflection Curves of the Coupon Test and the FE Simulation (5 s-1, Warp Direction Tension)

In Figure 5-18, it is seen that Ls-Dyna coupon simulation matches with real coupon tests considerable well. Elastic moduli value of the material model is very close to real tests. On the other hand, failure strength result of the simulation is less than average failure strengths obtained in real tests. It is considered that conservative approach can be accepted.

For the strain rate of 50 s^{-1}, warp tension test and simulation results are given in Figure 5-19.

Figure 5-19 Force-Deflection Curves of the Coupon Test and the FE Simulation (50 s-1, Warp Direction Tension)

In Figure 5-19, linear behavior of test and simulation is clearly seen. Nonlinear viscoelastic behavior could not be investigated from results of both simulation and real tests in the longitudinal direction. This is because of the dominant characteristics of carbon fibers in the longitudinal and transverse directions. Elastic moduli values obtained from the simulation and real tests are seen to be very close to each other. It is concluded that laminated composite fabric material model gives very accurate results at high strain rates.

5.2.2.2 Comparison of Coupon Tests and Simulation (Weft Direction Tension)

For the strain rate of 5 s^{-1}, weft tension test and simulation results are given in Figure 5-20.

Figure 5-20 Force-Deflection Curves of the Coupon Test and the FE Simulation (5 s-1, Weft Direction Tension)

In Figure 5-20, similar linear behavior is observed in real coupon tests and simulation results. Composite materials are quite brittle in the longitudinal and in the transverse direction due to linear characteristics of carbon fibers. There is almost no plastic deformation before rupture in the coupons because nonlinear viscoelastic behavior of resin is not effective in the weft direction. Elastic modulus values are almost same for real tests and coupons. In addition, failure strength value of simulation is acceptable when it is compared with real coupon test results.

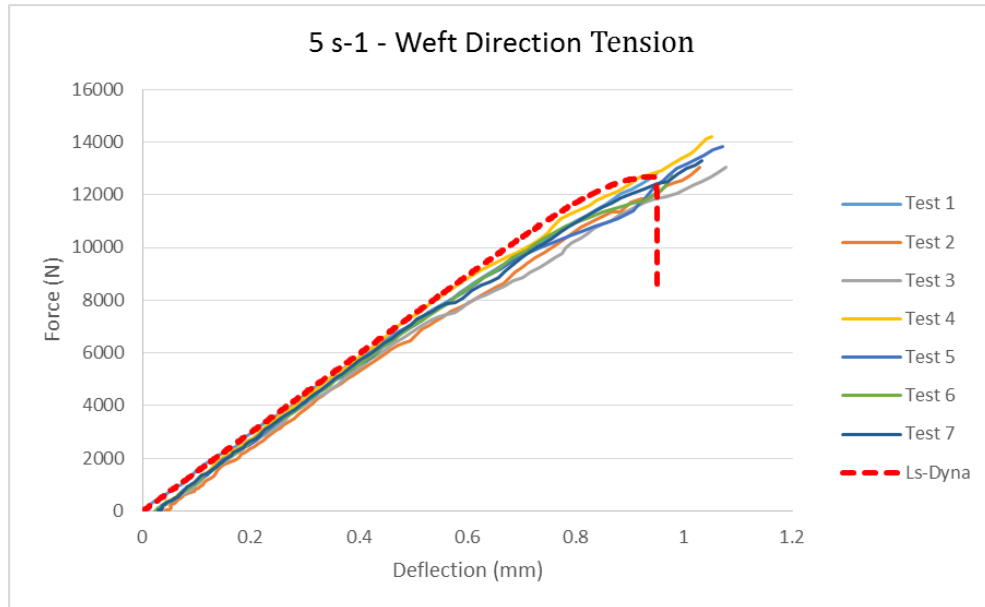For the strain rate of 50 s^{-1}, weft direction tension test and simulation results are given in Figure 5-21.
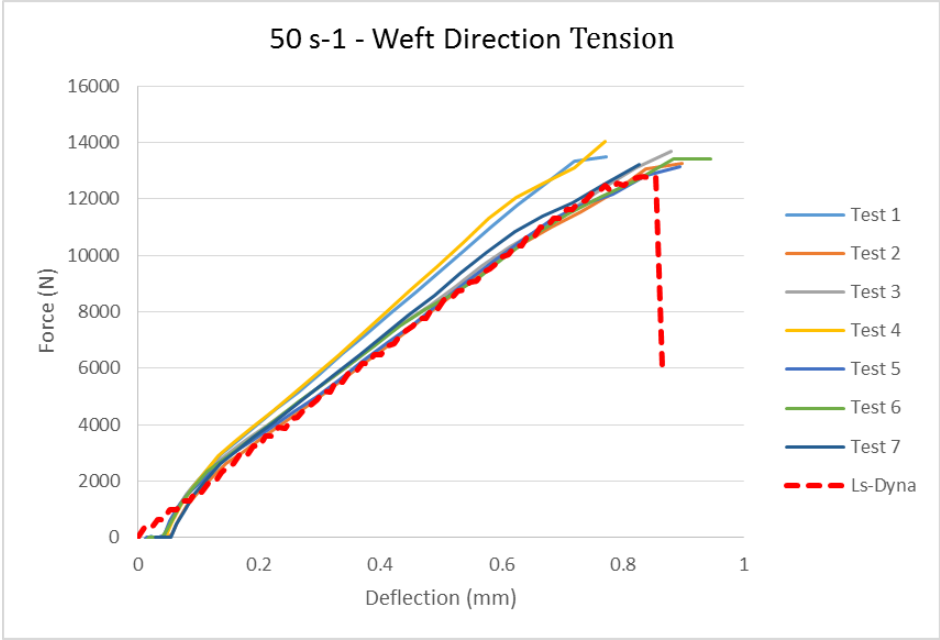
Figure 5-21 Force-Deflection Curves of the Coupon Test and the FE Simulation (50 s-1, Weft Direction Tension)

In Figure 5-21, it is seen that coupons 4 and 5 give larger elastic moduli values than other 5 coupon tests. Imperfections in the coupons and manufacturing effects can be the main reason of this difference. It is seen that simulation result matches with the real coupon tests except for coupons 4 and 5. Elastic modulus values obtained in the tests and the by the FE simulation are almost same. Similarly, failure strength result of simulations is conservative and acceptable. It is considered that laminated composite fabric material model gives accurate and acceptable results based on the comparison of the tests and the simulation.

5.2.2.3 Comparison of Coupon Test and Simulation for the 45° Tension Specimens

For the strain rate of 5 s^{-1}, 45° tension test and simulation results are given in Figure 5-22.

Figure 5-22 Force-Deflection Curves of the Coupon Test and the FE Simulation (5 s-1, 45° Tension)

In Figure 5-22, nonlinear viscoelastic behavior is observed in the off-axis tests. Contribution of resin material is very effective in this type of nonlinear behavior while carbon fibers exhibit almost linear elastic response. Actually, this shows the nonlinear mechanical response in off-axis tests while strength values are almost same in longitudinal and transverse tests. Resin material has a great influence on mechanical property, failure strengths and plastic deformation.

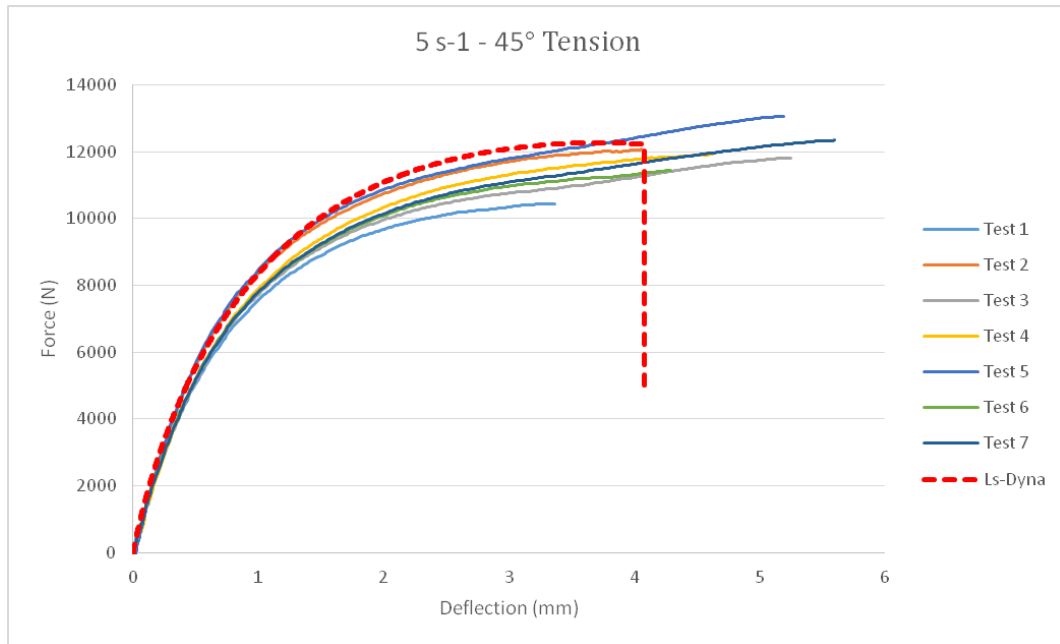For the strain rate of 50 s^{-1}, 45° tension test and simulation results are given in Figure 5-23.

Figure 5-23 Force-Deflection Curves of the Coupon Test and the FE Simulation (50 s-1, 45° Tension)

In Figure 5-23, off-axis tests conduct nonlinear mechanical response at 45° direction. Failure strength of simulation gives almost same results with real coupon test results. It should be noted that mechanical property test results provide data to calibrate the nonlinear material parameters of laminated composite fabric material model. Similarly, dynamic off – axis test exhibit and provide viscoelastic property of composite material. It is noted that laminated composite fabric material model gives sufficient and accurate results compared to the real material tests. Therefore, it is concluded that laminated composite fabric material model can be used to model carbon prepreg composite material in impact problem because strain rate sensitive property is already available in this material model.

In summary:

Material model for composite material is chosen as laminated composite fabric which is available in Ls-Dyna material model library. In this chapter, the work stated in the following items is accomplished.

- Continuum damage mechanics theory of laminated composite fabric material model is described.
- Carbon Prepreg composite material characterization is performed.
- From experimental test data, material parameters and strain rate vs. strength graphs are prepared.
- To validate the material model, dynamic coupon tests are simulated in Ls-Dyna.
- Force-deflection graphs from experimental test data and simulations are obtained.
- Comparison of test and simulation results is performed. This comparison leads to the validated material models for carbon prepreg composite material.

CHAPTER 6

WING LEADING EDGE BIRD STRIKE ANALYSIS

6.1 Metallic Leading Edge Bird Strike Analysis

After deciding on the suitable material models for the soft impactor and the metallic aircraft material, bird strike simulations on wing leading edge are performed. For the bird strike analysis, a generic aircraft wing is used because the main aim of this study is to show the process of bird strike analysis. The generic aircraft wing is totally made of AL 2024 T3 and dimension of the wing is shown in Figure 6-1. Skin thickness of the impact region is 2 mm.

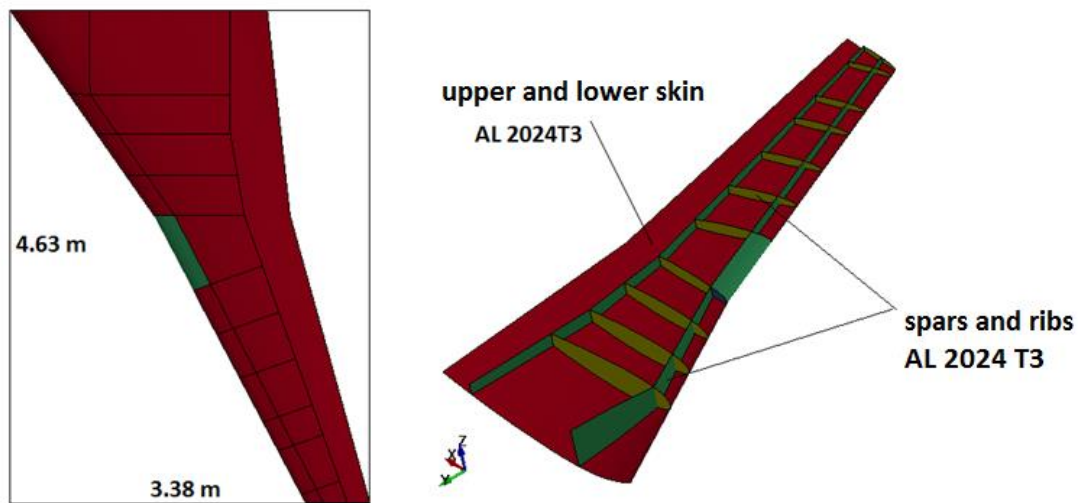Figure 6-1 Dimension of the Generic Aircraft Wing

Finite Element Model:

In the model, soft body impactor (bird) is modeled by SPH formulation and its material is defined as Null material model. Gruneisen equation of state model is selected as EOS of the bird. For the metallic wing structure, Johnson Cook material model is used with EOS Gruneisen. Illustrative picture about FE model is given in Figure 6-2
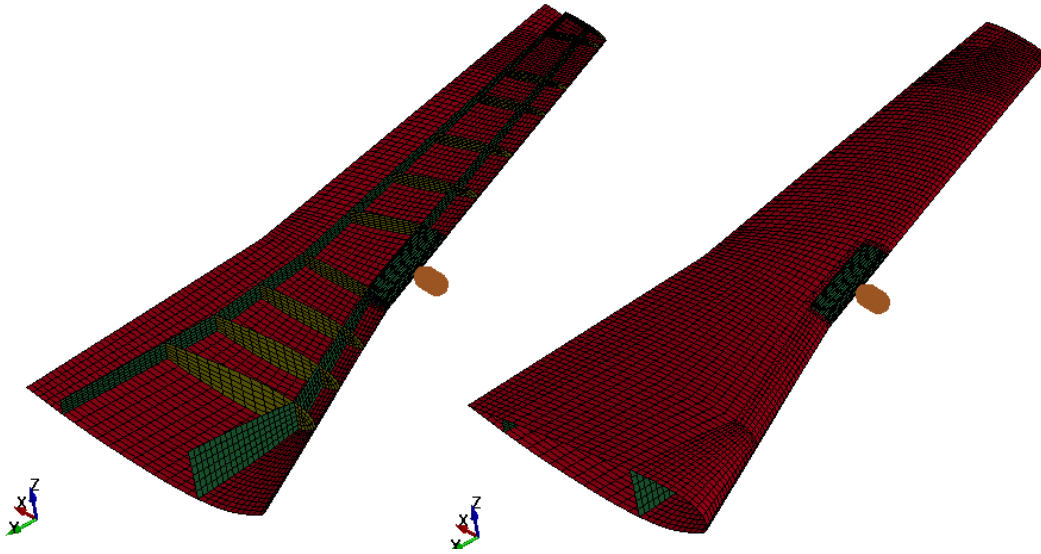
Figure 6-2 Finite Element Model of Generic Aircraft Wing

Finer mesh size is used in impact region of the leading edge to provide better accuracy and contact behavior. The green colored region is chosen as bird impact region and fine mesh is applied here. Fine mesh in the impact region is shown in Figure 6-3. Mesh size in impact region is 7.5 mm while mesh size of other region is 50 mm.

Figure 6-3 Fine Mesh Distribution in the Impact Region

Soft body impactor is modeled by using Smoothed particle hydrodynamics method. Its dimension and weight is standardized in FAA regulations. Dimension of the bird and SPH model are shown in Figure 6-4.
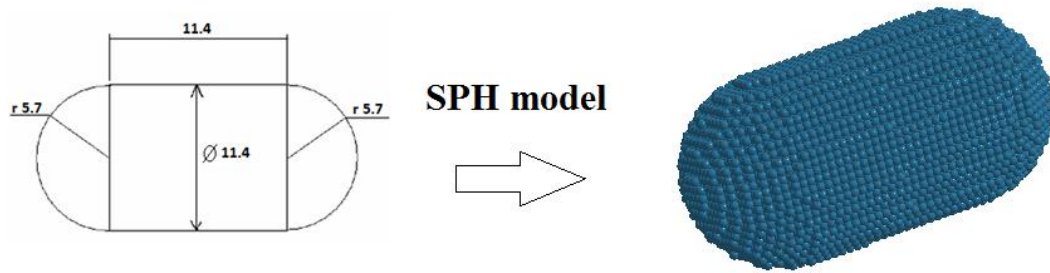
Figure 6-4 SPH Model of Soft Body Impactor (all dimension is given in cm)

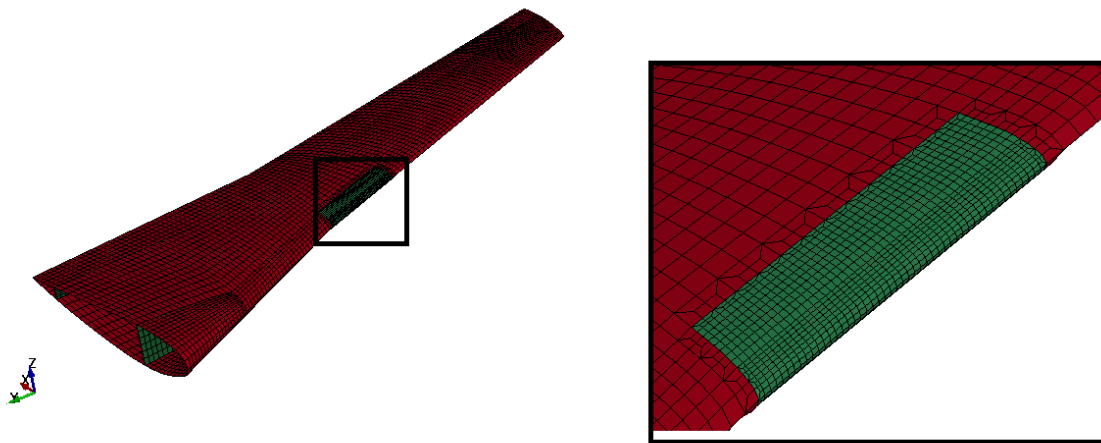In Figure 6-4, the geometry of the soft body impactor is simply defined as cylinder with hemi-spherical ends and its weight is 4 Ib. 15000 SPH particles are used to model soft body impactor.

The details of the model can be summarized as follows;

- The bird dimensions and the weight are taken from FAA standards.
- MAT_NULL and EOS_Gruneisen are used for the bird model. The required parameters are same as given in Chapter 4.
- Impact velocity is about 240 knots or 125 m/s
- The complete wing structure is made of AL 2024 T3.
- Johnson Cook and EOS_Gruneisen are used for wing structure. The required parameters are taken from Chapter 5.
- Finer mesh is applied to the impact region to get more accurate results and to provide a better contact behavior.

Analysis results of the bird strike on the metallic leading edge are given in Figure 6-5.

Figure 6-5 Metallic Wing Leading Edge Deformation Results (t = 2.5 ms)
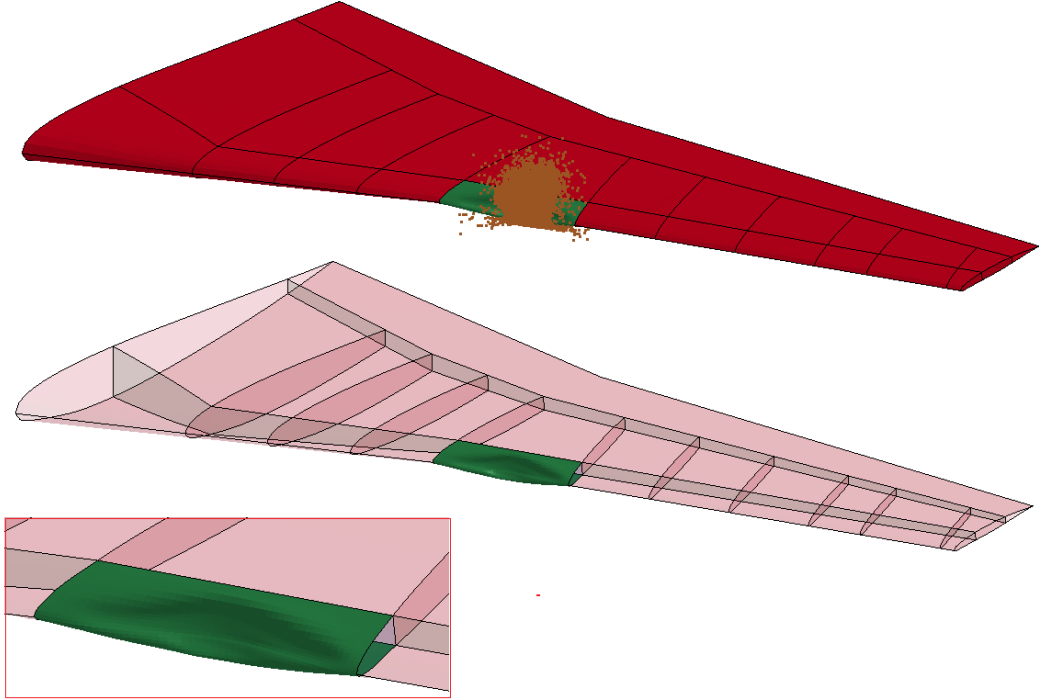
In Figure 6-5, deformation of metallic wing leading edge is illustrated at 2.5ms after the impact. It is clear that aerodynamics profile of leading edge is highly distorted and this may lead to instability during flight. However, total fracture of metallic leading edge does not occur because aluminum alloy exhibits ductile characteristics in plastic deformation.

Plastic deformation and von Mises stress plots of the metallic leading edge are given in Figure 6-6.
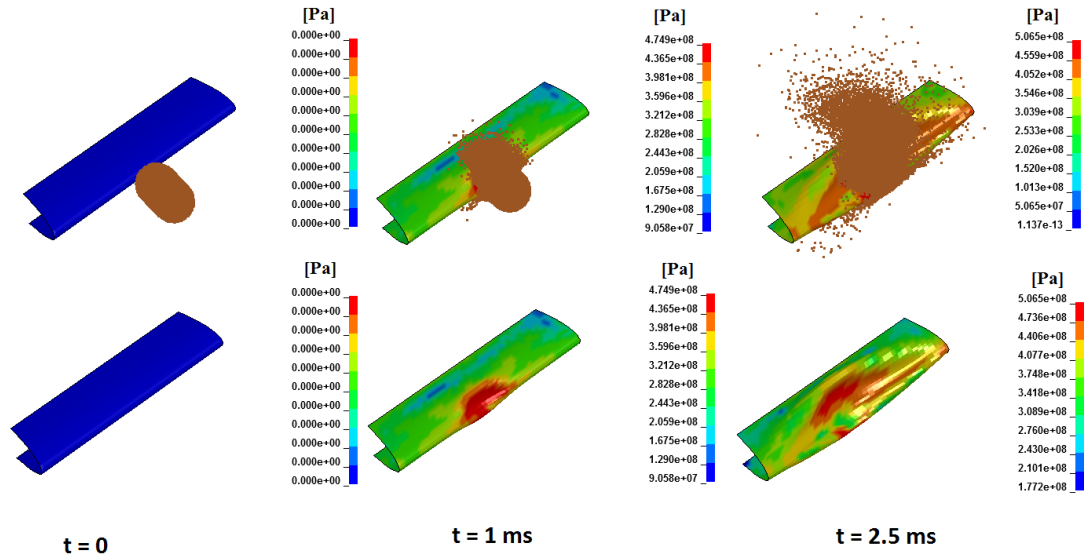
Figure 6-6 Metallic Impact Region Bird Strike Results (von Mises Stress Distribution [Pa])

In Figure 6-6, significant effect of bird strike on leading edge can be seen. Plastic deformation continuously propagates during impact and metallic leading edge cannot resist this impact load. Aerodynamic characteristic of leading edge is changed sharply. Deformation profile of bird after impact seems acceptable because bird essentially disintegrates after impact and behaves like fluidic material.

Parametric study is performed by changing impact velocity to see effect of impact velocity in bird strike problem. Five different impact velocities such as 25 m/s, 50 m/s, 75 m/s, 100 m/s and 125 m/s are chosen to see effect of soft body impactor on metallic leading edge. Impact velocity vs. logarithmic displacement graph is given in Figure 6-7.

25 m/s	50 m/s	75 m/s	100 m/s	125 m/s
$d_{max} = 0.1$ mm	$d_{max} = 0.2$ mm	$d_{max} = 0.4$ mm	$d_{max} = 28$ mm	$d_{max} = 73$ mm
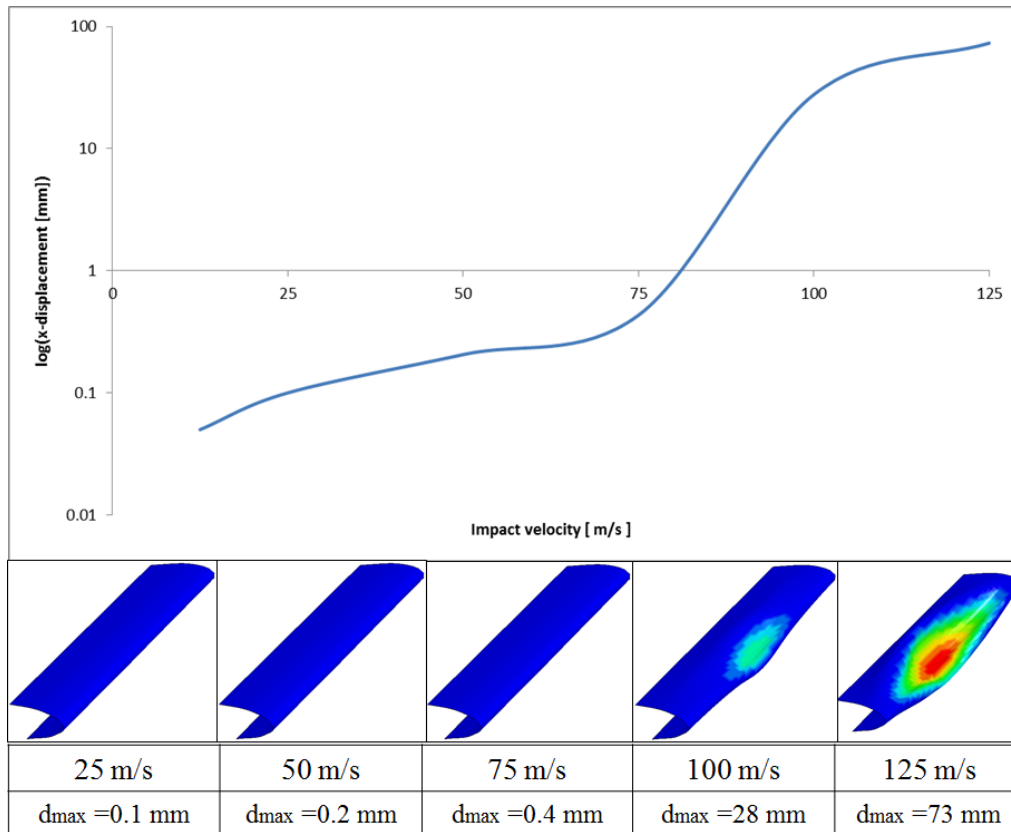
Figure 6-7 Impact Velocity vs. Logarithmic x-displacement (impact direction) of the Impact Region

In Figure 6-7, the impact velocity vs. logarithmic x-displacement curve is given together with the deformation fringe plot of the impact region. From Figure 6-7, it is clear that metallic wing leading edge provides enough resistance to the bird strike up to 75 m/s. After this threshold value, the leading edge is not able to resist this impact force and starts to deform sharply.

In addition to the investigation of the impact region, other part of the wing can also be examined according to Von Mises stress distribution which is given in Figure 6-8.
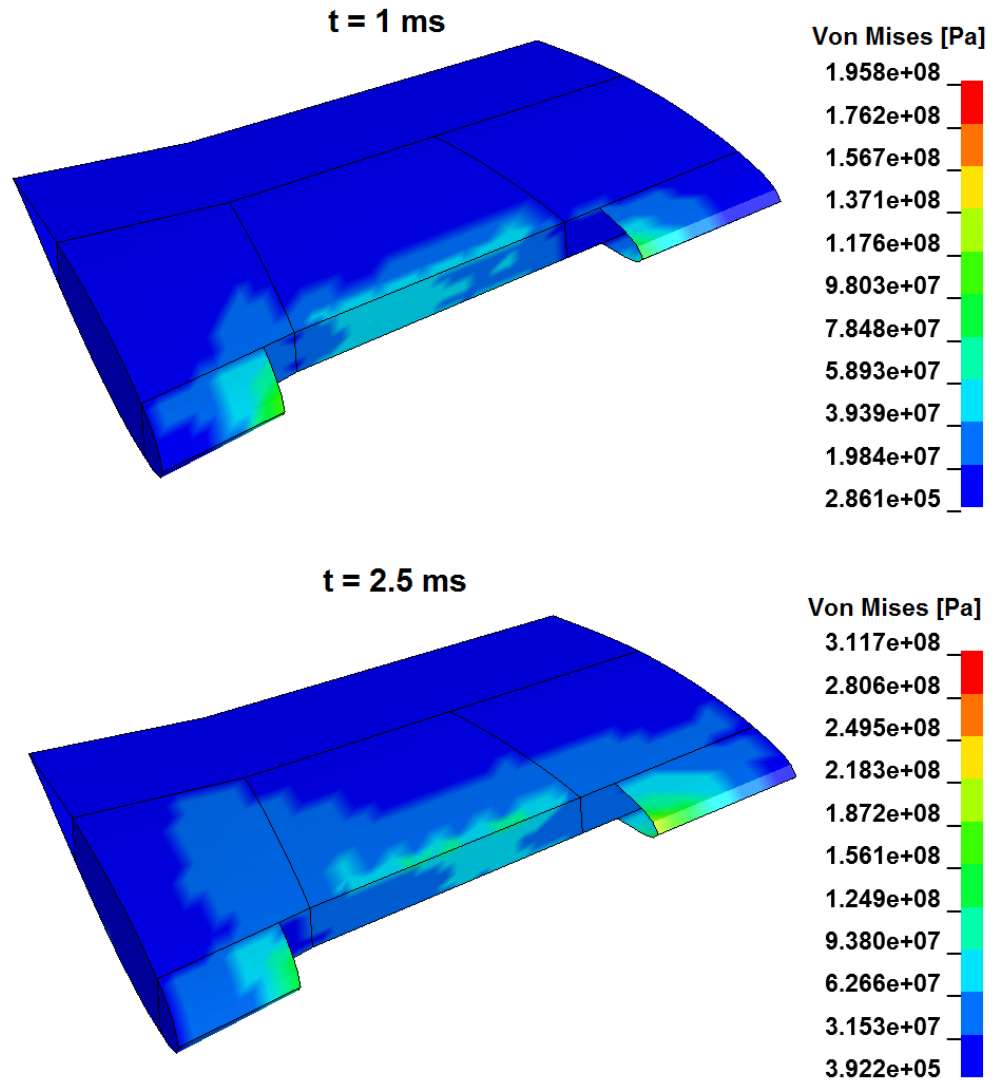
Figure 6-8 Stress Distribution around the Impact Zone

In Figure 6-8, effect of bird strike around the impact region is clearly seen. At time is equal to 1 ms, von Mises stress distribution is about 200 MPa at front spar and leading edge regions. Also, at time is equal to 2.5 ms, stress value increases up to 300 MPa which is non negligible stress value for primary structures such as front spar and upper/lower panels.

In this thesis, wing structure is fully modeled to investigate effect of the bird strike. If the impact region is only examined, local finite element model can also be used. In Figure 6-9, local finite element model is shown. The other part of the wing is not modeled. Displacement boundary condition is applied at left and right side of this local mesh to model essential boundary condition.
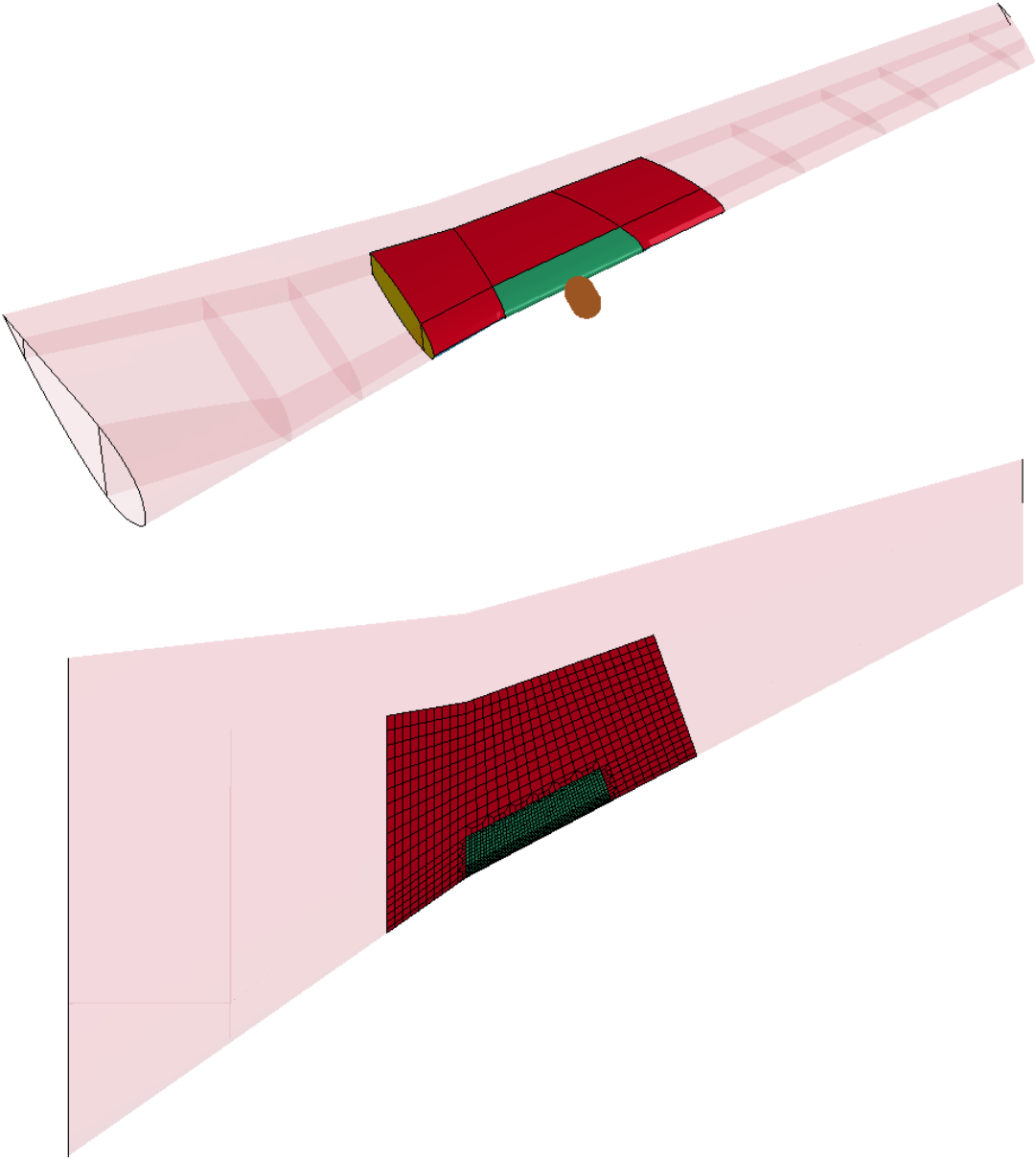
Figure 6-9 Local Finite Element Model of Wing Structure

Comparison of plastic strain history for local and global model is given in Figure 6-10. Also, comparison of plastic strain values is given in Table 6-1.
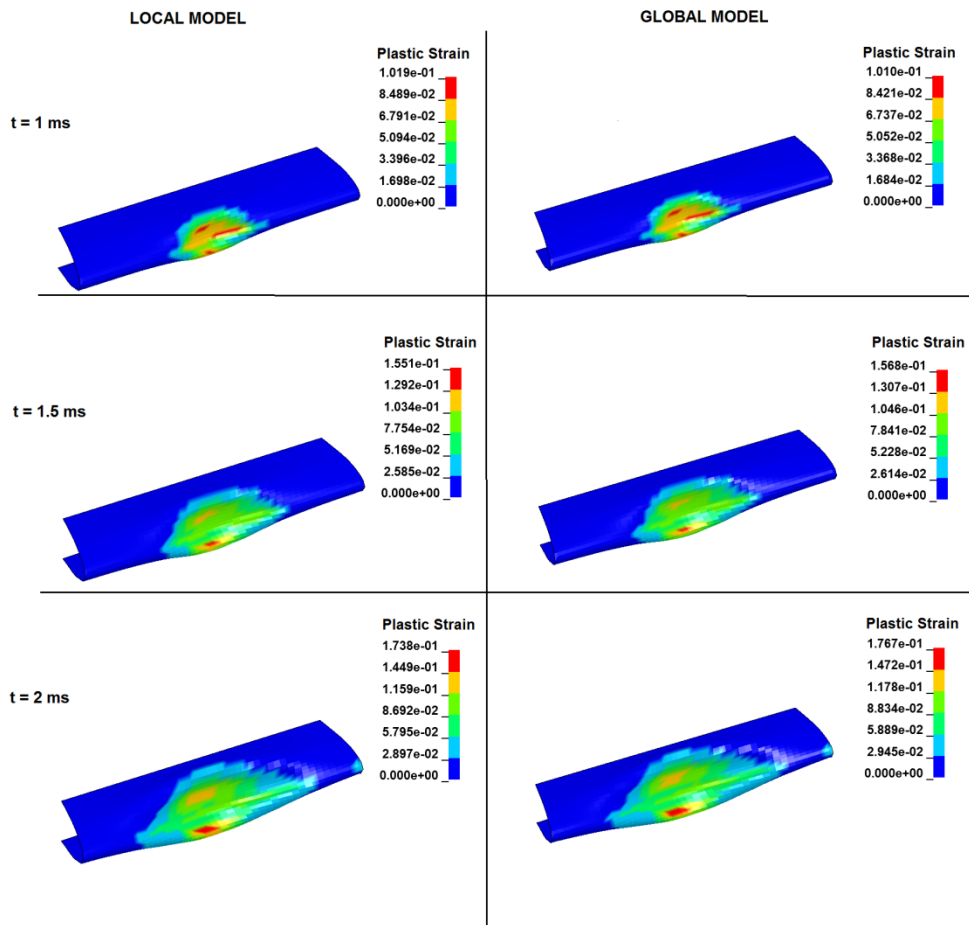
Figure 6-10 Comparison of the Plastic Strain Results for Local and Global Models

Table 6-1 Comparison of Plastic Strain Values for Local and Global Models

| | Plastic Strain [mm/mm] | | Difference |
	Local Model	Global Model	(%)
at t = 1ms	0.102	0.101	0.99
at t = 1.5 ms	0.155	0.157	1.08
at t = 2 ms	0.174	0.177	1.64

In Figure 6-10, deformation profile of local and global models is quite similar. Moreover, difference in plastic strain values is about 1 % which is provided in Table 6-1. Therefore, local modeling technique can also be used in bird strike analyses to reduce modeling and solution time if impact region is only investigated.

6.2   Composite Leading Edge Bird Strike Analysis

In this part, the behavior of the composite leading edge during the bird strike is analyzed. The same generic wing is used to model the bird strike except for the leading edge material. In this case, the material of the impact region of the wing is changed to carbon prepreg composite material that is characterized in Chapter 5 in detail. Dimensions and materials used in the wing are given in Figure 6-11. It can be seen that the impact region which is plotted as green in Figure 6-11 is defined as composite material. All other parts of the wing are again made from Al 2024 T3.
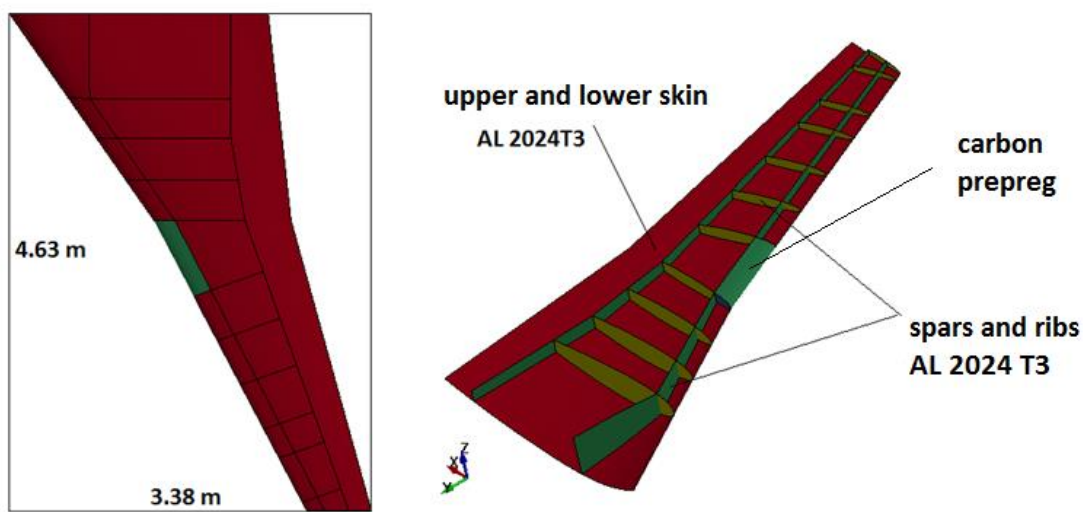
Figure 6-11: Dimension of the Generic Wing

Summary of model details is given as:

- The bird dimensions and the weight are taken from FAA standards.
- Null material model and Gruneisen EOS are used for bird model. The required parameters are same as Chapter 4.
- The impact velocity is about 240 knots or 125 m/s.
- The wing is made of AL 2024 T3 except for the impact region of leading edge. This region is assigned as composite material.
- Johnson Cook and Gruneisen EOS are used for the wing structure. The required parameters are taken from Chapter 5
- Stacking sequence of the composite leading edge is taken [0°/45°/0°/45°]s and each layer has a thickness of 0.2 mm.

- Laminated composite fabric material model is used for the composite impact region.
- A finer mesh is applied to the impact region to get more accurate results and to provide a better contact behavior. In Figure 6-12, the impact region with fine mesh is given.
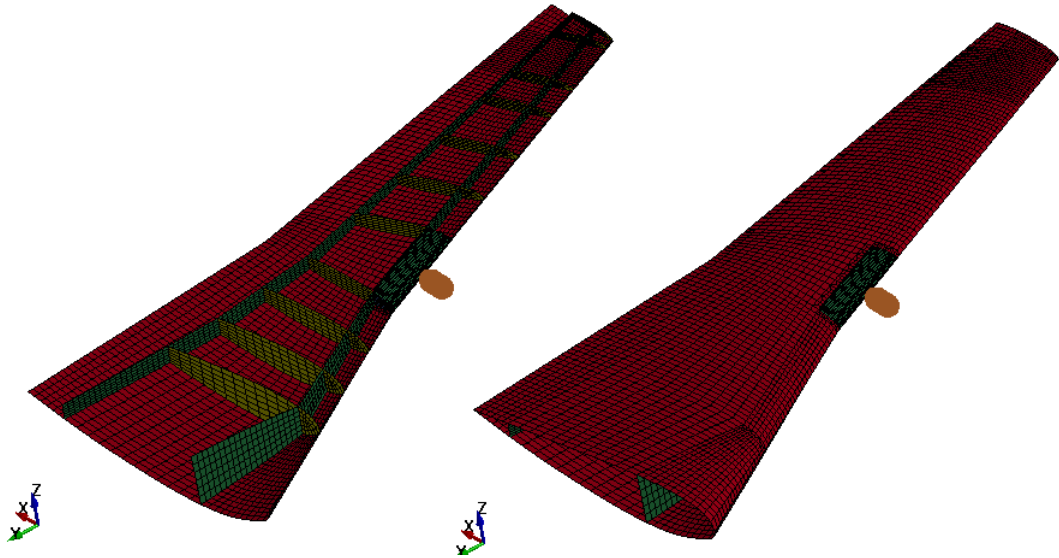
Figure 6-12 Finite Element Model of Generic Aircraft Wing

A finer mesh size is used at the impact region of the leading edge to provide a better accuracy and contact behavior. The green colored region is chosen as the bird impact region and a finer mesh is applied here. The fine mesh is shown in Figure 6-13.
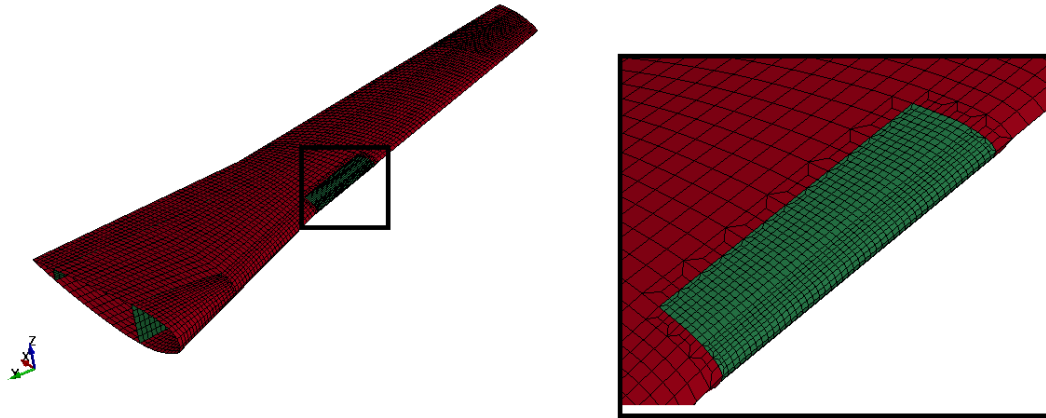
Figure 6-13 Finer Mesh Distribution in the Impact Region

Analysis results of the bird Strike on the metallic leading edge are given in Figure 6-14.
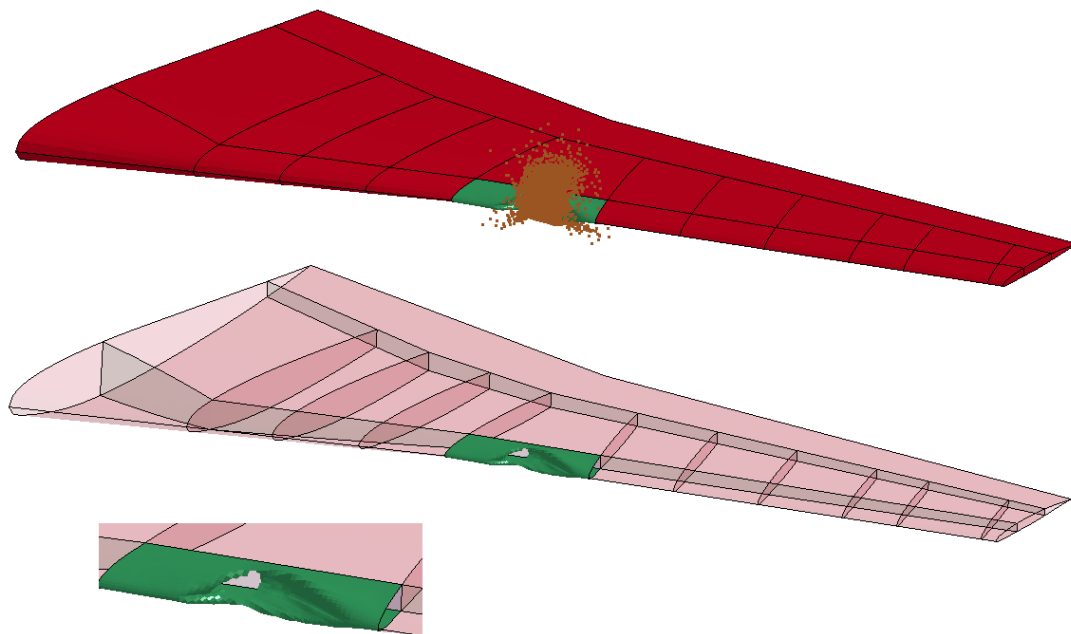
Figure 6-14 Composite Wing Leading Edge Deformation Results (t = 2.5 ms)

In Figure 6-14, deformation of the composite wing leading edge is given. It is obvious that aerodynamics profile of leading edge is highly distorted and this may lead to an instability or catastrophic failure during flight because total fracture of composite leading edge occurs due to brittle nature of composite materials.

74

Composite materials are commonly used in aviation industry because of their lightweight and strength. However, composite materials are also very brittle and they cannot provide enough toughness during impact problems. Therefore, this type of brittle material has to be reinforced against impact force effects. Failure index distribution in warp direction for composite leading edge is illustrated in Figure 6-15.
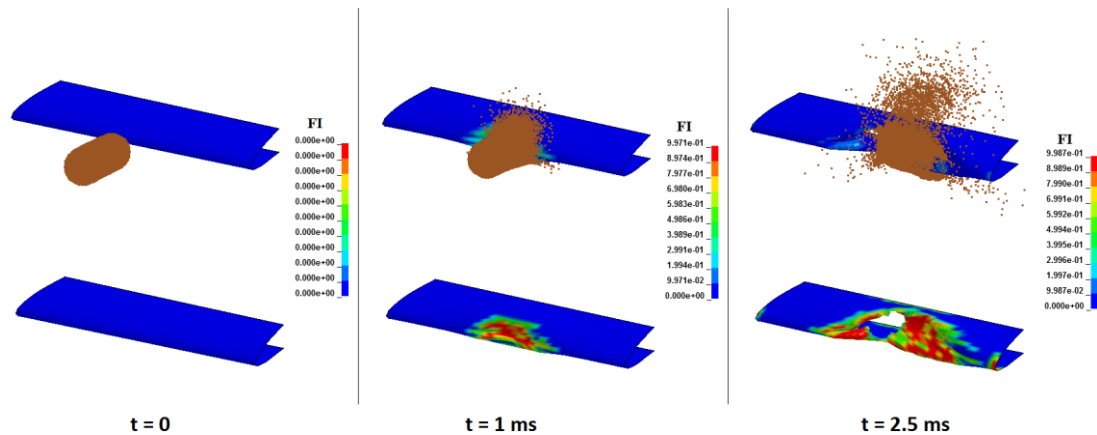
Figure 6-15 Composite Impact Region Bird Strike Results (Failure Index in longitudinal direction)

Failure of composite leading edge continuously propagates during impact. Total failure can be seen clearly from failure index results and this may yield to catastrophic failure of the aircraft during flight. Brittle nature of composites is disadvantageous against impact loads.

A parametric study is again performed by changing the impact velocity to see the behavior of composite leading edge under impact load. Five different impact velocities 25 m/s, 50 m/s, 75 m/s, 100 m/s and 125 m/s are chosen.

25 m/s	50 m/s	75 m/s	100 m/s	125 m/s
dmax =0.22 mm	dmax =1.02 mm	dmax =3.3 mm	dmax =96 mm	dmax =162 mm
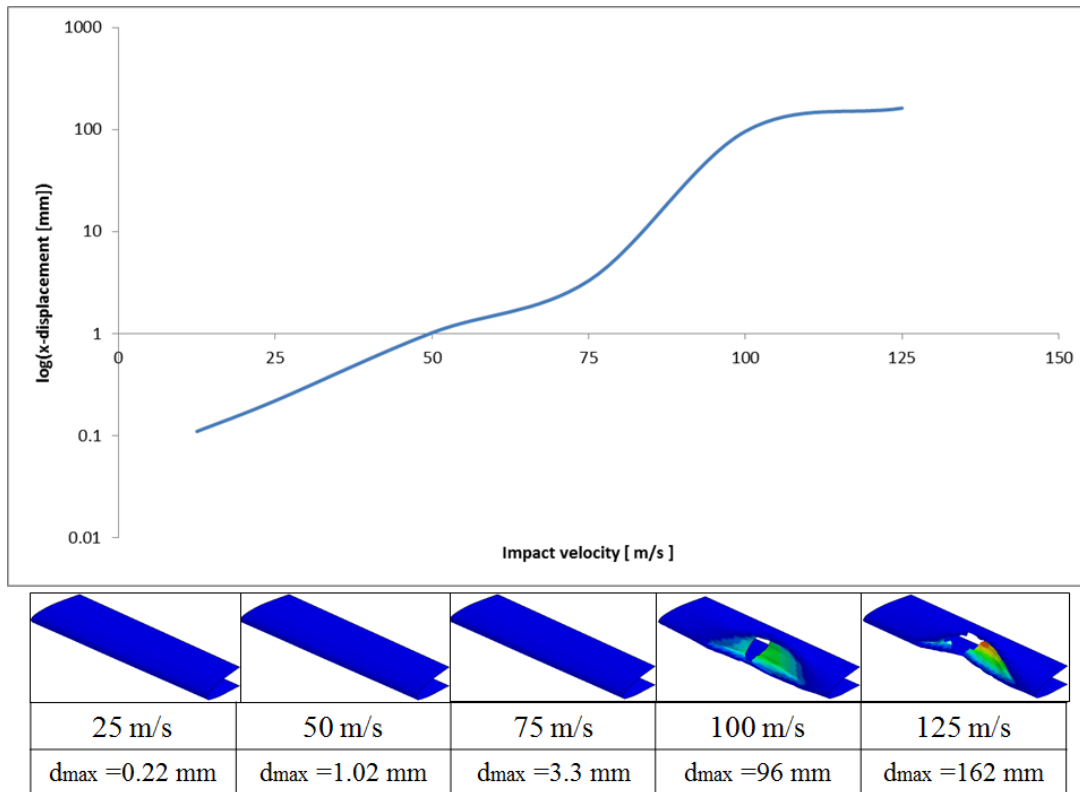
Figure 6-16 Impact Velocity vs. Logarithmic x-displacement (impact direction) of Impact Region

In Figure 6-16, the impact velocity vs. logarithmic x-displacement of the impact region graph is given with fringe plots of the impact region. It is obvious that the composite wing leading edge provides enough resistance to bird strike up to 75 m/s. After this threshold value, the leading edge is not able to cover this impact force and starts to deform sharply and total failure occurs at the impact region. In this case, it can be said that the composite leading edge resists to the bird strike until the impact velocity of 75 m/s. However, a catastrophic failure immediately propagates when the stress value reaches to the strength limit of the composite material. This parametric study indicates that the composite fabrics may lead to catastrophic failure during flight because of the brittle nature. This can be considered as a deficiency of composite materials under impact loads. To overcome this issue, the composite structure has to be reinforced by increasing the thickness or providing secondary structure.

CHAPTER 7

REINFORCEMENT STUDY

7.1   Theoretical Background

Use of honeycomb material is one of the recommended solutions against bird strike. Honeycomb is a very stiff material in compression and impact loads while it is quite inefficient in tension and shear loads. Cellular honeycomb structure provides a secondary lightweight construction element. A comparison study which shows advantages of using honeycomb is done by Hexcel Inc. [22]. The summary table of this comparison study is given in Figure 7-1.
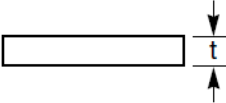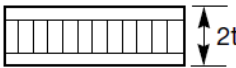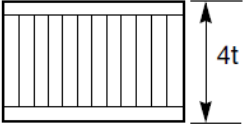
	Solid Metal Sheet	Sandwich Construction	Thicker Sandwich
Relative Stiffness	100	700 7 times more rigid	3700 37 times more rigid!
Relative Strength	100	350 3.5 times as strong	925 9.25 times as strong!
Relative Weight	100	103 3% increase in weight	106 6% increase in weight

Figure 7-1 Investigation of Effect of Honeycomb in Impact Loading [22]

Typical mechanical property of honeycomb material is given in Figure 7-2
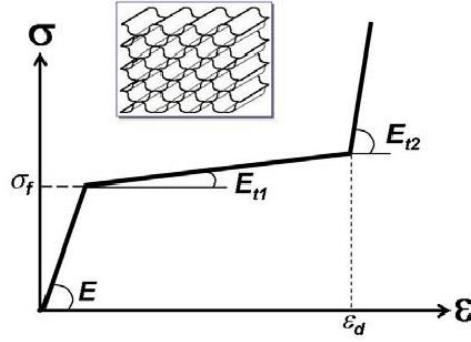
Figure 7-2 Typical Mechanical Behavior of Honeycomb Material [8]

To investigate the effect of honeycomb in soft body impact analysis, honeycomb is added to the finite element model. Honeycomb material model is used for modeling of honeycomb available in Ls-Dyna material model library.

Honeycomb material model [19]:

The major use of this material model is for honeycomb and foam materials with real anisotropic behavior. A nonlinear elastoplastic material behavior can be defined separately for all normal and shear stresses. These are considered to be fully uncoupled. This material model is referenced as MAT_026_HONEYCOMB in Ls-Dyna material model library.

The behavior before compaction is orthotropic where the components of the stress tensor are uncoupled, i.e., a component of strain will generate resistance in the local a-direction with no coupling to the local b and c directions.

$$E_{aa} = E_{aau} + \beta(E - E_{aau})$$
$$E_{bb} = E_{bbu} + \beta(E - E_{bbu})$$
$$E_{cc} = E_{ccu} + \beta(E - E_{ccu})$$
$$G_{ab} = G_{abu} + \beta(G - G_{abu})$$
$$G_{bc} = G_{bcu} + \beta(G - G_{bcu})$$
$$G_{ca} = G_{cau} + \beta(G - G_{cau})$$

(7.1)

where

$$\beta = max\left[min\left(\frac{1-V}{1-V_f}\right), 0\right]$$

(7.2)

V_f is final volume and V indicates relative volume

Description of required parameters is given in Table 7-1.

Table 7-1 Parameter Description of Honeycomb Material Model

Parameter	Description
ro	Density
E	young modulus of compressed honeycomb
pr	poisson's ratio of compressed honeycomb
vf	relative volume
mu	material viscosity coefficient
Eaau	Elastic modulus of uncompressed honeycomb in a direction
Ebbu	Elastic modulus of uncompressed honeycomb in b direction
Eccu	Elastic modulus of uncompressed honeycomb in c direction
Gabu	Shear modulus of uncompressed honeycomb in ab plane
Gbcu	Shear modulus of uncompressed honeycomb in bc plane
Gacu	Shear modulus of uncompressed honeycomb in ca plane

and G is the elastic shear modulus for the fully compacted honeycomb material

$$G = \frac{E}{2(1 + v)} \tag{7.3}$$

The honeycomb is modeled by using hex elements. The 3D finite element model of honeycomb is given in Figure 7-3.
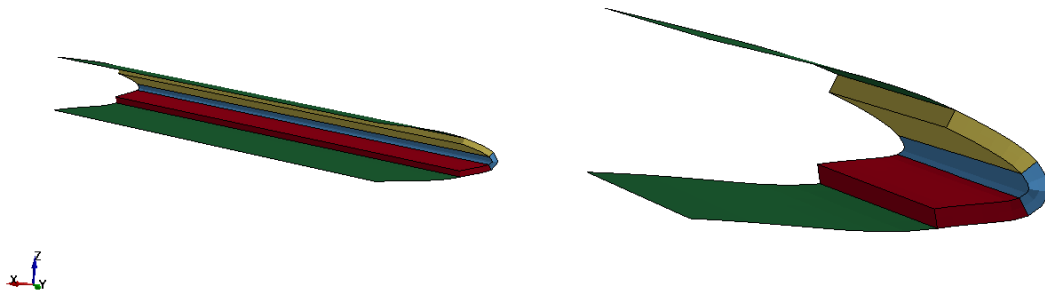
Figure 7-3 3D Finite Element Model of Honeycomb

Parameters are obtained from the Hexcel product catalog [22] for the honeycomb material model in Table 7-2.

Table 7-2 Honeycomb Material Parameters [22]

ro [kg/m3]	E [Pa]	pr	Sigy [Pa]	vf	mu
198.62	1.37E+11	0.33	2.80E+08	0.15	6.00E-02
Eaau [Pa]	Ebbu [Pa]	Eccu [Pa]	Gabu [Pa]	Gbcu [Pa]	Gacu [Pa]
1.45E+09	1.45E+09	1.38E+11	2.00E+09	2.00E+10	4.00E+10

7.2 Bird Strike Analysis with Honeycomb Reinforced Leading Edge

7.2.1 Metallic Leading Edge Case

Deformation results of bird strike analysis with the honeycomb reinforced metallic leading edge are given in Figure 7-4. Impact velocity is taken as 125 m/s.
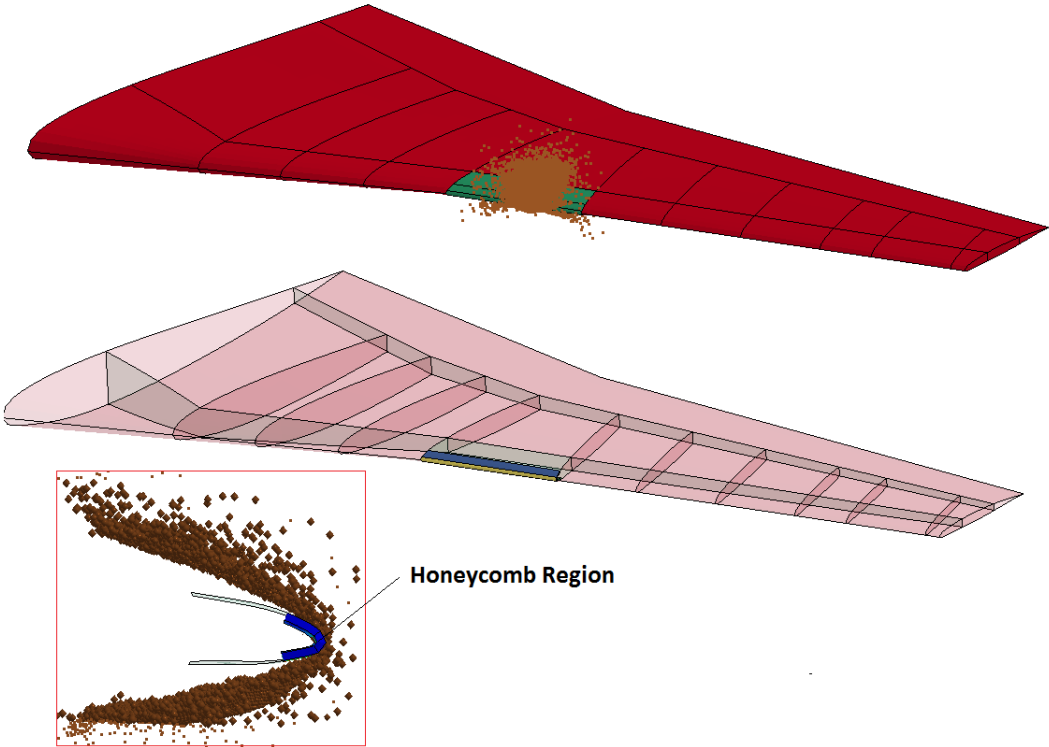
Figure 7-4 Deformation Results of Bird Strike Analysis with Honeycomb Reinforcement in the Wing Leading Edge

Plastic strain contour plots of the metallic leading edge without and with honeycomb reinforcement are given in Figure 7-5. It is noted that plastic strain is much higher in original model which does not have honeycomb reinforcement. On the other hand, honeycomb reinforced leading edge shows excellent resistance against impact loading.
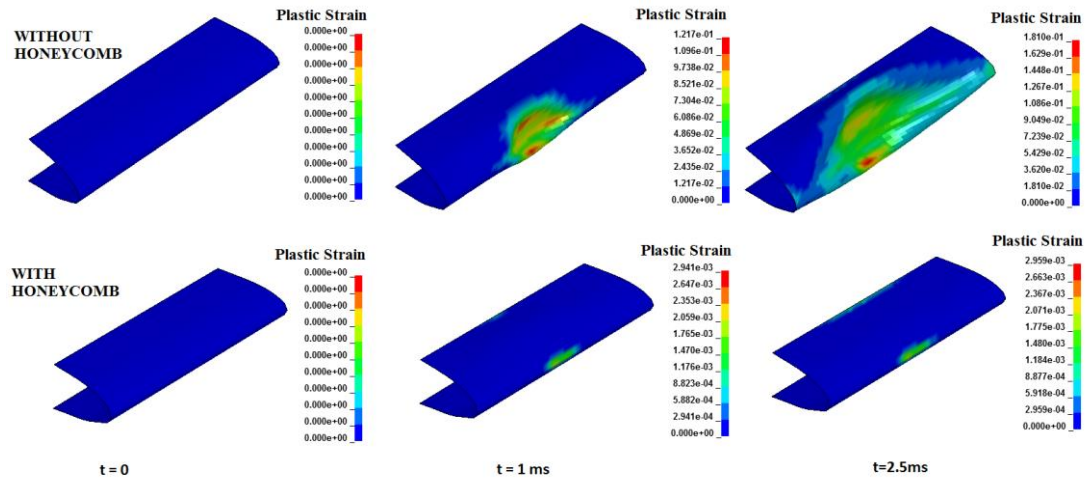
Figure 7-5 Plastic Strain Results of Metallic Leading Edge with Honeycomb Reinforcement

Section view of impact region is given in Figure 7-6. When the sectional view of impact region is investigated, it is clear that honeycomb reinforced leading edge successfully resists to impact. Aerodynamic profile of reinforced metallic leading edge does not distort much.
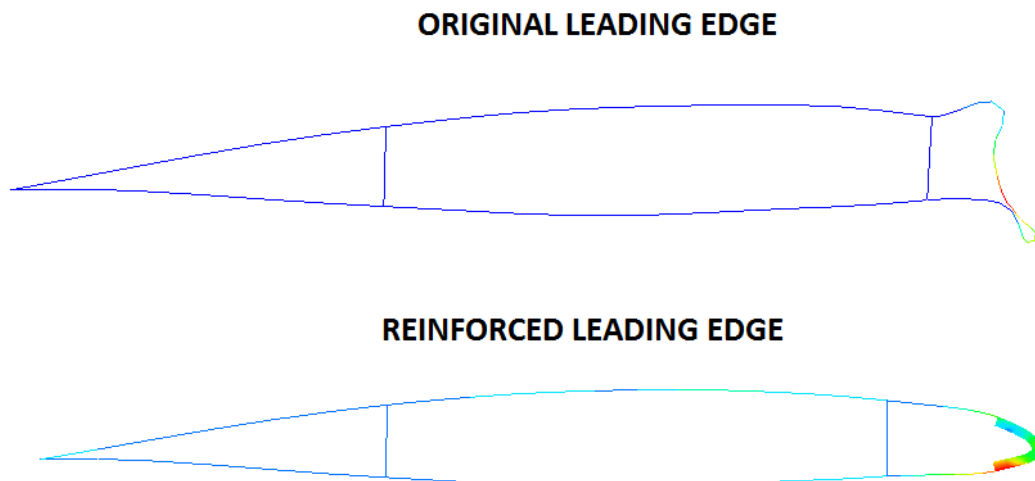
Figure 7-6 Section View of the Impact Region (t = 2.5ms)

In Figure 7-7, sectional deformation plots of metallic leading edge are given at different times after the impact event. Positive effect of honeycomb in maintaining the aerodynamic shape of the leading edge during impact is clearly seen in Figure 7.7.

| t = 0 | t = 1.25 ms | t = 2.5 ms |

I : ORIGINAL METALLIC LEADING EDGE   II: REINFORCED METALLIC LEADING EDGE
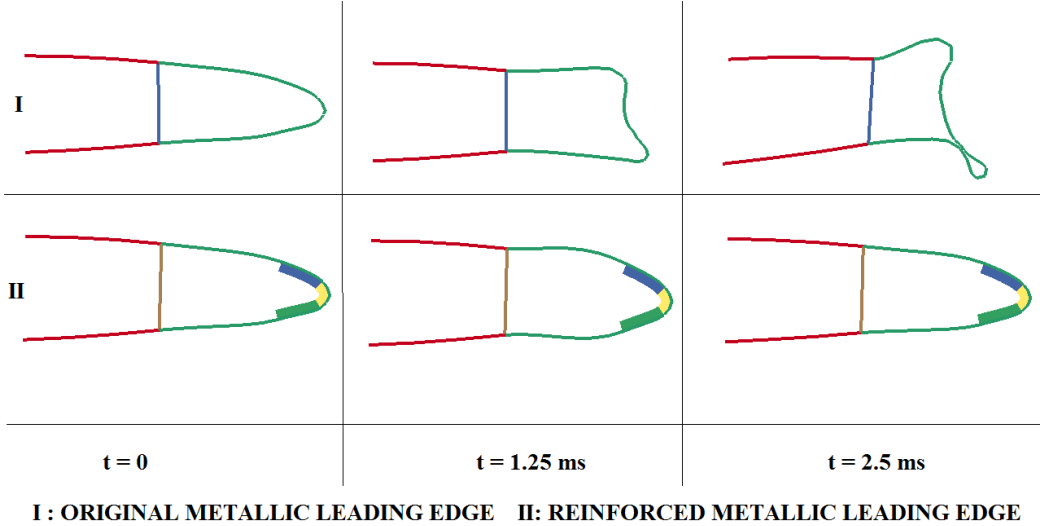
Figure 7-7 Sectional Views of the Metallic Leading Edge

7.2.2   Composite Leading Edge Case

Deformation results of bird strike analysis with the honeycomb reinforced composite leading edge are given in Figure 7-8. It is clear that honeycomb provides efficient resistance against impact loading also for the composite leading edge. Soft body impactor follows aerodynamic surface profile and there is no significant distortion in the profile of composite leading edge.
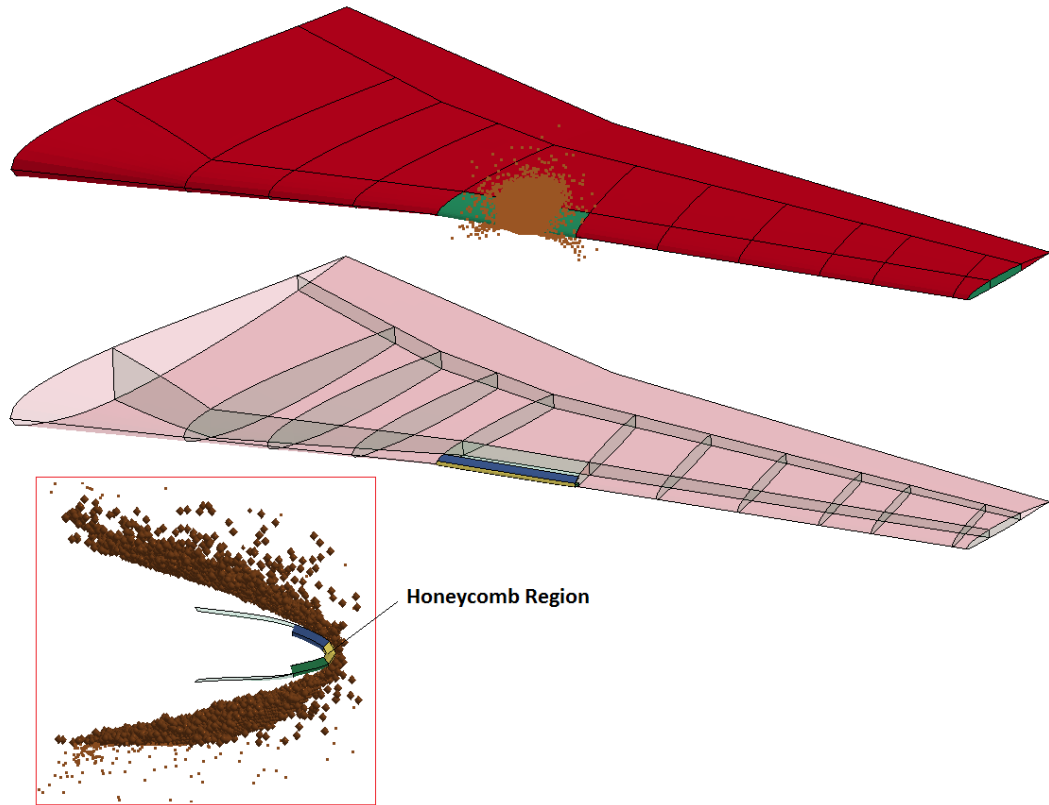
Figure 7-8 Deformation Results of Bird Strike Analysis of Composite Leading Edge
Honeycomb Reinforcement

Failures Index plots of the composite fabric are given in Figure 7-9. It is seen that
failure does not happen in the honeycomb reinforced composite leading edge. In
other words, honeycomb reinforced composite leading edge shows excellent
resistance against the impact loading.
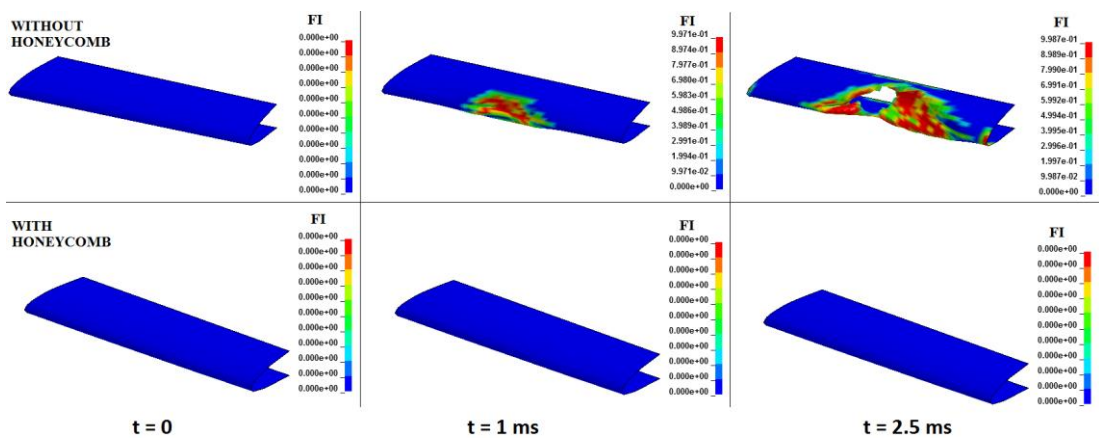
Figure 7-9 Failure Index Results of Bird Strike Analysis of the Composite Leading
Edge with Honeycomb Reinforcement (Failure Index in the longitudinal direction)

Sectional view of the impact region is given in Figure 7-10. When sectional view of the impact region is investigated, it is clear that honeycomb reinforced composite leading edge behaves in excellent impact resistant manner.

ORIGINAL LEADING EDGE

REINFORCED LEADING EDGE
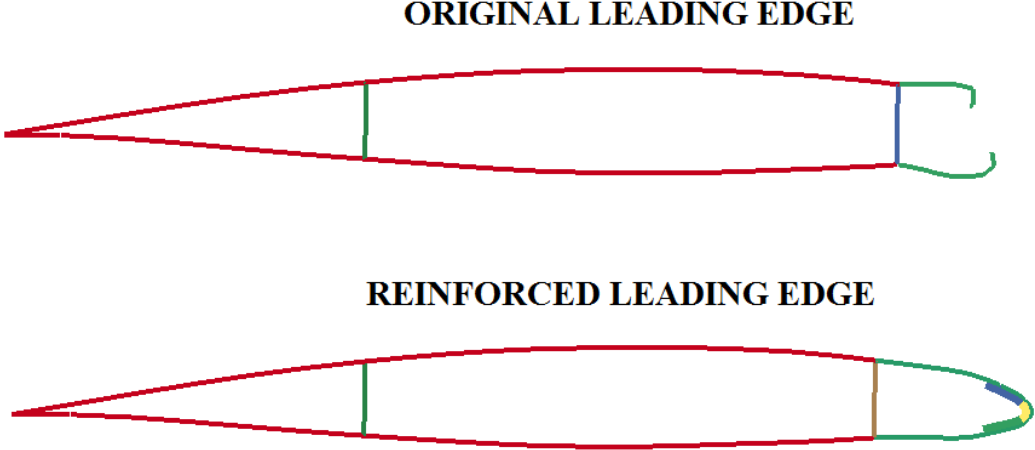
Figure 7-10 Section view of the Impact Region of the Composite Wing Leading Edge (t = 2.5 ms)

In Figure 7-11, sectional deformation plots of composite leading edge is given at different times after impact. Again for the composite wing leading edge, positive effect of the honeycomb reinforcement is clearly seen during impact.

I : ORIGINAL COMPOSITE LEADING EDGE   II : REINFORCED COMPOSITE LEADING EDGE
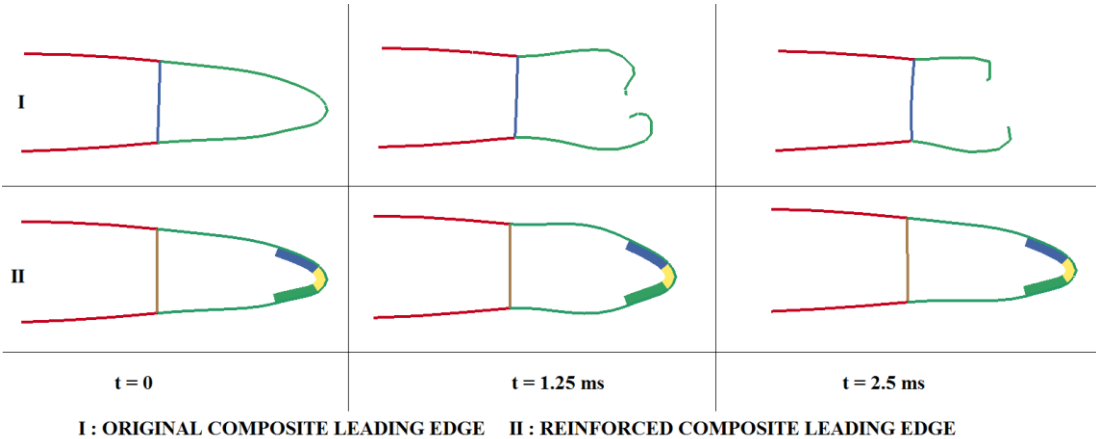
Figure 7-11 Section Views of Composite Leading Edge With Honeycomb Reinforcement

In summary:

In this chapter, theoretical background of honeycomb usage is investigated. Honeycomb material model in Ls-Dyna material library is described. Modeling of honeycomb with 3D elements is shown. Also, material parameter of honeycomb material model is given.

Bird strike analyses for reinforced leading edge are preformed and deformation, plastic strain and failure index results are given. As a result of the bird strike analyses, it is seen that honeycomb material behaves in excellent impact resistant manner. In reinforced metallic leading edge analysis, there is sufficient improvement in plastic strain in metallic leading edge panel. Similarly, in reinforced composite leading edge analysis, failure is not predicted in the composite leading edge panel. Honeycomb material provides low weight and high impact resistant mechanical property. In other words, honeycomb materials are effective secondary structural elements with low ratio of weight/stiffness in impact loading. If the wing leading edge panel of bird strike region is only taken in terms of weight consideration, honeycomb material increases the weight of this panel is around 20 %. Weight increase caused by honeycomb reinforcement for the metallic and composite wing leading edge is summarized in Table 7-3.

Table 7-3 Leading Edge panel of Bird Impact Region Weight Summary

Material of Leading Edge Panel	Weight (kg) without honeycomb	Weight (kg) with honeycomb	Difference (%)
composite	0,782	0,954	22
metallic	0,932	1,103	18

It should be noted that although honeycomb reinforcement causes approximately %20 weight increase in the wing leading edge panel, the absolute weight increases in kg are very low. However, for the wing leading edge extending along the whole span of the wing with honeycomb reinforcement, the weight increase in absolute value will be higher. Nevertheless, honeycomb reinforcement can be used in selected regions along the wing span and provide the required resistance against bird impact.

CHAPTER 8

CONCLUSION

In this thesis, the bird strike problem on wing leading edge is investigated by using the explicit finite element method. Aircraft structures are faced with various problem and 90 % of all incidences are caused by foreign object damage such as bird strike. Wings, nose, engines are reported as most common aircraft components struck by birds. Experiments and/or numerical simulations are typical design tools to optimize aircraft structures against the bird strike problem. Nowadays, advanced engineering software allows to model highly nonlinear problems. Bird strike proof design is validated by using computer aided engineering tools and final design is tested. In the last decades, many researchers focused their bird strike research by using computer and the related software.

Bird strike problem can be divided into four parts. Aviation standards may be defined as starting point of analyzing the bird strike problem. There are some milestones in constructing a model for bird strike such as problem definition, bird impactor modeling, metallic and composite material models of the aircraft part that is hit by the bird and the bird strike analysis. Firstly, Federal Aviation Administration's regulation provides impact speed and bird dimension for various aircraft type. Secondly, modeling of soft body impactor has to be characterized according to available solution formulation. Explicit finite element solver, Ls-Dyna, provides various solution formulations such as Lagrangian, Eulerian, ALE and SPH. Suitable formulation has to be selected according to a benchmark study which just includes a comparison process. Thirdly, suitable material models for metallic and composite aircraft structures have to select. In general, parameters of composite material or metallic material models have to be obtained from material characterization tests. However, for metallic materials one can find the parameters of the material model in the literature. Finally, bird strike problem on aircraft components can be analyzed by using all information which is obtained from previous steps.

Bird impactor modeling can be done by using explicit finite element formulation. There are some solution formulations such as Lagrangian, Eulerian, ALE and SPH. Conventional Lagrangian solution method cannot be used practically for bird modeling because of the distortion of Lagrange elements may lead to instability/divergence problems. In this thesis, a benchmark study among Eulerian, ALE and SPH solution formulations is performed. Bird dimensions are taken from FAA standards and the bird is modeled by using Eulerian, ALE and SPH formulation. Impact speed is taken as 100 m/s. Bird strikes to a square plate which is totally rigid. After performing all steps, deformation plots and impact force results are compared. As a result of the benchmark study, it is concluded that SPH solution formulation yields acceptable results which is also supported by the study of Ensan et al. [8]. Therefore, after introducing available solution technique and performing a benchmark study, it is decided to use SPH for modeling of soft body impactor.

Material model for aircraft structure is another subject that has to be clarified. Aluminum alloys are often used in aviation industry and there are some advanced material models such as Johnson Cook and Piecewise Linear Plasticity in Ls-Dyna material model library. In this thesis, another benchmark study is done between Johnson Cook and Piecewise Linear Plasticity material models. Bird dimension and the impact speed are taken from Federal Aviation Administration's regulations. Flexible plate is modeled to determine the failure characteristics of material model. The plate material is assigned as AL 2024 T3. Failure profile of the metallic part is obtained to be similar manner for both Johnson Cook and the Piecewise Linear Plasticity material models. Internal and kinetic energy comparison obtained by the both material models showed good agreement. However, in the light of comparison data and literature review, Johnson Cook material model is selected for modeling of the metallic aircraft structure. Secondly, material model for composite material has to be selected. Ls-Dyna material library provides a few material model and laminated composite fabric material model is used for modeling of laminated fabrics. Required parameters are determined from coupon tests. On-axis tests provide elastic and shear moduli, Poisson's ratio and failure strength values. Off-axis test is simply used for calibrating nonlinear material parameters. To validate the material model, coupon simulations are performed. A finite element model of coupon is prepared and analyzed. According to the comparison of coupon tests and simulations, mechanical

response of material model yields very similar results to the real coupon tests. Therefore, laminated composite fabric is considered to be a suitable material model for modeling of woven composite material that is used in the wing leading edge.

After the determination of the solution formulation for the bird impactor and suitable material models for metallic/composite aircraft structures, bird strike analyses on the wing leading edge are performed. Bird dimensions and impact speed are referenced from FAA standards. Metallic structures are modeled by using Johnson Cook elasto-viscoplastic material model. Laminated composite fabric material model is used to model the composite leading edge. After bird strike analysis, it is seen that for metallic leading edge, aerodynamic profile of leading edge is highly distorted and this may lead to instability during flight. Total fracture does not happen due to ductile mechanical response of aluminum alloy. A parametric study is performed by changing the impact velocity to see effect of impact velocity on the bird strike problem. It is seen that metallic leading edge exhibits enough toughness to impact speeds up to 75 m/s. After this velocity, plastic deformation propagates continuously with the increase of the impact speed. For the composite leading edge, failure index results are given. Composite materials are very brittle material and they cannot provide enough stiffness against impact force. Catastrophic failure occurs in the composite leading edge due to the brittle mechanical response of the composite. This leads to instability and threats the flight. The effect of impact velocity on composite leading edge is also investigated. Composite leading edge resists safely for impact speeds up to 75 m/s. Beyond this speed, after the stresses reach threshold strength values, leading edge has total failure. In the light of these information, it be concluded that leading edge can resist bird impacts up to a certain speed. However, leading edge is faced with a plastic deformation for the metallic case and total failure for the composite case during flight. This issue may lead to instability and catastrophic failure and it is concluded that leading edge has to be reinforced with secondary structural elements.

Finally, honeycomb material is used as secondary structural elements for reinforcing the leading edge against soft body impact problem. Honeycomb is very stiff material in compression and impact loads while it is quite inefficient in tension ad shear loads. Ls-Dyna also provides material models for honeycombs. Honeycomb material model is used to model the honeycomb and 3D finite elements are added to the model for

modeling of the honeycomb. After analyzing reinforced leading edges for metallic and composite cases, it seen that honeycomb material provides excellent impact resistance during the soft body impact. There is sufficient improvement in the plastic strain for metallic leading edge. For the reinforced composite leading edge, failure is not predicted. It is concluded that honeycomb material provides low weight and high impact resistance in bird impact.

For the future studies, bird impact analyses can be performed for a specific wing structure rather than a generic wing. This can provide actual wing geometry, thickness, connection types, etc. and can leads to more accurate results. Secondly, Ls-Dyna is suitable for user defined material model application. A specific material model can be prepared for composite materials and analyses results can be improved. Thirdly, although static and dynamic coupon test results are available for woven fabric material, there are no impact test results for composite fabric. Impact test setup can be established to test impact problem for composite material. From this type of impact test results, linear and nonlinear material parameters can be obtained to calibrate and improve composite material model. Bird impact analyses can also be done for different parts of aircraft such as node/radome, canopy and tails. Especially, bird impact problem on the canopy can be challenge according to modeling of glass material. Finally, bird impact analyses for different parts of the wing can be performed. Different strike angles and higher speed can also be future studies.

REFERENCES

[1] Cleary, E., et al., "Wildlife Strikes to Civil Aircraft in the United States 1990-2006," Federal Aviation Administration National Wildlife Strike Database, No. 13, July 2007.

[2] McCallum, S., C., Constantinou, C., "The influence of bird-shape in bird-strike analysis" , 5th European LS-DYNA Users Conference, 2005

[3] Guida, M., "Study, Design and Testing of Structural Configurations for the Bird-Strike Compliance of Aeronautical Components" Department of Aerospace Engineering University of Naples "Federico II", Naples, ITALY, Doctoral Thesis, December 2008

[4] Guida, M., Grimaldi, A., Marulo, F., Meo, M., Olivares, G., " Bird Impact on Leading Edge Wıng with SPH Formulation"

[5] Lavoie, A, Gakwaya, A, Ensan, M, N, "Application of the SPH Method for Simulation of Aerospace Structures under Impact Loading", 10th International LS-DYNA Users Conference, 2008

[6] Shmotin, Y., N., Chupin, P., V., Gabov, D.,V., "Bird Strike Analysis of Aircraft Engine Fan", 7th European LS-DYNA Conference,

[7] Heimbs, S., "Bird Strike Simulation on Composite Aircraft Structures" , EADS, Innovation Works, Munich, GERMANY.

[8] Tho, C., Smith, M., R., "Accurate Bird Strike Simulation methodology for BA609 Tiltrotor", Bell Helicopter Textron Inc., Fort Worth, Texas

[9] Goyal, V., K., Huertas, C., A., Vasko, T., J., " Smooth Particle Hydrodynamics for Bird- Strike Analysis Using LS-DYNA", American Transactions on Engineering & Applied Sciences, 2013

[10] Kim, M., Zammit, A., Siddens, A., Bayandor, J., " An Extensive Crashworthiness Methodology for Advanced Propulsion Systems, Part I: Soft Impact Damage Assessment of Composite Fan Stage Assembiles", 49th AIAA Aerospace Sciences Meeting including the New Horizons Forum and Aerospace Exposition, 4-7 January 2011, Orlando, Florida

[11] Heimbs, S., 2010, "Computational Methods for Bird Strike Simulations: A Review", EADS, Innovation Works, Munich, Germany.

[12] Liu, J., Li, Y., Gao, X., 2014, "Bird Strike on a Flat Plate: Experiments and Numerical Simulations", International Journal of Impact Engineering.

[13] Salem, S., C., Viswamurthy, S., R., Sundaram, R., 2011, "Prediction of Bird Impact Behavior through Different Bird Models Using Altair Radioss", Hyperworks Technology Conference.

[14] Hanssen, A., G., Girard, Y., Olovsson, L., Berstad, T., Langseth, M., 2006, "A Numerical Model for Bird Strike of Aluminum Foam Based Sandwich Panels", International Journal of Impact Engineering, pp: 1127-1144

[15] Willows, M. L., "Final report on the European Aerospace GARTEUR group on bird strike (AG23)", QinetiQ, 2005.

[16] Federal Aviation Administration, Issue Paper G-1, FR Doc. E7-19053, September, 2007.

[17] LS-Dyna® Keyword User's Manual, Version 971, Livermore Software Technology Corporation, May, 2007

[18] Lucy, L.B., "A Numerical Approach to the Testing of the Fission Hypothesis," Astronomical Journal, Vol. 82, 1977, pp.1013-20.

[19] LS-Dyna®Keyword User's ManualVol II, Version R7.1, Livermore Software Technology Corporation, May, 2014

20] Meyer, M., A., "Dynamic Behavior of Materials", John Wiley & Sons, Inc., University of California, San Diego, 1994, pp. 328

[21] Rueda, F, Beltran, F, Maderuelo,C, Climent,H, "Birdstrike analysis og the wing slats of EF-2000" EADS-CASA, Spain

[22] Hexcel Inc., "HexWeb Honeycomb Attributes and Properties", Product Catalog

APPENDIX A

DIMENSION AND STACKING SEQUENCE OF COUPONS

Material characterization is done by using coupons which have the following dimensions and stacking sequences. Dimension of tension test coupons and their stacking sequence are given in Figure A1 for warp and weft directions. Please note that, definition of stacking sequence direction such as 0° and 90° direction indicates that 0° is warp direction and 90° is weft direction.
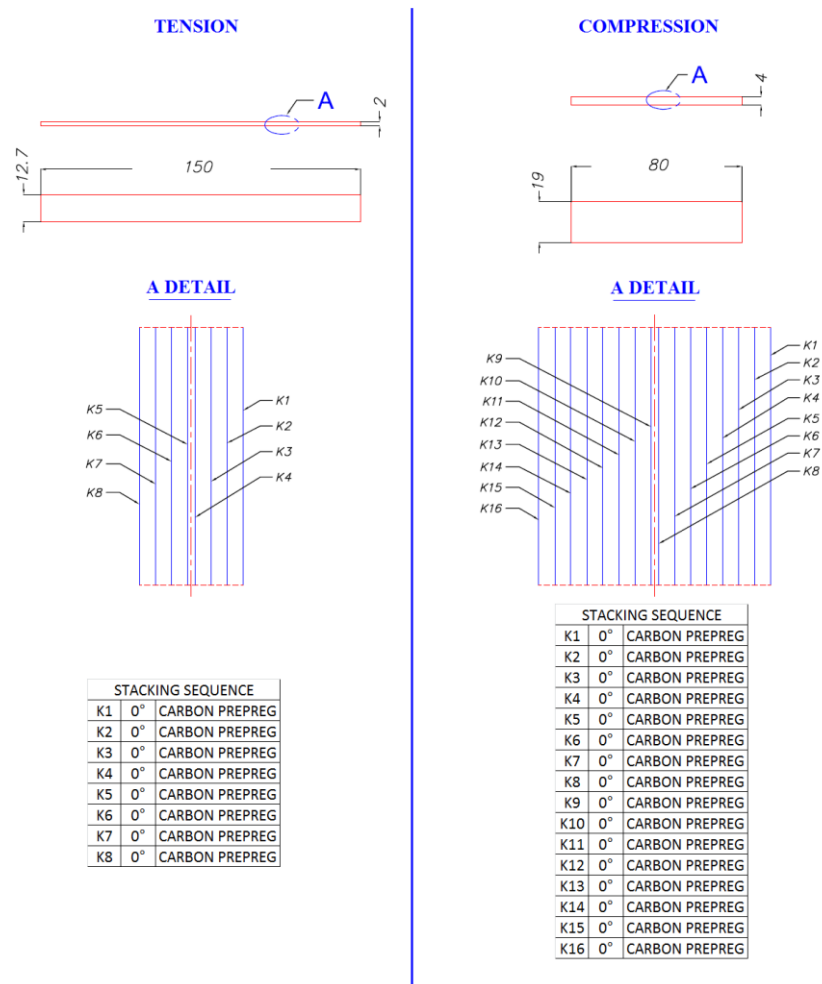

Figure A1 Coupon Dimensions (mm) and Stacking Sequence of Tension/Compression Coupons at warp and weft direction

45° direction tension/compression/shear tests are performed according to following dimension and stacking sequence information. Coupon dimension and stacking sequence are given in Figure A2.
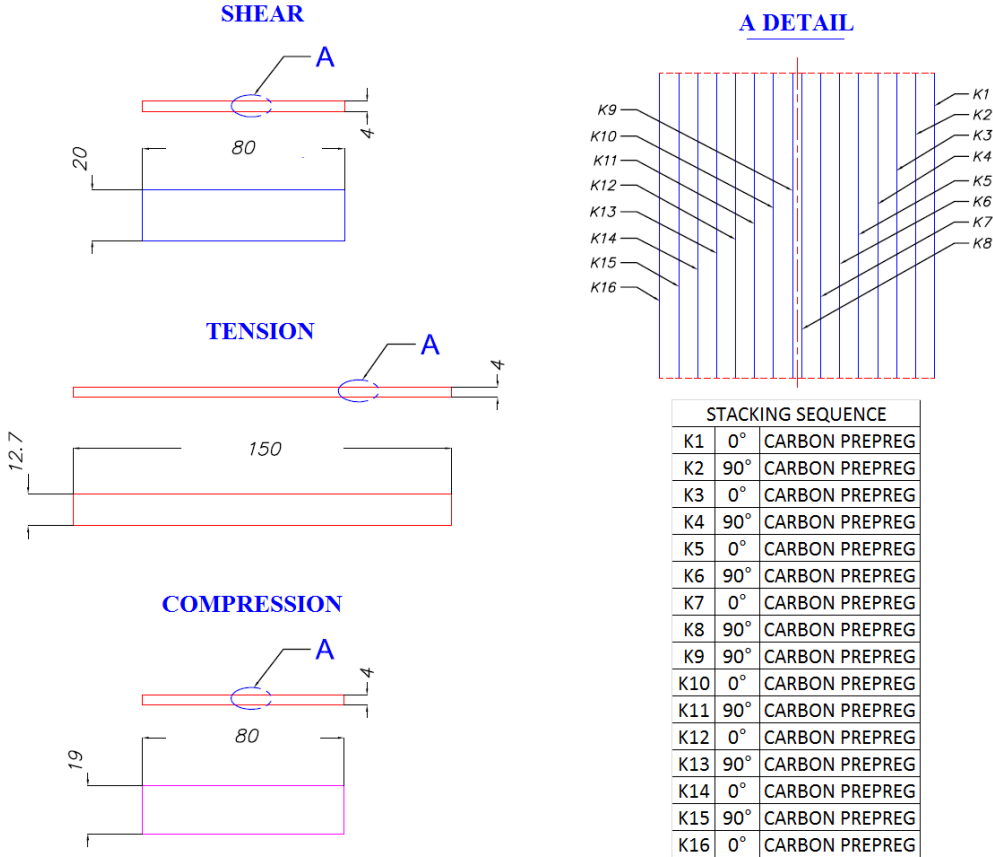

Figure A2 Dimensions and Stacking Sequence of Tension / Compression / Shear Coupons at 45° Direction

APPENDIX B

INFORMATION ABOUT UNIVERSAL TESTING MACHINES

B.1. Instron 5582 Eletromechanical UTM

Wide range of mechanical properties testing is performed by the Instron 5582 Universal Testing Machine. Measurement of tensile, flexural and compressive properties can be done by simply changing setup of the test machine.

Operation range of the test machine is:

Load: 2N to 100 kN, Temperature: -70° C to 300°C, Speed: 0.05 to 500 mm/min

Application: Poisson's ratio, Young's modulus, shear modulus, elongation measurement, tension/compression/shear stress-strain data and strength values. Picture about the testing machine is given in Figure B1.

Figure B1 Instron 5582 Electromechanical UTM

B.2. Instron 8872 Servohydrolic UTM

This machine can be modified to allow high speed tensile, bending and compression tests. Non-ambient conditions can be provided by using a conditioning oven. The Servohydrolic framework allows for fatigue testing in tension, bending and compression.

Operating range of the machine is: Load range: 2 N to 25 kN, Temperature range: -70° C to 300° C and Test Speed Range: 0.005 to 60000 mm/min.

Main applications are elongation measurements, Poisson's ratio, Young's modulus, shear modulus, fatigue and tension/compression/shear stress-strain data. Picture of the testing machine is given in Figure B2.
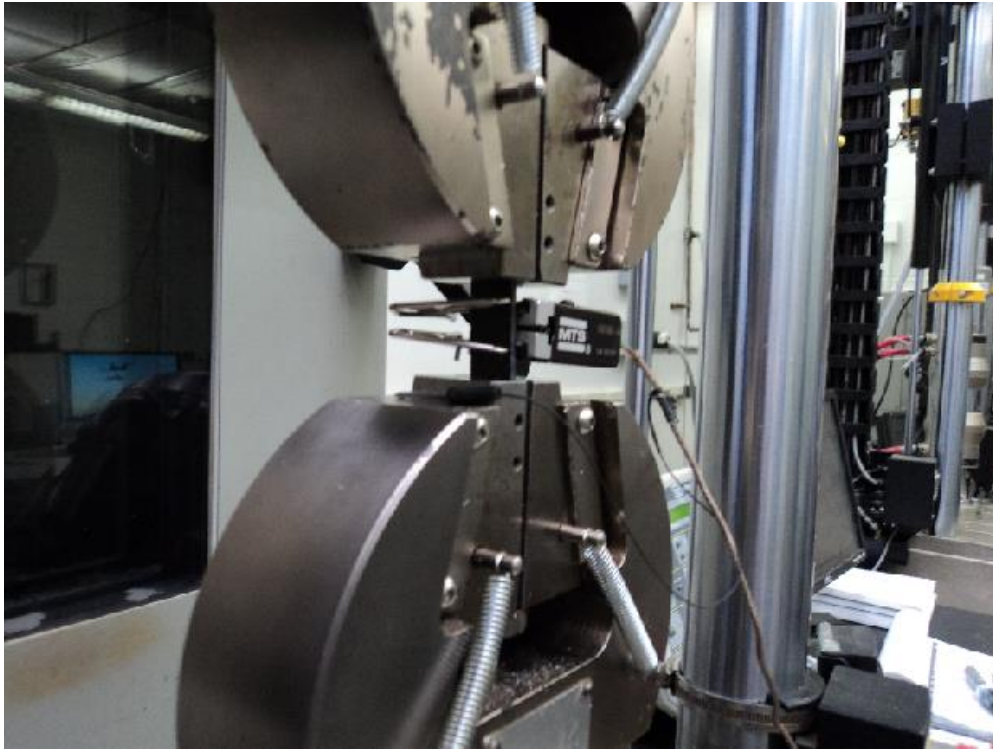

Figure B2 Instron 8872 Servohydrolic UTM